

STATUS OF THESIS

Title of thesis

Design and Fabrication of a Surface pH Sensor for a Real-Time Corrosion Monitoring

I, SAEID KAKOOEI

hereby allows my thesis to be placed at the Information Resource Center (IRC) of Universiti Teknologi PETRONAS (UTP) with the following conditions:

1. The thesis becomes the property of UTP
2. The IRC of UTP may make copies of the thesis for academic purposes only.
3. This thesis is classified as

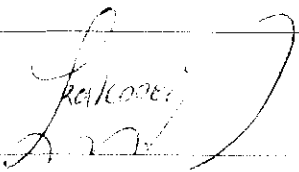
Confidential

Non-confidential

If this thesis is confidential, please state the reason:

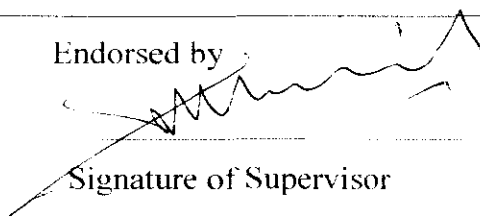
The contents of the thesis will remain confidential for _____ years.

Remarks on disclosure:



Signature of Author

Endorsed by



Signature of Supervisor

Permanent Address:

4th Floor, 1st Building, Andisheh 9 Alley,

Shahid Beheshti Street, Amol, Mazandaran,

Postcode: 46158/49468

Date: 23/12/13

Name of Supervisor:

Assoc. Prof. Ir. Dr. Mokhtar Che Ismail

Date: 23/12/13

UNIVERSITI TEKNOLOGI PETRONAS

DESIGN AND FABRICATION OF A SURFACE pH SENSOR FOR A REAL-
TIME CORROSION MONITORING

By

SAEID KAKOOEI

The undersigned certify that they have read, and recommend to the Postgraduate Studies Program for acceptance this thesis for the fulfillment of the requirements for the degree stated.

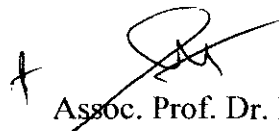
Signature:



Main Supervisor:

Assoc. Prof. Ir. Dr. Mokhtar Che Ismail

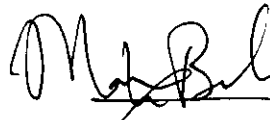
Signature:



Co-Supervisor:

Assoc. Prof. Dr. Bambang Ari-Wahjoedi

Signature:



Head of Department:

Ir. Dr. Masri M Bahar

Ir. Dr. Masri Baharem
Head of Department/Associate Professor
Department of Mechanical Engineering
Universiti Teknologi PETRONAS
Bandar Seri Iskandar, 31750 Tronoh,
Perak Darul Ridzuan, Malaysia

Date:

3/12/13

DESIGN AND FABRICATION OF A SURFACE pH SENSOR FOR A REAL-
TIME CORROSION MONITORING

by

SAEID KAKOOEI

A Thesis

Submitted to the Postgraduate Studies Programme

as a Requirement for the Degree of

DOCTOR OF PHILOSOPHY

DEPARTMENT OF MECHANICAL ENGINEERING

UNIVERSITI TEKNOLOGI PETRONAS

BANDAR SERI ISKANDAR

PERAK

December 2013

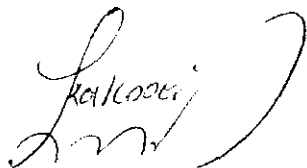
DECLARATION OF THESIS

Title of thesis

DESIGN AND FABRICATION OF A SURFACE pH SENSOR FOR
A REAL-TIME CORROSION MONITORING

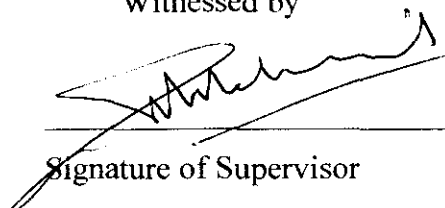
I, SAEID KAKOOEI

hereby declare that the thesis is based on my original work except for quotations and citations, which have been duly acknowledged. I also declare that it has not been previously or concurrently submitted for any other degree at UTP or other institutions.



Signature of Author

Witnessed by



Signature of Supervisor

Permanent Address:
4th Floor, 1st Building, Andisheh 9 Alley, Shahid
Beheshti Street, Amol, Mazandaran, Iran

Postcode: 46158/49468

Date: 03/12/13

Name of Supervisor:

Assoc. Prof. Ir. Dr. MokhtarChe Ismail

Date: 03/12/13

DEDICATION

To my beloved wife, beautiful daughter and my dearest supportive family members.

ACKNOWLEDGEMENTS

“In the name of God, the most Beneficent, the most Merciful”

First and foremost I wish to express my sincere appreciation to my Advisor and Supervisor Associated Professor Ir. Dr. Mokhtar Che Ismail who help me technically and spiritually. I appreciate his help and the father-like care from the bottom of my heart.

I would like to express my appreciation to the help and cooperation from Assoc. Prof. Dr. Bambang Ari-Wahjoedi , my co-supervisor, for his valuable discussion on sensor preparation and fabrication process.

I would like to express my deep love and appreciation to my beloved wife, my dear family also my friends who without their encouragement and moral support this thesis work would not be possible.

I also thank personnel of Hi-Tech Instruments Sdn Bhd. For their help in characterization part of my project.

Not to forget my colleagues and all staff of Centre for Corrosion Research (CCR), I thank you sincerely.

I express my thanks to Ministry of Higher Education (ERGS Grant No: 158200327) for their financial support.

Further I would appreciate UniversitiTeknologi PETRONAS (UTP) for providing education facilities and financial support (I-GEN grant and Ph.D. full scholarship).

ABSTRACT

The aim of this research is to design and fabricate a new pH sensor that can be used to measure hydrogen ion activity on corroding metal surface in bulk solution or under deposit. Iridium oxide (IrO_x) is used for proposed design as pH sensitive material. IrO_x is a potentiometric sensor which its open circuit potential regarding a reference electrode is representative of pH. The electrodeposition method of cyclic voltammetry approach is used for coating of IrO_x on stainless steel substrate. The effects of scan rate, temperature, and number of cycles on the coating thickness of IrO_x electrodeposited on a stainless steel substrate were investigated in a statistical system. The central composite design, combined with response surface methodology, was used to study condition of electrodeposition. Electrochemical experiments were conducted to characterize the IrO_x -pH sensor as well as monitor the pH on a metal surface in conjunction with the fabrication of a pH microelectrode-designed system. The fabricated pH sensor was calibrated by using a commercial glass pH probe. The pH response measured by OCP at 25 °C was 75.3 mV/pH unit. Results of statistical investigation showed that the proposed pH sensor design can be used for real-time corrosion monitoring by surface pH measurement. Increasing of surface pH during CO_2 corrosion was detected by proposed pH sensor. Results showed that scan rate significantly affects the thickness of the electrodeposited layer. Also, the number of cycles has a greater effect than temperature on the IrO_x thickness. Cyclic voltammetry (CV), scanning electron microscopy (SEM), energy-dispersive X-ray spectroscopy (EDX), atomic force microscopy (AFM), X-ray Diffraction (XRD), Transmission electron microscopy (TEM), Electrochemical Impedance Spectroscopy (EIS), Linear polarization resistance (LPR), Infinite Focus Microscope (IFM) and open circuit potential (OCP) are used for CO_2 corrosion and iridium oxide film characterization.

Keywords: CO₂ corrosion; pH microelectrode; IrO₂; Electrodeposition; Surface pH measurement; Cyclic voltammetry; stainless steel; response surface methodology; central composite design

ABSTRAK

Tujuan kajian ini adalah untuk mereka bentuk dan menghasilkan satu sensor pH baru yang boleh digunakan untuk menguji dan memantau aktiviti ion hidrogen pada permukaan logam yang berkarat dalam larutan pukal atau di bawah deposit. Iridium oksida (IrO_x) telah digunakan sebagai bahan sensitif pH untuk bentuk rekaan yang dicadangkan. IrO_x adalah pengesan potentiometrik di mana nilai voltan litar terbuka antara sensor ini dengan elektrod rujukan mewakili nilai pH. Kaedah penyaduran elektrik dengan pendekatan cyclic voltammetry telah digunakan untuk menghasilkan lapisan IrO_x pada substrat keluli tahan karat.

Kesan kadar imbasan, suhu dan bilangan kitaran pada ketebalan lapisan IrO_x yang telah disadurkan pada substrat keluli tahan karat telah dikaji dalam sistem statistik. Reka bentuk komposit berpusat, digabungkan dengan kaedah gerak balas permukaan, telah digunakan untuk mengkaji keadaan penyaduran. Eksperimen elektrokimia telah dijalankan untuk mencirikan sensor IrO_x -pH serta memantau pH pada permukaan logam beserta penghasilan sistem rekaan pH microelectrode. Sensor pH yang direka ini telah ditentukan dengan menggunakan alat penentu pH kaca yang komersil. Reaksi pH yang diukur dengan kaedah voltan litar terbuka pada 25°C adalah 75.3 mV /unit pH . Hasil kajian menunjukkan bahawa reka bentuk sensor pH yang dicadangkan yang boleh digunakan untuk memantau hakisan masa sebenar dengan pengukuran pH permukaan. Peningkatan pH permukaan semasa hakisan CO_2 telah dikesan oleh sensor pH yang dicadangkan. Hasil kajian menunjukkan bahawa kadar imbasan telah memberi kesan ketara kepada ketebalan lapisan saduran. Selain itu, bilangan kitaran mempunyai kesan yang lebih besar berbanding suhu kepada ketebalan IrO_x . Cyclic voltammetry (CV), scanning electron microscopy (SEM), energy-dispersive X-ray spectroscopy (EDX), atomic force microscopy (AFM), X-ray Diffraction (XRD), Transmission electron microscopy (TEM), Electrochemical Impedance Spectroscopy (EIS), Linear polarization resistance (LPR), Infinite Focus Microscope (IFM) dan

open circuit potential (OCP) telah digunakan untuk pencirian hakisan CO₂ dan filem Iridium oksida. .

Kata kunci: kakisan CO₂; elektrod pH mikro; IrO_x ; penyaduran elektrik ; ukuran pH permukaan; cyclic voltammetry ; kelulitahan karat; kaedah gerak balas permukaan ; reka bentuk komposit berpusat.

In compliance with the terms of the Copyright Act 1987 and the IP Policy of the university, the copyright of this thesis has been reassigned by the author to the legal entity of the university,

Institute of Technology PETRONAS Sdn Bhd.

Due acknowledgement shall always be made of the use of any material contained in, or derived from, this thesis.

© Saeid Kakooei, 2013

Institute of Technology PETRONAS SdnBhd

All rights reserved.

TABLE OF CONTENT

STATUS OF THESIS	1
ABSTRACT	vii
ABSTRAK	ix
LIST OF TABLES	xvi
LIST OF FIGURES	xvii
LIST OF ABBREVIATION AND SYMBOLS	xxiii
CHAPTER 1 INTRODUCTION	1
1.1 Background	1
1.2 Problem Statement	3
1.3 Research Objectives	3
1.4 Scope of Study	4
1.5 Organization of the Thesis	4
CHAPTER 2 BACKGROUND AND LITERATURE REVIEW	6
2.1 Chapter Overview	6
2.2 CO ₂ corrosion	6
2.3 Surface pH measurement	10
2.4 Electrodeposition theory	13
2.4.1 Nernst Equation	15
2.5 Cyclic Voltammetry	17
2.6 Open Circuit Potential	19
2.7 Electrochemical Impedance Spectroscopy	20
2.8 Potentiometric pH sensor	22
2.9 Iridium oxide pH sensor	22
2.9.1 Iridium oxide pH sensor fabrication method	28
2.9.1.1 Sol–gel processes	28
2.9.1.2 Electrochemical or thermal oxidation of iridium and iridium salts	28
2.9.1.3 Sputtering	30
2.9.1.4 Anodic or cathodic electrodeposition	31
2.9.1.5 Other methods	35

2.9.2 Applications of IrO ₂ electrode.....	35
2.9.2.1 Biomedical and Biological applications.....	35
2.9.2.2 Industrial applications.....	36
2.10 Design of Experiments.....	37
2.10.1 Response Surface Methodology.....	37
2.10.2 Central Composite Design.....	38
2.10.3 Analysis of Variance.....	39
CHAPTER 3 METHODOLOGY AND CHARACTERIZATION TOOLS.....	40
3.1 Methodology Overview.....	40
3.2 Design of experiments, analysis, and model fitting.....	40
3.3 Design and Fabrication of pH Sensor.....	42
3.3.1 Chemicals and Materials.....	42
3.3.2 Preparation of Electrodeposition Solution.....	43
3.3.3 Preparation of IrO _x electrode for electrochemical experiments.....	44
3.3.4 Preparation of IrO _x pH sensor for surface pH measurements.....	46
3.3.5 Preparation of IrO _x pH sensor for under deposit pH measurement.....	47
3.4 Research Test matrix of pH sensor application.....	48
3.5 Electrochemical investigation.....	51
3.5.1 Linear polarization resistance (LPR).....	51
3.5.2 Electrochemical impedance spectroscopy (EIS).....	52
3.5.3 Open Circuit Potential (OCP).....	52
3.5.4 Cyclic Voltammetry (CV).....	53
3.6 Surface Morphology Characterization.....	53
3.6.1 Field Emission Scanning Electron Microscope (FESEM).....	54
3.6.2 Energy Dispersive X-rays Analysis (EDX).....	55
3.6.3 Atomic force microscopy (AFM).....	55
3.6.4 X-rays diffraction (XRD).....	56
3.6.5 Infinite Focus Microscope (IFM).....	56
3.6.6 Transmission electron microscopy.....	57
3.6.7 Fourier Transform Infrared Analysis.....	57
CHAPTER 4 RESULTS AND DISCUSSIONS.....	59
4.1 Chapter Overview.....	59

4.2 Electrodeposition of Iridium Oxide on Stainless Steel.....	59
4.2.1 Preparation of the Deposition Solution	59
4.2.2 Fabrication of Iridium Oxide Electrode	60
4.2.3 The Cyclic Voltammetry Growing of IrO _x Electrode.....	62
4.2.4 The Sensitivity of IrO _x Electrode.....	64
4.2.5 The Cyclic Voltammetry of IrO _x Electrode	66
4.2.6 The electrochemical impedances and Equivalent circuit models of IrO _x Electrode	67
4.2.7 The Surface Morphology of IrO _x Electrode (SEM, EDX, AFM, TEM, and XRD).....	71
4.2.8 Stability of IrO _x Electrode	76
4.2.9 Conclusion.....	77
4.3 Statistical investigation of iridium oxide electrodeposition on stainless steel.	78
4.3.1 Fabrication of pH electrodes	78
4.3.2 Open-Circuit Potential Response	78
4.3.3 Cyclic voltammetry of IrO _x electrodes	80
4.3.4 Electrochemical Impedance Spectroscopy of IrO _x electrodes	83
4.3.5 SEM and EDX of IrO _x electrodes.....	84
4.3.6 Response surface methodology model equations.....	87
4.3.7 Coded experimental model equations for oxide thickness	90
4.3.8 Interactions between independent variables	92
4.3.9 Conclusion.....	93
4.4 Surface pH measurement in CO ₂ corrosion with a novel microelectrode pH probe	93
4.4.1 Design and fabrication of a novel microelectrode pH probe.....	93
4.4.2 Surface pH measurement in CO ₂ corrosion at three different temperatures	94
4.4.3 SEM/EDX of corrosion product at three different temperatures.....	100
4.4.4 Conclusion.....	106
4.5 Under deposit pH measurement in CO ₂ corrosion with a novel microelectrode pH probe	107

4.5.1 pH probe and experimental set-up for under deposit pH measurement	107
4.5.2 Surface pH measurement under deposit in CO ₂ corrosion at three different temperatures	108
4.5.3 SEM/EDX of corrosion product at three different temperatures.....	114
4.5.4 Corrosion rate in bulk pH=4.....	118
4.5.5 Conclusion.....	119
CHAPTER 5 CONCLUSIONS AND FUTURE WORK.....	120
5.1 Conclusions.....	120
5.2 Recommendation for Future Works	121

LIST OF TABLES

Table 2.1: Application and characterization of IrO ₂ electrodes fabricated by electrodeposition technique[7].....	32
Table 3.1: Codified and normal values of the experimental design levels	41
Table 3.2: Experimental design and actual response of the thickness and pH sensitivity of pH electrode.	42
Table 3.3: Composition of X52 carbon steel	49
Table 3.4: Test matrix for surface pH measurement and under deposit pH measurement	49
Table 4.1: Experimental design for IrO _x electrodeposition on stainless steel.....	61
Table 4.2: Experimental design and actual response of the thickness and pH sensitivity of pH electrode.....	80
Table 4.3: Suggested Model Summary Statistics by DOE software.....	91
Table 4.4: 2FI Model summary statistics.....	92
Table 4.5: 2FI Model Summary Statistics Result after improvement.....	92

LIST OF FIGURES

Figure 2.1: Sketch of the test specimens mounted in the specimen holder; FS1 and FS2: specimens will be covered with sand deposit, NS: specimen will be directly exposed to the brine, RE: A carbon steel wire can be used as pseudo-reference electrode [25].	9
Figure 2.2: Interfacial pH measurement setup. (CE, counter electrode; WE, working electrode; RE, reference electrode.) [44]	12
Figure 2.3: Schematic of an electrodeposition cell; CE (Counter electrode), RE (Reference electrode), WE (working electrode)	14
Figure 2.4: Graphical diagram of an electrodeposition process	15
Figure 2.5: An example voltammogram with relevant features marked [14].	19
Figure 2.6: Crystal structure of IrO ₂ [75].	24
Figure 2.7: The proposed reaction at the anhydrous IrO _x electrode	25
Figure 2.8: The proposed reaction at the hydrous IrO _x electrode	26
Figure 2.9: The schematic structure of hydrous IrO _x electrode	26
Figure 2.10: CV of iridium oxide in PBS at 50 mV/s showing the area used to calculate the CSC of the film [66].	27
Figure 2.11: Stacked voltammograms of iridium oxide potentiodynamically cycled between -0.25 V _{SCE} and 1.27 V _{SCE} at 50 mV/s for 2, 4, 8, and 24 hr in deaerated 0.5 M H ₂ SO ₄ aqueous solution [67].	30
Figure 3.1: Four iridium oxidation state in iridium tetrachloride	43
Figure 3.2: Solution preparation and electrodeposition setup	44
Figure 3.3: IrO _x electrodeposited on stainless steel substrate for electrochemical investigations.	45
Figure 3.4: A high-performance potentiostat/galvanostat (Autolab/PGSTAT128N, the Netherlands) used for pH sensor fabrication, calibration and all electrochemical investigations.	45
Figure 3.5: Schematic diagram of an electrodeposition setup: (1) Pt mesh counter electrode, (2) stainless steel (working electrode), (3) Ag/AgCl (3M KCl) reference electrode.	46
Figure 3.6: Schematic Design of pH probe for surface pH measurement of corroding carbon steel.	47

Figure 3.7: Schematic Design of pH measurement probe for monitoring of pH and corrosion under deposit (Agar).	48
Figure 3.8: SEM image of polished X52 carbon steel before testing	50
Figure 3.9: Field Emission Scanning electron microscopy (FESEM) system	54
Figure 3.10: A schematic diagram of the AFM operation [121]......	55
Figure 3.11: Infinite Focus Microscope (IFM) system	56
Figure 3.12: Transmission electron microscope	57
Figure 3.13: Fourier Transform Infrared Spectrometer	58
Figure 4.1: The UV–vis spectra of fresh and aged deposition solutions	60
Figure 4.2: Schematic of an electrodeposition setup: (1) Pt mesh counter electrode, (2) stainless steel (working electrode), (3) Ag/AgCl reference electrode.	62
Figure 4.3: Growth of iridium oxide on stainless steel substrate by cyclic voltammetry method at a scan rate of 50 mV/s.	63
Figure 4.4: The area used to calculate CSC_C in EIROF electrode	63
Figure 4.5: Typical potentiometric response of the EIROF electrode to a series of universal buffer solutions. . This response is in agreement with published reports for iridium oxide.(Please refer to Table 4.1 for detail of a, b, c, and d).....	64
Figure 4.6: Schematic titration of IrO_2 pH sensor by adding 1M KOH to buffer solution.....	65
Figure 4.7: OCP response of an EIROF prepared by cyclic voltammetry on stainless steel in a universal buffer while it is titrated with KOH.	66
Figure 4.8: Cyclic voltammetry of bare stainless steel and EIROF electrodes in pH 7 standard buffer solution at a scan rate of 50 mV/s. (Please refer to Table 4.1 for detail of a, b, c, and d)	67
Figure 4.9: Nyquist plot of EIROF electrode on stainless steel (Please refer to Table 4.1 for detail of a, b, c, and d)	68
Figure 4.10: Equivalent circuit models; (a) circuit model of IrO_x coated stainless steel physical properties, (b) representing an equivalent circuit model of fitting EIS data	68

Figure 4.11: AC Impedance of bare stainless steel and EIROF electrodes as a function of cycles and scan rate (Please refer to Table 4.1 for detail of a, b, c, and d).....	70
Figure 4.12: (1) Element Maps of IrO ₂ coated stainless steel ((a) Mixed map, (b) Carbon Ka1 2(blue), (c) Oxygen Ka1(green), (d) Iron Ka1 (black), (e) Iridium La1(red)); (2)EDX spectra of iridium oxide electrodeposited on stainless steel substrate.....	72
Figure 4.13: FESEM images of EIROF electrode	73
Figure 4.14: AFM image of iridium oxide fabricated by CV.	74
Figure 4.15: TEM images of iridium oxide electrodeposited by cyclic voltammetry .	75
Figure 4.16: XRD result of iridium oxide electrodeposited by cyclic voltammetry....	76
Figure 4.17: Cyclic voltamograms of IrO _x electrode before and after ultrasonic test.	77
Figure 4.18: (a) and (b), Equilibrium potential as a function of pH for electrodeposited IrO _x films on stainless steel substrates deposited at different scan rates, temperatures, and number of cycles by cyclic voltammetry (CV).	79
Figure 4.19: Cyclic voltammetry results of bare stainless steel and EIROF electrodes in a pH 7 universal buffer solution at a scan rate of 50 mV/s are shown in a, b, and c. SS = stainless steel electrode without coating.	82
Figure 4.20: (a) and (b), A Bode plot showing the total impedance module versus the frequency of bare stainless steel and IrO _x electrodeposited on stainless steel electrodes. SS = stainless steel electrode without coating.	84
Figure 4.21: EDX result of IrO _x on stainless steel	85
Figure 4.22: FESEM images of IrO _x electrodeposited layer with an increasing number of cycles. (a) 100, (b) 200, (c) 400, and (d) 500.	86
Figure 4.23: Actual versus predicted response plot of the IrO _x coating thickness.....	87
Figure 4.24: Response surface and contour plot of IrO _x coating thickness (nm) as a function of the number of cycles and scan rate (mV/s) at minimum and maximum temperatures: (a) 25 °C (b) 65 °C.	88
Figure 4.25: Changes in IrO _x coating thickness (nm) with different variables: (a) cycle (b) Temperature (°C) and (c) Scan rate (mV/s).	90

Figure 4.26: Potentiometric response of a IrO_x pH electrode in the pH range of 4–9 at a temperature of 25 °C.	94
Figure 4.27: Set-up for measuring near surface pH on carbon steel corroding surface at three different temperatures; 25, 50, and 80 °C.	96
Figure 4.28: Surface pH measurement during X52 carbon steel corrosion under bulk pH 4.0; $p\text{CO}_2=0.97$ bar, temperature= 25 °C, and $[\text{NaCl}]= 3\text{wt}\%$	97
Figure 4.29: Surface pH measurement during X52 carbon steel corrosion under bulk pH 6.0; $p\text{CO}_2=0.97$ bar, temperature= 25 °C, and $[\text{NaCl}]= 3\text{wt}\%$	97
Figure 4.30: Surface pH measurement during X52 carbon steel corrosion under bulk pH 4.0; $p\text{CO}_2=0.88$ bar, temperature =50 °C, and $[\text{NaCl}] = 3\text{wt}\%$	98
Figure 4.31: Surface pH measurement during X52 carbon steel corrosion under bulk pH 6.0; $p\text{CO}_2=0.88$ bar, temperature =50 °C, and $[\text{NaCl}] = 3\text{wt}\%$	98
Figure 4.32: Surface pH measurement during X52 carbon steel corrosion under bulk pH 4.0; $p\text{CO}_2=0.53$ bar, temperature= 80 °C, and $[\text{NaCl}] = 3\text{wt}\%$	99
Figure 4.33: Surface pH measurement during X52 carbon steel corrosion under bulk pH 6.0; $p\text{CO}_2=0.53$ bar, temperature= 80 °C, and $[\text{NaCl}] = 3\text{wt}\%$	99
Figure 4.34: Electrochemical and chemical reaction on carbon steel surface during CO_2 corrosion.	100
Figure 4.35: SEM image of corroded X52 carbon steel surface at 25 °C, bulk pH=4.	101
Figure 4.36: EDX result of CO_2 corrosion product of X52 carbon steel at 25 °C, bulk pH=4.	101
Figure 4.37: SEM image of corroded X52 carbon steel surface at 80 °C, bulk pH=4.	102
Figure 4.38: EDX result of CO_2 corrosion product of X52 carbon steel at 80 °C, bulk pH=4.	102
Figure 4.39: SEM image of corroded X52 carbon steel surface at 25 °C, bulk pH=6.	103
Figure 4.40: EDX result of CO_2 corrosion product of X52 carbon steel at 25 °C, bulk pH=6.	103
Figure 4.41: SEM image of corroded X52 carbon steel surface at 80 °C, bulk pH=6.	104

Figure 4.42: EDX result of CO ₂ corrosion product of X52 carbon steel at 80 °C, bulk pH=6.	104
Figure 4.43: XRD spectrum for corrosion product on the surface of X52 carbon steel in CO ₂ -saturated 3% NaCl solution at 80 °C, bulk pH=6.....	105
Figure 4.44: Surface of pH probe and carbon steel before (a) and after (b) exposure in CO ₂ -saturated 3% NaCl solution.	105
Figure 4.45: Potentiometric response of aIrO _x pH electrode in the pH range of 4–9 at a temperature of 25 °C.....	108
Figure 4.46: Set-up for measuring corrosion rate and near surface pH on carbon steel corroding surface under deposit at three different temperatures; 25, 50, and 80 °C.	109
Figure 4.47: Surface pH measurement under deposit during X52 carbon steel corrosion under bulk pH 4.0; pCO ₂ =0.97 bar, temperature= 25 °C, and [NaCl]= 3wt%.....	111
Figure 4.48: Surface pH measurement under deposit during X52 carbon steel corrosion under bulk pH 4.0; pCO ₂ =0.97 bar, temperature= 25 °C, and [NaCl]= 3wt%.....	111
Figure 4.49: Surface pH measurement under deposit during X52 carbon steel corrosion under bulk pH 4.0; pCO ₂ =0.88 bar, temperature =50 °C, and [NaCl] = 3wt%.....	112
Figure 4.50: Surface pH measurement under deposit during X52 carbon steel corrosion under bulk pH 6.0; pCO ₂ =0.88 bar, temperature =50 °C, and [NaCl] = 3wt%.....	112
Figure 4.51: Surface pH measurement under deposit during X52 carbon steel corrosion under bulk pH 4.0; pCO ₂ =0.53 bar, temperature= 80 °C and [NaCl] = 3wt%.....	113
Figure 4.52: Surface pH measurement under deposit during X52 carbon steel corrosion under bulk pH 6.0; pCO ₂ =0.53 bar, temperature= 80 °C and [NaCl] = 3wt%.....	113
Figure 4.53: SEM image of corroded X52 carbon steel surface at 25 °C, pH=4.....	114
Figure 4.54: SEM image of corroded X52 carbon steel surface at 25 °C, pH=6.....	115

Figure 4.55: EDX result of CO ₂ corrosion product of X52 carbon steel at 25 °C, pH=6.	115
Figure 4.56: SEM image of corroded X52 carbon steel surface at 80 °C, pH=4.....	116
Figure 4.57: SEM image of corroded X52 carbon steel surface at 80 °C, pH=6.....	116
Figure 4.58: EDX result of CO ₂ corrosion product of X52 carbon steel at 80 °C, pH=6.	117
Figure 4.59: Surface of pH probe and carbon steel after exposure in CO ₂ -saturated 3% NaCl solution under deposit.	117
Figure 4.60: Corrosion rate of X52 carbon steel in the 3% NaCl solution at 25 °C under deposit, bulk pH=4.....	118
Figure 4.61: Corrosion rate of X52 carbon steel in the 3% NaCl solution at 80 °C under deposit, bulk pH=4.....	119

LIST OF ABBREVIATION AND SYMBOLS

<i>A</i>	Surface area of the steel in m ²
API	American Petroleum Institute
<i>B</i>	Stern Geary coefficient
<i>b_a</i>	Anodic curve Tafel slope
<i>b_c</i>	Cathodic curve Tafel slope
CCD	Central Composite Design
CV	Cyclic Voltammetry
CR	Corrosion rate in mm/year
CPE	Constant Phase Element
EDX	Energy Dispersive X-rays Analysis
EIS	Electrochemical Impedance Spectroscopy
<i>F</i>	Faraday constant, 96500 C/mole
FESEM	Field Emission Scanning Electron microscopy
<i>i_{corr}</i>	Corrosion current density in A/cm ²
IrO _x	Iridium Oxide
LPR	linear polarization resistance
<i>n</i>	Number of electron
OCP	Open Circuit Potential
P	Pressure in MPa
ppm	Part Per Million
<i>R</i>	Universal gas constant, $R=8.314 J/(mol K)$
RSM	Response Surface Methodology
<i>R_p</i>	Resistance polarization in ohm
<i>R_s</i>	Solution Resistance in ohm
<i>R_t</i>	Charge Transfer Resistance in ohm
SCE	Saturated Calomel Electrode
<i>T</i>	Temperature

TP	Tafel polarization
Z	Atomic weight in g/mol

CHAPTER 1

INTRODUCTION

1.1 Background

Corrosion damages play a major role on the world economy. A corrosion cost of \$276 billion per year was reported by the US Department of Transportation in 2002 which \$1.4 billion of it was annual direct costs for corrosion related to oil/gas exploration/production and a \$5.0 billion related to gas distribution [1]. The most important form of corrosion in the oil and gas industry is CO₂ corrosion [2,3]. Carbon steel is one of the most commonly used materials for pipelines in the industry because of low cost and availability. CO₂ corrosion governed not only by material characteristics of the pipelines but also by operating conditions such as flow rate, temperature, pH, and CO₂ partial pressure [4].

In CO₂ corrosion, the study of corrosion mechanism requires understanding of interfacial reactions between the pipeline material and local environment. The most important parameters is surface pH measurement. Local surface chemistry condition can be different from bulk solution when chemical reactions happen at a metal interface with solution. Surface pH is long recognized as a key local parameter that influences electrochemical reaction mechanisms and rates [5].

Furthermore, in CO₂ corrosion, the precipitation of FeCO₃ occurs when the pH of the CO₂-containing solution is sufficiently high [6]. The difficulty in recent research is to explain the formation of FeCO₃ deposit in low pH environment based on the pH measurement of bulk solution . The result obtained from localized pH measurements can be used for real-time corrosion monitoring because corrosion is a pH-dependent phenomenon. Unfortunately, commercial pH electrodes cannot monitor pH changes

on metal surfaces. Therefore, a novel pH electrode design is needed for monitoring of reactions occurring in metal-solution interfaces.

Successful corrosion monitoring requires understanding of electrochemical and chemical reaction on the metal surface. These reactions on the metal surface can change nature of metal/liquid interface and decrease or increase the surface pH. The main idea of this thesis is to measure and monitor pH changes of corroding carbon steel by a novel IrO_x pH probe design.

The glass pH sensor is the oldest electrochemical sensors which have some disadvantages such as lack of stability in alkaline and fluoridric acid solutions and their mechanical fragility [7,8]. New techniques for measuring pH include optical fiber-based pH sensor, mass-sensitive pH sensor, conducting polymer pH sensors, Nano-constructed cantilever-based pH sensor, ion-sensitive field effect transistors (ISFET) -based pH sensor, pH-image sensor, and metal oxide pH sensor [7].

The past decades, IrO_x became a superior material for reference electrode and pH measurements in various fields such as biological media, food-industry, nuclear field, and oil and gas industry. Iridium oxide can provide a rapid and stable response in different media because of its high conductivity and low temperature coefficient [9]. The possibility to design and fabricate a robust and accurate surface pH sensor based on IrO_x provide significant benefits for oil and gas industry.

Since iridium is an expensive metal, most of IrOX fabrication methods are also expensive. Among them, electrodeposition has offered several advantages such as: a) cheaper fabrication process, b) potential for using cheaper substrates, c) low-temperature process even appropriate for plastic substrates, and d) adaptability of sensor shapes and designs made possible with electrodeposition on substrates of different geometries. Most researchers used gold, platinum and some other expensive metal as substrate for IrOX electrodeposition. Using a cheaper substrate like stainless steel needs a precise optimization of electrodeposition factor s to achieve a stable and proper IrOX film on substrate. An statistical approach is needed to be used for investigation of effect of various factors on IrOX electrodeposition process.

1.2 Problem Statement

Measuring surface pH or pH in metal/solution interface is indispensable to understand accurate corrosion mechanism. Surface pH measurement of corroding carbon steel cannot be measured by conventional pH sensor. Thus, a requirement of a new pH sensor design is necessary for this purpose. IrO_x as pH sensitive material is a perfect candidate for this aim due to its significant properties.

Researchers in oil and gas industries are interested to know and monitor reactions which happen under a deposit. Lack of proper facility for doing pH measurement under deposit is commonly highlighted. A proper design of experiment is necessary to be designed for surface pH measurement of a corroding metal under deposit.

1.3 Research Objectives

In order to study and monitor surface pH of corroding metal surface, a stable and accurate pH sensor is required. To understand CO₂ corrosion mechanism, several factors should be considered which one of most important of them is surface pH measurement. Regarding to this matter, an attempt has been done to study and find a design and method for fabrication of a novel surface pH sensor which bring following objectives:

- The capability of electrodeposition of IrO_x on stainless steel by cyclic voltammetry method.
- To statistically investigate effect of various factors on electrodeposition of IrO_x film.
- Investigation of an effective design and deployment of a simple and applicable surface pH probe for direct measurement of in-situ surface pH at a corroding metal surface.
- Using proposed pH sensor probe for measuring and monitoring of surface pH of corroding metal under deposit.

1.4 Scope of Study

The research focuses on design and fabrication of a novel probe design for surface pH measurement and pH measurement under deposit. Cyclic voltammetry approach as electrodeposition method was used for forming of IrO_x pH sensitive film on stainless steel substrate.

Statistical tools, RSM in conjunction with CCD, were used for investigation of different variable factors on properties of IrO_x film.

1.5 Organization of the Thesis

This thesis consists of four chapters. Chapter 1 describes the research background related to significant role of surface pH monitoring in corrosion understanding and monitoring.

Chapter 2 contains literature reviews on different fabrication method, electrodeposition, iridium oxide pH sensor, surface pH measurement, CO₂ corrosion and design of experiment.

Chapter 3 describes the details on the methodology, general principles underlying the operation of the characterization tools, and experimental setup, consists of sample preparations, electrodeposition solution preparation. This chapter also proposed pH sensor design for surface pH measurement of corroding carbon steel.

Chapter 4 is divided to four parts. First part describes electrodeposition of iridium oxide on stainless steel, consisting of characterization of electrodeposition solution and investigation of IrO_x film growing on stainless steel substrate. Second part discuss about statistical investigation of iridium oxide electrodeposition on stainless steel by means of RSM. The effects of three different variable factors of electrodeposition were studied on electrodeposited IrO_x film properties in this part. Third part of this chapter is dedicated to surface pH measurement of corroding carbon

steel in CO₂-Containing 3% NaCl solution. In last part of this chapter, 5 mm deposit layer was used to simulate CO₂ corrosion of carbon steel under deposit.

Finally, Chapter 5 remarks the conclusion and recommendations. This chapter covers summarize of experiment's finding and recommendation for future work.

CHAPTER 2

BACKGROUND AND LITERATURE REVIEW

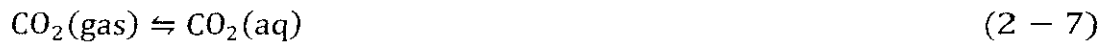
2.1 Chapter Overview

Iridium oxide pH sensor can be used in many applications. It is a robust pH sensor which can be made in different shape by using electrodeposition method. Investigation of electrochemical reaction on the metal/ liquid interface is an attractive topic for the researcher which needs high-tech and special tools. One of the most interesting fields is corrosion monitoring, which needs understanding of electrochemical and chemical reaction on the metal surface. These reactions on the metal surface can change nature of metal/liquid interface and decrease or increase the surface pH. The main idea of this thesis is to measure and monitor pH changes of corroding carbon steel by a novel IrO₂ pH probe design. Methods for fabrication and characterization of IrO₂ pH sensor are reviewed from both theoretical and experimental aspects. Moreover, surface pH measurement has been considered as an interesting topic recently.

2.2 CO₂ corrosion

CO₂ corrosion accounts for 55% of corrosion damage in oil and gas industries [10]. Sweet corrosion occurring in CO₂-containing solution is affected by various parameters such as pH, temperature, and CO₂ partial pressure [11]. CO₂ gas hydrates in water, creating carbonic acid that can cause internal corrosion in the petroleum pipeline [12]. Generally, the following reactions are observed in CO₂ corrosion: (a) four chemical reactions occurring in a solution and (b) four electrochemical reactions — one anodic and three cathodic — occurring on metal surfaces [12-15]:

a) Chemical reactions:



b) Electrochemical reactions:



Cathodic Reactions:



FeCO_3 , an insoluble corrosion product, can be formed at this stage, as follows:



Under certain conditions, the films can be very protective and offer great protection from corrosion by forming a barrier through blocking some parts of the metal surface which indirectly reduce the corrosion rate.

Many researchers had investigated parameters influencing CO_2 corrosion [3,16-18]. Notable parameters affecting CO_2 corrosion includes pH, temperature, CO_2 partial pressure, flow rate and presence of corrosion products. In this study we investigated changes of surface pH at corroding metal versus various temperature.

The temperature strongly influences the CO₂ corrosion due to its effect on the rate of scale formation. Besides, it also has correlation with corrosion rate. Formation of protective film will reduce the corrosion rate by act as a diffusion barrier on metal surface [2]. At lower temperatures (< 60°C) the solubility of FeCO₃ is high. This situation will cause the precipitation rate is slow and thus the protective films will not form unless the pH is increased. On the other hand, at higher temperatures (> 60°C) the solubility of FeCO₃ is reduced and lead the precipitation rate become much faster. Thus, allowing the formation of protective iron carbonate films to occur. Under this condition, dense crystalline films are formed which often give good protection. The existence of film will influence the corrosion rate. It was concluded that the surface coverage by the iron carbonate film was increased by increasing the temperature. This is due to the higher precipitation rate was occurred [19,20].

Precipitation of FeCO₃ deposits occurs when the pH of the CO₂-containing solution is sufficiently high [5]. Regarding the electrochemical reaction, pH on metal surfaces varies from that in bulk solution. The result obtained from localized pH measurements can be used for real-time corrosion monitoring because corrosion is a pH-dependent phenomenon. Meanwhile, commercial pH electrodes cannot monitor pH changes on metal surfaces. Therefore, a novel pH electrode design is needed to aid scientists in monitoring reactions occurring in metal-solution interfaces.

Under deposit corrosion is one of significant reason for main damage of boiler tubes [21], oil and gas pipelines [22,23], oil and gas production systems [24].

Nyborg *et al.* [25] investigated under deposit corrosion by developing a new test method. They used three carbon steel working electrode in conjunction with a reference electrode which were mounted together in an assembly as shown in figure 2.1. Sand was used as deposit to cover two of the specimens. The galvanic current and potential difference between sand covered and not covered specimens were

determined. They measured the corrosion rate of all three specimens by LPR measurements, while the galvanic current is measured by zero resistance ammetry.

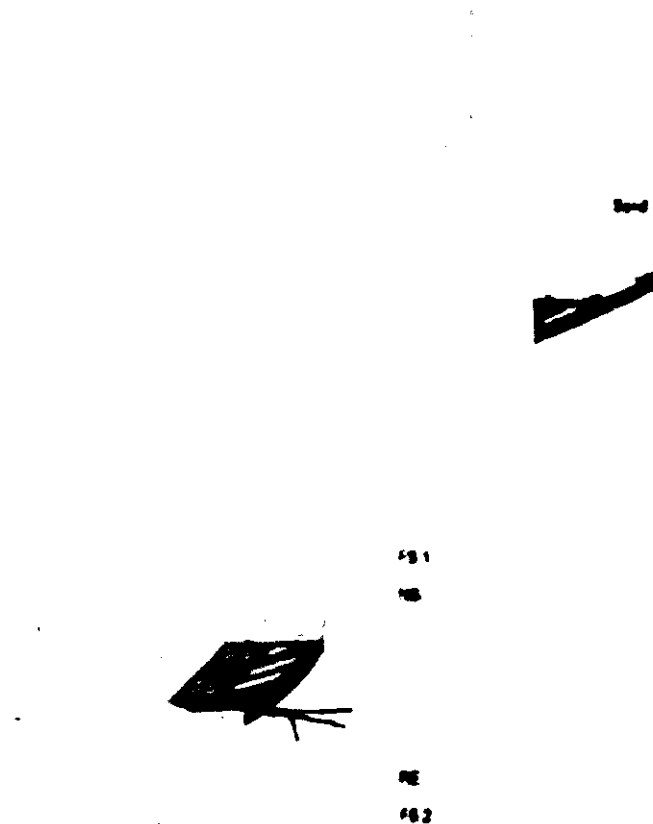


Figure 2.1: Sketch of the test specimens mounted in the specimen holder; FS1 and FS2: specimens will be covered with sand deposit. NS: specimen will be directly exposed to the brine, RE: A carbon steel wire can be used as pseudo-reference electrode [25].

Cathodic reaction and the reduced mass transport in corroding steel surface covered by deposit can cause pH increasing which is favour for precipitation of FeCO_3 on the steel surface. Created FeCO_3 film may decrease overall corrosion rate if cover metal surface. otherwise discontinuous film may increase corrosion rate due to local galvanic corrosion which result in pitting attacks [25].

Internal pitting corrosion of X80 pipeline steel under deposited sand bed in CO₂-saturated solutions was investigated by Huibin *et al.* [26]. They used a Pt-Ir microelectrode to map the current of the specimen surface. They found that corrosion pits could begin and grow on the steel surface under a layer of sands. Corrosion pits keep growing with the increase of test time which caused a drop of local impedance and an increase of the peak current density. Besides, the increase of chloride concentration in the solution and the solution flow velocity is another reason of the corrosion pits growing.

2.3 Surface pH measurement

The mechanisms mentioned above still have some unproven assumption; in CO₂ corrosion the local pH at a corroding steel surface will be greater than that of the bulk, especially the pH under a FeCO₃ film. In fact it can be expected that this pH will be sufficiently high to create passivation of the mild steel surface.

Our main motivation in this thesis is to display the outcomes of experiments that were conducted to precisely examine this hypothesis and complete the suggested mechanism of CO₂ corrosion.

It is a fact that local surface chemistry conditions could be very different than those in the bulk and get critical when chemical reactions happen on an interface [4]. Surface pH is recognized as a significant local parameter that affects electrochemical reaction mechanisms and rates [5,27]. Mathematical modelling which is built on thermodynamic, kinetic and transport theories, has facilitated in the quantification of surface pH conditions [28]. Though, a very little has been accomplished regarding of direct surface pH estimation at a corroding surface because of troubles with investigation design, manufacturing and operation.

Surface pH can be measured directly as reported by several researchers. The pH microelectrode, a quiet generally utilized direct surface pH measurement device, specifically intended for surface pH measurement [29-34]. Microtips, commonly ranging from 1 to 20 μ m in diameter [35], have been created as the sensing components of microelectrode pH probes; these have been applied in corrosion surface pH measurement [36,37] along with dissemination layer pH profiling. An important deficiency of this design is that it meddles with the mass transfer boundary layers close to the solid surface.

Romankiw [27,38] has come up with one more direct surface pH probe design for electrolysis systems. The model design comprises of an even sensor pH probe with a tip which is stuck to a metal mesh. Surface pH can be checked during the corrosion of the mesh. This surface pH probe design was additionally adapted for rotating [39-41] or fixed metal meshes [5,42]. Specific provisions were accounted for surface pH measurement during jet impingement tests [43], electrodeposition [42,44] and electrochemical reduction reactions [45].

Diaz *et al.* [44] measured local pH during ZnFe anomalous electrodeposition. Their proposed design for measuring surface pH during electrodeposition process is shown in Figure 2.10. They used a Pt rotating disc electrode as substrate combined with a commercial pH electrode as shown in Figure 2.2.

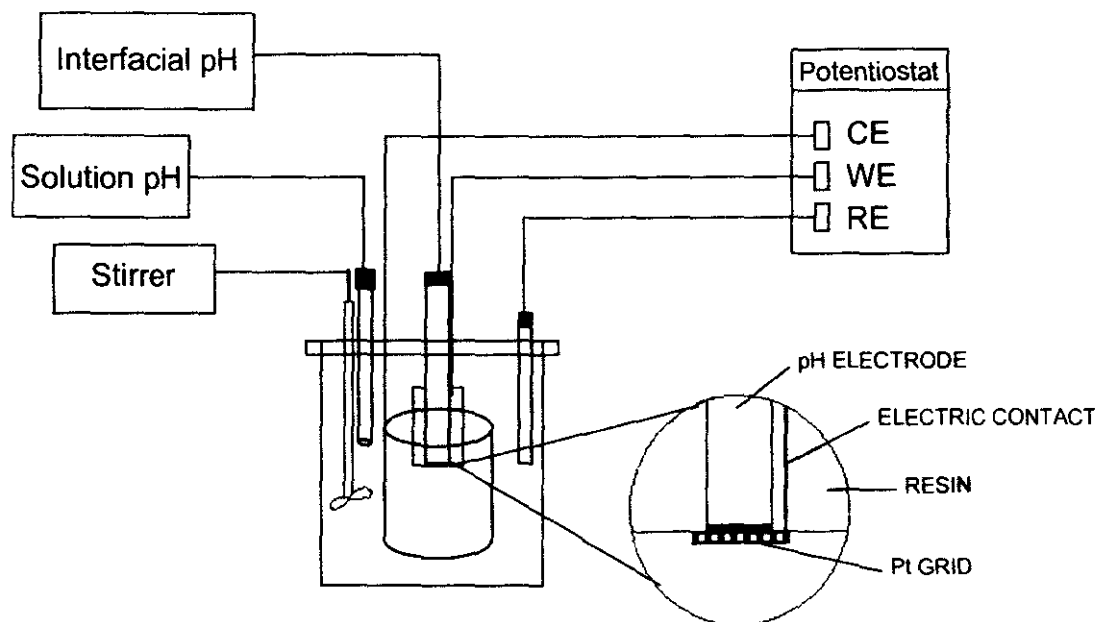


Figure 2.2: Interfacial pH measurement setup. (CE, counter electrode; WE, working electrode; RE, reference electrode.) [44]

Some surface pH probe designs have been formerly stated for indirect pH estimations throughout the electrolysis procedures. It is a pH-mapping [46,47] method in which a semiconductor contacts the solution and reacts to the pH owing to exhaustion of its protecting layer. The subsequent capacitance change can be documented with a generated photocurrent. This design is comparatively complicated and includes components which are not simple or inexpensive to get or produced. Another indirect technique is surface pH measurement by means of a rotating ring electrode [48]. This method is dependent upon the pH potential relation as described by the Nernst equation and does not offer itself simply to extend to distinctive corroding systems.

The objective of the present undertaking relied on a suitable design and employment of a simple and adaptable surface pH probe for direct measurement of surface pH and pH under deposit at a corroding surface.

2.4 Electrodeposition theory

Electrochemical deposition, or electrodeposition for short, is a technique used for depositing material onto a conducting surface of a substrate from a solution containing ionic species. This fabrication method is usually employed to create thin films of material on the surface of a substrate to enhance its external properties such as to increase abrasion resistance, corrosion protection, improve decorative quality, or simply to deposit a layer which is part of a more complicated device.

Electrodeposition was initially used to create decorative and protective coatings by Luigi Brugnatelli in 1805 [49].

As shown in Figure 2.3, the working electrode is the object which will be plated, the counter electrode is used to complete the electronic circuit, and the reference electrode is used as a fixed reference point for the potentiostat. An electric field is then applied across the working electrode in such a way as to give electrons to the ions in solution so that they form uncharged elements or compounds which prefer to adhere to the surface of the working electrode rather than remain dissolved in solution. The strength of the electric field or the potential is measured versus the reference electrode, but the actual current flows between the working and counter electrodes.

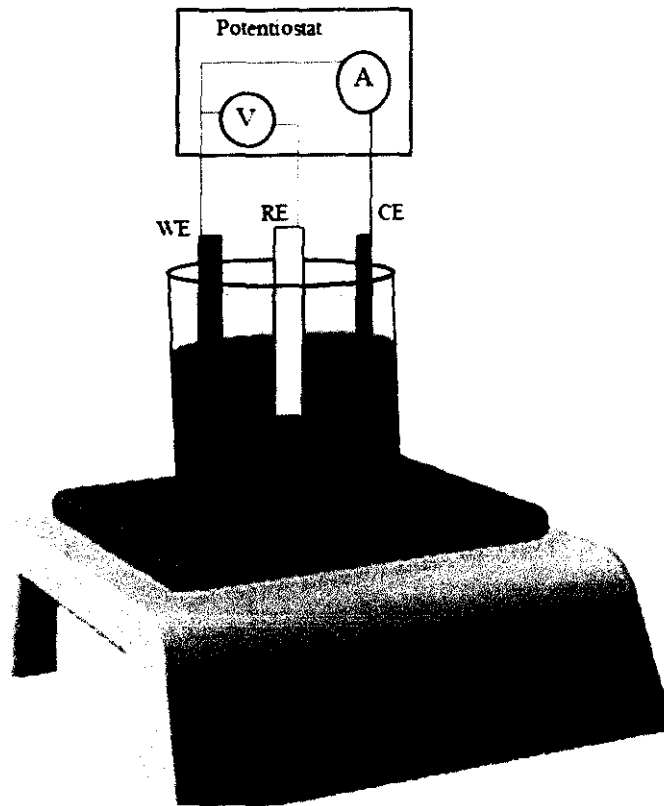


Figure2.3: Schematic of an electrodeposition cell; CE (Counter electrode), RE (Reference electrode), WE (working electrode)

The electrolyte is an ionic conductor, where chemical species containing the metal of interest are dissolved into a suitable solvent or brought to the liquid state to form a molten salt. The solvent is most often water, but recently various organic compounds and other ionic liquids are being used for selected electroplating processes.

As shown in Figure 2.4, in the process of metal electrodeposition metal ions are reduced at the substrate, forming adsorbed atoms that diffuse on the substrate surface; these adsorbed atoms will eventually contact other adatoms, forming atomic clusters that may be stable or unstable. Unstable clusters will eventually disappear, while stable clusters will be able to grow, finally forming the film [49,50].

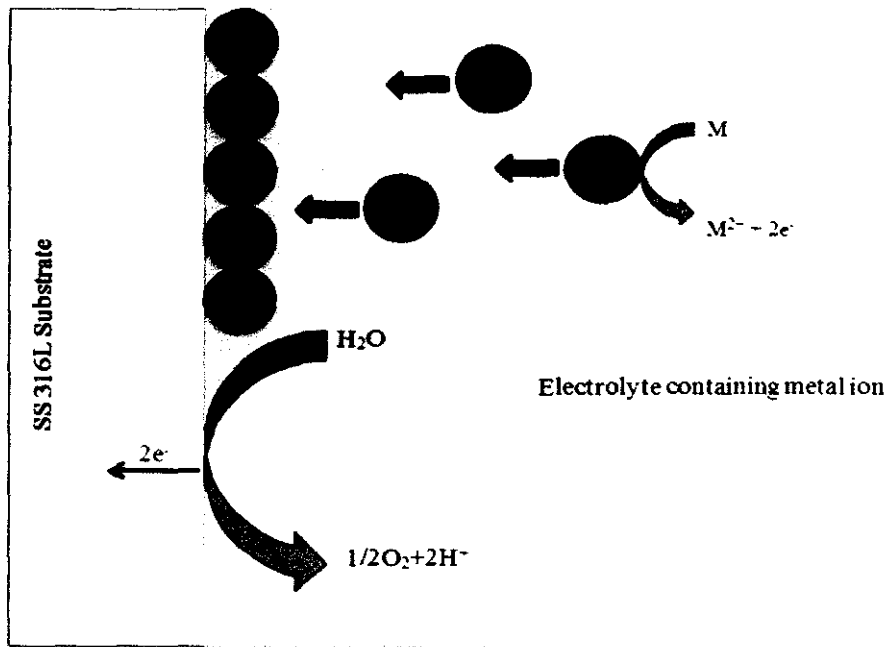


Figure 2.4: Graphical diagram of an electrodeposition process

Charge transfer of electrodeposition process can be applied by application of an electrical potential from a potentiostat (power source) as depicted in Figure 2.1. This applied potential (E) forces electrons in the Fermi level of the electrode, allowing for the flow of electrons from the electrode to a species in solution or vice versa [49].

It is accepted to assume that nucleation and crystal growth are consecutive steps of the phase transition; however, from the phenomenological standpoint these steps cannot strictly be separated: in fact, the two processes coincide. For example, if we consider the critical nucleus, the addition of the last atomic species to a subcritical cluster is assigned to a nucleation process, while the identical addition of the next adatom would constitute crystal growth [50].

2.4.1 Nernst Equation

In its usual form, the Nernst equation is a thermodynamic relationship between the equilibrium potential and reactant concentrations at the electrode surface. Since

the Nernst equation is a result of thermodynamics, not kinetics, it only applies when the system is at equilibrium. The equation can be derived from three basic expressions in thermodynamics. The first is the chemical equilibrium expression for the Gibbs free energy:

$$\Delta G = \Delta G^0 + RT \ln Q = \Delta G^0 + RT \ln \frac{a_R}{a_O} \quad (2 - 1)$$

Where Q is the equilibrium constant and a_i is the activity of species i. The second and third relate the Gibbs free energy to the cell potential:

$$\Delta G = -nFE \quad (2 - 2)$$

$$\Delta G^0 = -nFE^0 \quad (2 - 3)$$

In these expressions, ΔG is the Gibbs free energy, ΔG^0 is the standard Gibbs free energy, E is the equilibrium cell potential, and E^0 is the standard equilibrium cell potential. The Nernst equation can be derived simply by equating the first two expressions and substituting in the third. For a reversible redox reaction $O + ne^- \rightleftharpoons R$ where O is the oxidized materials and R is the reduced materials, the Nernst equation can therefore be written as:

$$E = E^0 + \frac{RT}{nF} \ln \frac{a_O}{a_R} = E^0 + \frac{RT}{nF} \ln \frac{Y_O C_O}{Y_R C_R} \quad (2 - 4)$$

where Y_i is the activity coefficient of species i. As one would expect, C_O and C_R are the surface concentrations of O and R respectively. Since it is difficult work with activity coefficients, the equation is usually written as:

$$E = E^{0'} + \frac{RT}{nF} \ln \frac{C_O}{C_R} \quad (2 - 5)$$

where $E^{0'}$ is the formal potential and related to E^0 . This conveniently does away with the need to explicitly calculate activity coefficients. The formal potential can also be defined as the measured potential of the working electrode vs a normal hydrogen electrode (NHE) when the concentrations of O and R are equal. This corresponds to the potential at which equal concentrations of O and R will lead to no net reaction. In an electrochemical cell, this also corresponds to no net current. The formal potentials of many chemical reactions have been measured and tabulated in standard references. These tables are a valuable resource when investigating electrochemical phenomena. The purpose and importance of using a reference electrode like the NHE will be discussed in the next chapter. With the Nernst equation, one can calculate the equilibrium concentration ratio for a given applied potential. One can also do the opposite and calculate the potential that will develop at equilibrium if the concentrations are set to known values. This can be extremely useful when trying to interpret certain electrochemical measurements. However, it is important to remember that the Nernst equation only applies when the system is at equilibrium. A truly reversible process will always satisfy the Nernst equation. But if the reactions are slow or the potential is changed rapidly, thermodynamics may not apply and kinetic relationships must be used instead [51,52].

2.5 Cyclic Voltammetry

Cyclic voltammetry (CV) is a three-electrode measurement which measure the potential of a working electrode regarding to a reference electrode. CV is swept cyclically at a constant rate between two potential limits while allowing current to flow between the working electrode and a counter electrode. The potential provides the driving force for reactions at the working electrode, whereas the current is proportional to the rate of these reactions. CV identifies the presence of electrochemical reactions and provides information on the reversibility of the

reactions, the quantity of electro-active material on the electrode, and the stability of the electrode.

The peaks seen in a cyclic voltammogram result from a combination of chemical reaction and mass transport processes. Figure 2.3 is a simple example voltammogram marked with several important features [14].

It corresponds to an electrode that can undergo a single perfectly reversible reaction $R \rightleftharpoons O + ne^-$, where O is the oxidized species and R is the reduced species. As described earlier, positive current corresponds to the reaction moving from left to right, since electrons are produced in the forward reaction and flow out of the working electrode. Electrons flowing out means that a positive current is flowing in. Negative current corresponds to the reaction moving from right to left. As the voltage is swept from V_{\min} to V_{\max} and back again, the current follows the path shown in Figure 2.5, moving in the direction of the arrows. Starting near A, the current increases more and more rapidly as it approaches the formal potential E_0 . Near B, the rise in current begins to slow down, reaching a peak at C. The current continues to decay as it goes through region D. Eventually, the potential reaches V_{\max} at point E, the sweep direction reverses, and similar behavior is seen for the negative direction [53]. Cyclic voltammetry is covered extensively in *Electrochemical Methods* by Bard and Faulkner [54,55]. Another good introduction to the technique was published in *The Journal of Chemical Education* [56].

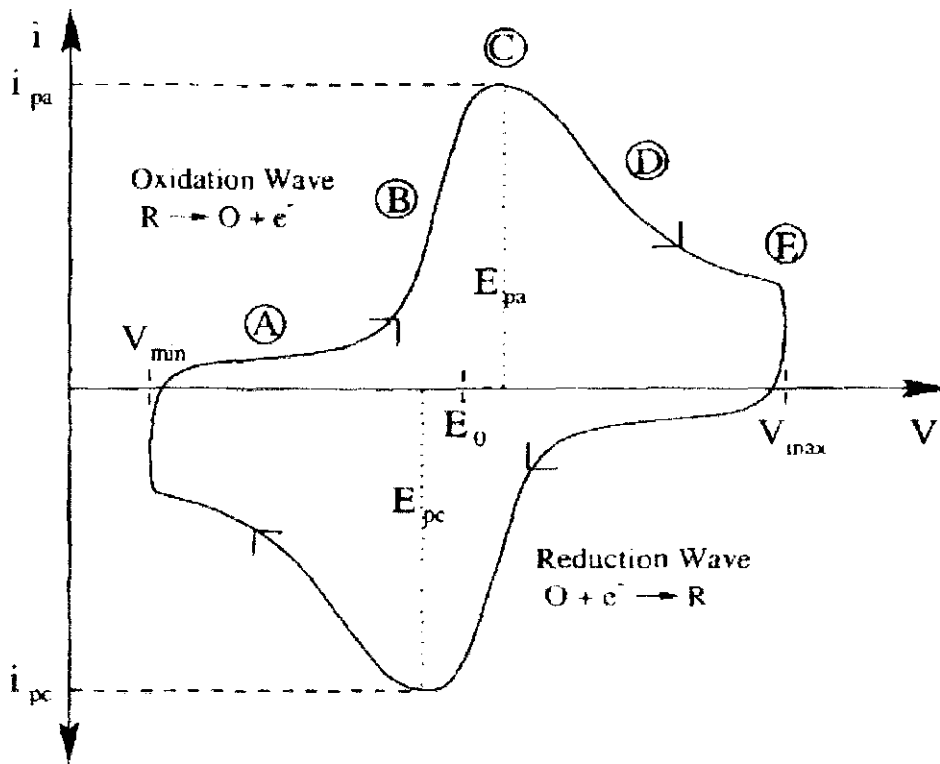


Figure 2.5: An example voltammogram with relevant features marked [14].

2.6 Open Circuit Potential

The open circuit potential (OCP) is the potential of the working electrode regarding to reference electrode when there is no current applied. The experiments based on the OCP measurement are known as potentiometric experiments. OCP measurement has many applications, although it is very simple. One of important application of OCP is a titration test which is based on the Nernst equation.

OCP in the Nernst equation relates the concentration of electroactive species at the electrode surface (C_s) to the potential at that electrode (E) regarding to the oxidation / reduction reaction of $O + e^- \rightleftharpoons R$.

$$E = E^{0'} + \frac{RT}{nF} \ln \frac{C_O}{C_R} \quad (2 - 5)$$

Where,

$E^{0'}$: The formal redox potential of the electron transfer reaction.

E: Potential measured between the working electrode and the reference electrode.

In OCP measurement the auxiliary electrode is disconnected for potentiometric measurements on the epsilon. The working electrode is selected such that its potential is sensitive to the concentration of the analyte in solution (e.g., a pH sensor), and the reference electrode (e.g., the Ag/AgCl electrode) supplies a stable potential for the measurement of the potential of the working electrode. Also, OCP technique can be used for investigation of the open circuit potential of a battery, and the corrosion potential of a corroding sample [57].

2.7 Electrochemical Impedance Spectroscopy

Electrochemical impedance spectroscopy (EIS) is the most commonly used technique for electrode modeling and characterization. It also has an important place in its history. Randles used a form of the technique to develop the model that bears his name [58]. Since then, a great deal of work has been done to refine the equipment and analysis tools needed to use it. EIS is very well suited for both model discovery and parameter fitting [59,60]. Unlike most electrochemical methods, the results of an EIS experiment can be interpreted almost completely in the electrical domain. Interpreting a spectrum in any other domain is in fact quite difficult.

The greatest strength and greatest weakness of the technique is that one can develop circuit models that completely encapsulate the observed behavior without

worrying about what physical processes are actually being represented. This section will describe the basic theory behind EIS measurements, explain some of the features commonly encountered in spectra, and provide examples for iridium oxide, gold, and platinum.

In an EIS experiment, an electrode is biased at some potential, usually its open circuit potential, and a small sinusoidal potential variation is applied. The magnitude and phase of the resulting current variation is measured and recorded. This is repeated over a range of frequencies, building up a complete spectrum. In more advanced experiments, the bias potential is also varied. The range of the bias is often quite limited, since holding the potential too far from its open circuit value can damage the electrode over time.

Impedance spectroscopy is in some ways the polar opposite of cyclic voltammetry. Both are controlled potential techniques, but whereas cyclic voltammetry is large-signal and low-frequency, EIS is small-signal and high-frequency. As a result, they provide completely different types of information about an electrode. Cyclic voltammetry focuses on the specifics of mass transport and chemical reactions, while impedance spectroscopy abstracts these away and focuses more on the electrical domain.

As a small signal technique, it is unable to directly model large signal electrode processes. The large signal predictions of EIS are often inaccurate [53,61]. There are several reasons for this. One reason is that electrode behavior tends to be highly nonlinear. Another reason is that simple circuit models rarely capture all of the behavior present in the spectrum. The fits are at best rough approximations of what is really there. Finally, most fitting is done with a global measure of accuracy, but most stimulation waveforms have a very limited set of frequency components. A good global fit often means poor local fits in some areas. Under limited circumstances, it is

possible for the small signal results to accurately predict the large signal behavior, but this is the exception not the rule.

2.8 Potentiometric pH sensor

pH measurements are proper means for controlling a wide range of processes in different industries such as petroleum, food, environmental, and clinical. Therefore, an accurate and reliable pH measurement is very important [62,63].

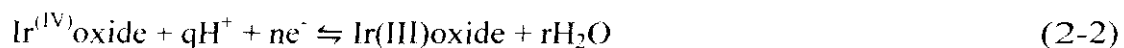
In potentiometric pH sensor; the recognition of hydrogen ion is done by the pH electrode, which is coupled with the reference electrode to complete the electrical circuit; and the sensor measures the potential difference between these two electrodes. As the name indicates the electrode is “selective for one ion, in preference to other ions”. The glass electrode is known as mother of all ion-selective electrodes which is sensitive to hydrogen ion concentration (pH). The glass pH sensor is the oldest electrochemical sensors which have some disadvantages such as lack of stability in alkaline and fluoridric acid solutions and their mechanical fragility [34,63].

New techniques for measuring pH include optical fiber-based pH sensor [34,64], mass-sensitive pH sensor [65], Conducting polymer pH sensors [32,33], Nano-constructed cantilever-based pH sensor [66], ion-sensitive field effect transistors (ISFET) -based pH sensor [67], pH-image sensor [68,69], and metal oxide pH sensor [70].

2.9 Iridium oxide pH sensor

The past decades, IrO_x became a superior material for reference electrode [71,72] and pH measurements in various fields such as biological media [73,74], food-

industry [75], nuclear field [76,77], and oil and gas industry [29,78,79]. Iridium oxide can provide a rapid and stable response in different media because of its high conductivity and low temperature coefficient. Potentiometric response of the Iridium to pH is a function of transition effect between two states Ir(III) and Ir(IV) oxide, which can be shown as follows [80]:



In 1996, Roc *et al.* [81] measured dissolved oxygen, pH, and ion currents on steel corroded surface using three closely spaced microelectrodes. They proposed a real time mapping of the pH distribution on the steel corroded surface.

Two properties of biocompatibility and corrosion resistance of iridium oxide electrodes are noticeable [67]. This fact made iridium oxide electrodes as a potential candidate for microbial induced corrosion investigation. A crystal structure of stoichiometric iridium oxide is shown in Figure 2.6.

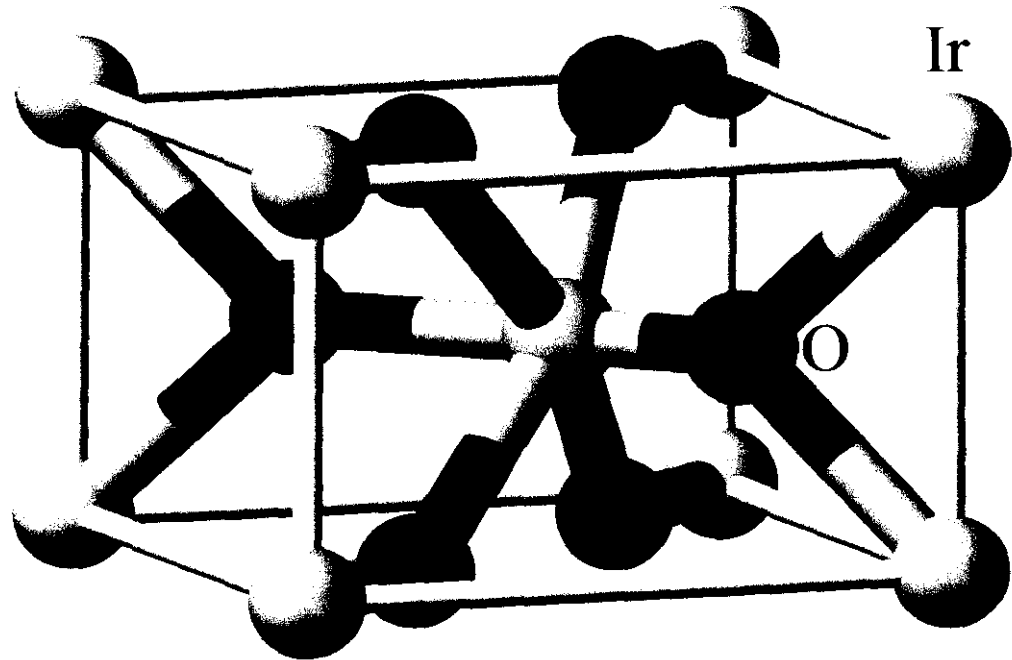
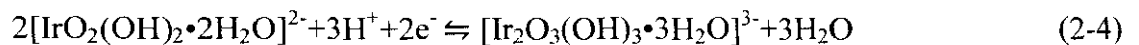


Figure 2.6: Crystal structure of IrO₂[75].

The difference between IrO_x pH sensor and traditional glass pH sensor is related to their mechanism for pH measuring. Glass pH electrode depends on solution-phase activities of the relevant electrode whereas IrO_x is dependent on H⁺ activity and oxidation state of IrO_x. The proposed reaction at the anhydrous IrO_x electrode shown as [82]:



And for a hydrous IrO_x electrode as follows reaction:



Hence the Nernstian response slopes for electrodes prepared by different methods can range between 59 and 88.5 mV/pH. Moreover, proposed Nernst equations are as follows:

$$E = E^0 - 2.3RT/2F \log [Ir_2O_3]/[IrO_2]^2[H^+]^2 \quad (2-5)$$

And

$$E = E^0 - 2.3RT/2F \log [Ir_2O_3]/[IrO_2]^2[H^+]^3 \quad (2-6)$$

It is proposed that any variation in the Ir^{3+}/Ir^{4+} ratio, IrO_x electrode preparation, IrO_x electrode's age, and deliberate exposure to redox agents such as $Fe(CN)_6^{3-/4-}$ have been shown to affect the pH response [82,83]. Another model for hydrous and anhydrous iridium oxide was proposed by Burke *et al.* [84] as shown in Figure 2.7 and 2.8 which discussed this high response in terms of the acid base properties of the films.

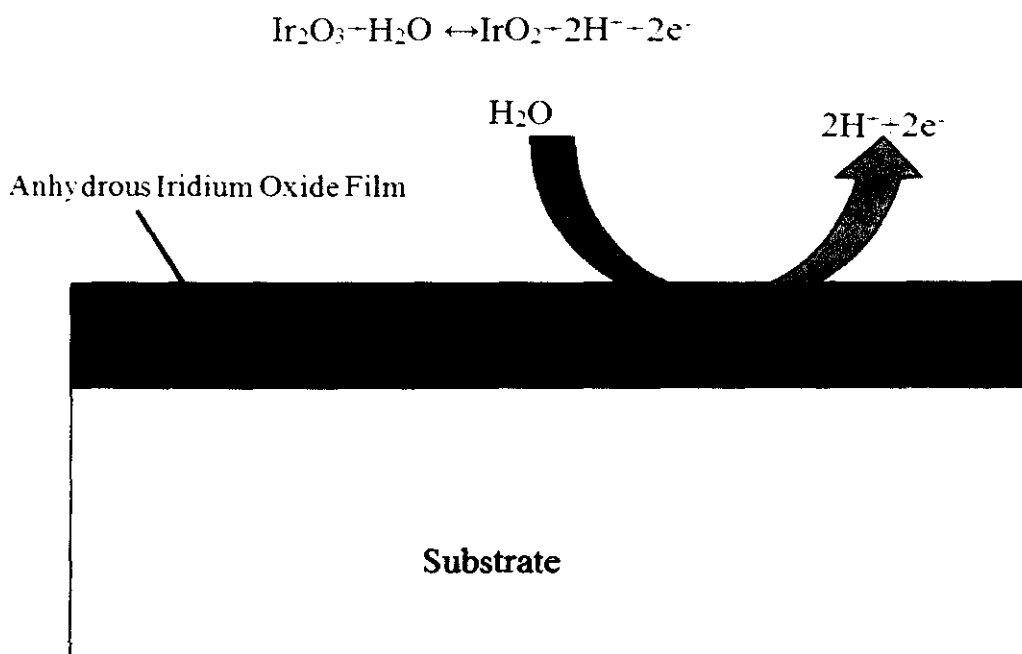


Figure 2.7: The proposed reaction at the anhydrous IrO_x electrode

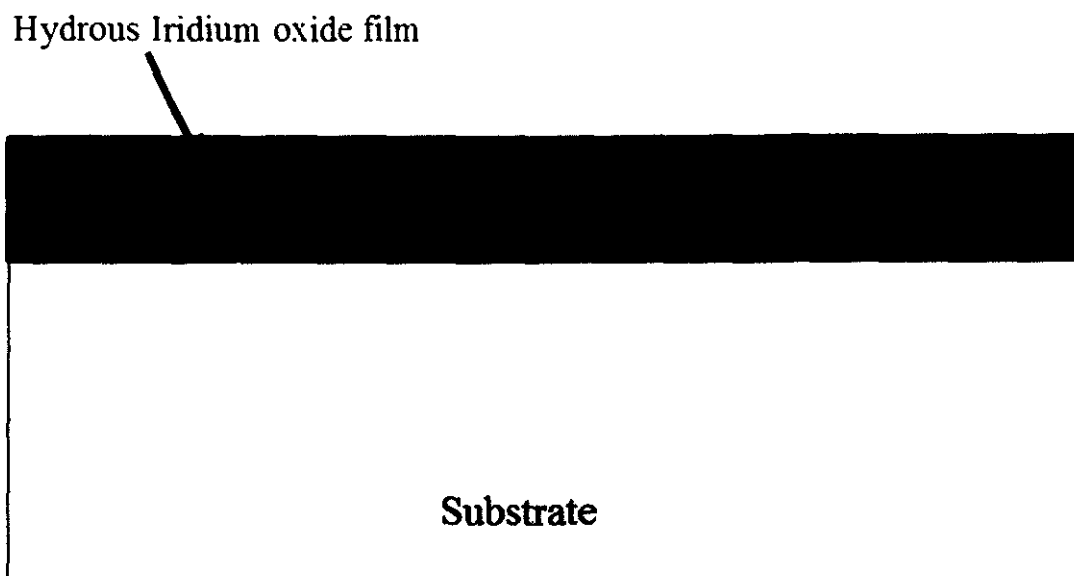


Figure 2.8: The proposed reaction at the hydrous IrO_x electrode

The schematic structure of a hydrated iridium oxide is shown in Figure 2.9.

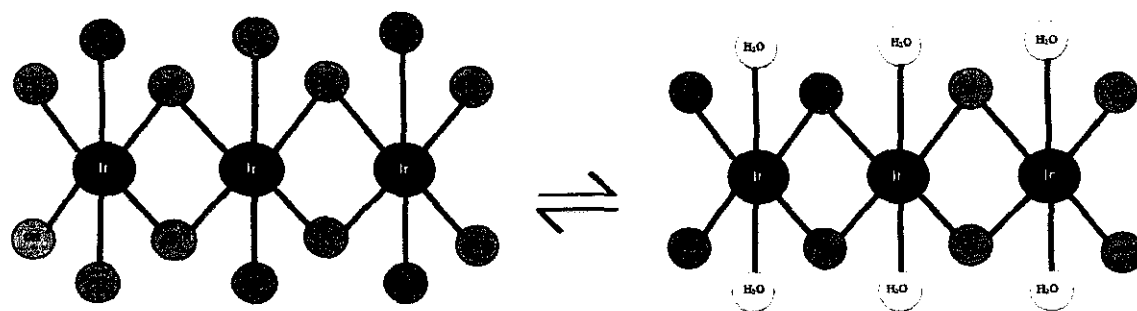


Figure 2.9: The schematic structure of hydrous IrO_x electrode

IrO_x films always are a combination of hydrous and anhydrous iridium oxides, in a ratio that significantly depends on the nature of the iridium oxides. Even a thermally prepared IrO_x film will contain some hydrated material caused by surface hydrolysis.

AIROFs, even though intensely hydrated, have a thin anhydrous oxide layer at the interface between the hydrated oxide and the parent metal [85].

Cathodic storage charge capacities (CSC_C) of the test samples will be calculated by integrating the cathodic area in cyclic voltammograms. The CSC_C data generally be used in the characterization of neural stimulation electrodes [32,33,65], although in some research work CSC_C calculated like this is approximately equal to the amount of Ir^{4+} on the substrate in thin electrodeposited layers. The calculated area above-mentioned is presented by the CV of an EIROF on Au in Figure 2.10 [66].

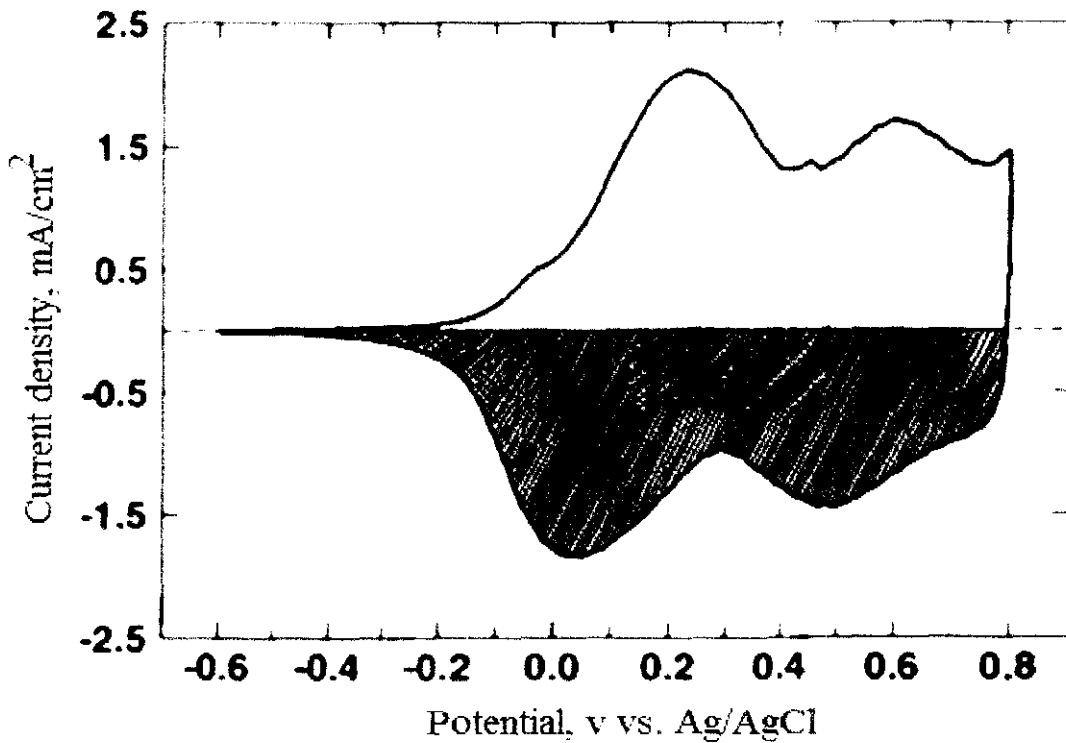


Figure 2.10: CV of iridium oxide in PBS at 50 mV/s showing the area used to calculate the CSC of the film [66].

2.9.1 Iridium oxide pH sensor fabrication method

It is clear that preparation methods play the main role in the pH response of the iridium oxide-based electrodes. Anhydrous iridium oxides were achieved by thermal oxidation or sputtering methods, which showed a pH response of 59 mV/pH, whereas iridium oxides fabricated by electrochemical technique are predominantly hydrated iridium oxides such as $\text{IrO}_2 \cdot 4\text{H}_2\text{O}$, $\text{Ir}(\text{OH})_4 \cdot 2\text{H}_2\text{O}$, which present a super-Nernstian response 90 mV/pH unit [86].

2.9.1.1 Sol-gel processes

Sol-gel method was used for a fabricated IrO_2 pH sensor on a flexible substrate [87,88]. Three different groups of pH sensors fabricated by the sol-gel process indicated similar near super-Nernstian response, good reversibility, and similar response times, which show better reproducibility and repeatability in this fabrication technique.

The sol-gel technique is well-known as a cheap method for advance material fabrication. Da Silva *et al.* [62] used a polymeric precursor approach to fabricate a low-cost pH sensor with substitution of IrO_x by TiO_2 . The best result was related to 70 % (IrO_x)-30% (TiO_2).

The challenge in sol-gel method is related to the drying process, which led to creating cracks in iridium oxide film due to its dehydration. This phenomenon can be decreased by using proper additives.

2.9.1.2 Electrochemical or thermal oxidation of iridium and iridium salts

Song *et al.* [67] fabricated an Ir/ IrO_2 pH sensor by using the potentiodynamically cycling method on an Ir electrode in 0.5 M H_2SO_4 aqueous solution at a 50 mV/s scan

rate with different exposure time (2, 4, 8, and 24 hr). According to Figure 2.11, they found that pH sensor fabricated by 2-hr and 4-hr treatment showed a more drift than those fabricated by 8-hr and 24-hr treatment.

Song *et al.* investigated the effect of bisulfite and thiosulfate ions on the Ir/IrO₂ pH sensor. The calibration of pH sensor significantly changed when exposed in solution test containing aforementioned ions.

The thermal oxidation iridium oxide film (TOIROF) proposes the possibility of optimizing electrodes for both charge injection and mechanical properties. The technology utilizes the high charge capacity of TOIROF without the expense of pure Ir metal or difficulty in forming pure Ir into shapes required for stimulation electrodes. Applications requiring electrodes and leads with high mechanical and flexural strength, such as intramuscular stimulation, need not be restricted to using large surface area electrodes because of the poor charge of the metal. However, formation of TIROF requires high temperatures of at least 400-500 °C [89].

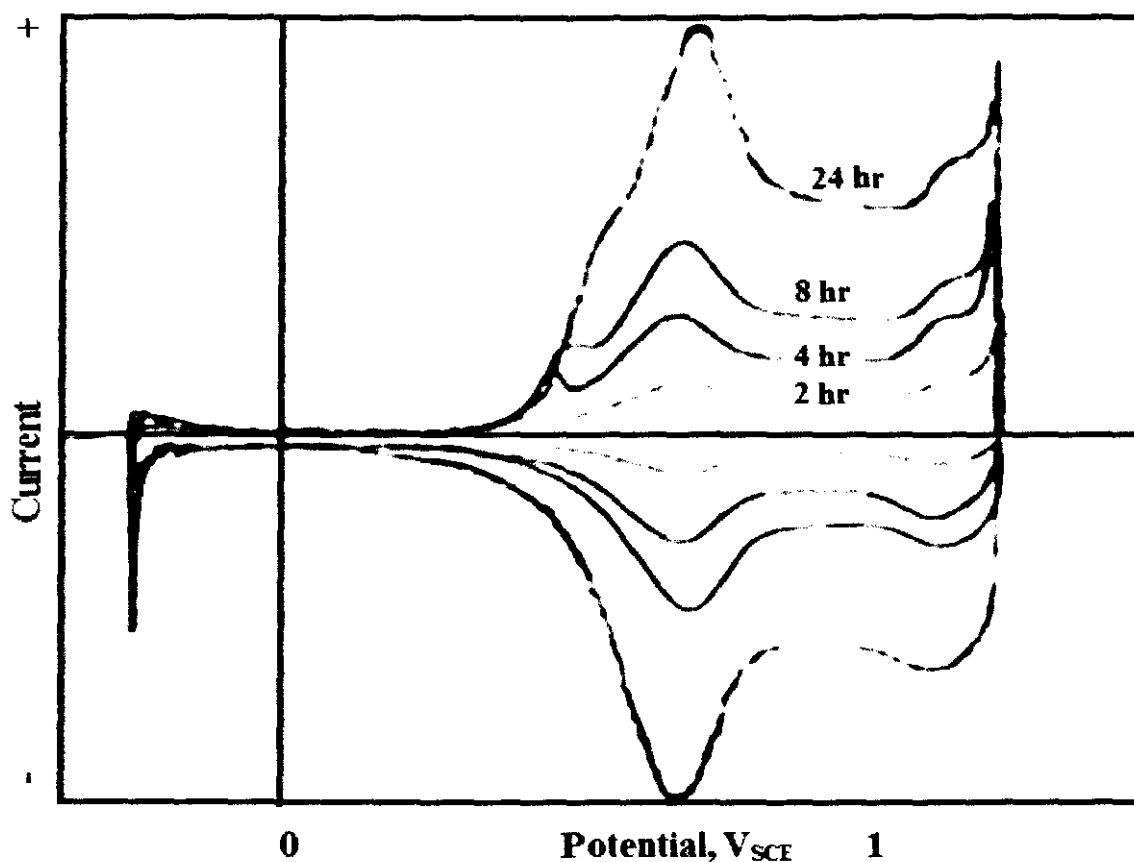


Figure 2.11: Stacked voltammograms of iridium oxide potentiodynamically cycled between $-0.25 V_{SCE}$ and $1.27 V_{SCE}$ at 50 mV/s for 2, 4, 8, and 24 hr in deaerated $0.5 \text{ M H}_2\text{SO}_4$ aqueous solution [67].

2.9.1.3 Sputtering

Sputtering method was used in most IrO_2 film fabrication for neural stimulation electrodes [65,68-70]. Kreider [77] in 1991 used sputtered iridium oxide as pH-sensing electrodes in high-temperature high-pressure saline solutions. Sputtered iridium oxide films were fabricated in mixed Argon and Oxygen environment in a 1:1 ratio at a total pressure of $\sim 0.40 \text{ Pa}$. The thickness of $0.5\text{-}0.7 \mu\text{m}$ thick depositions was made primarily on alumina circuit board at $30\text{-}40 \text{ }^\circ\text{C}$ and at $240 \text{ }^\circ\text{C}$. He found that with

increasing exposure time in saline solutions, pH sensitivity decreased at high temperature. The main disadvantage of sputtering method is the cost of its target material.

2.9.1.4 Anodic or cathodic electrodeposition

Yamanaka [90] proposed electrodeposition of iridium oxide for the first time for fabrication of display device. His suggested solution was based on a complex of IrCl_4 and oxalate component. After that a lot of researcher improved this solution or used it as described by Yamanaka [33,91-93].

Ryynänen *et al.* for first time used atomic layer deposition (ALD) for iridium oxide (IrO_x) fabrication as the pH sensitive layer with an average sensitivity of -67 mV/pH at 22 °C. They could coat 110 nm IrO_x layer on a glass substrate consists of 300 nm thick titanium electrodes. Their pH sensor was able to detect pH in a range from pH 4 to pH 10 [94].

Various metals have been used as substrate for IrO_2 coating such as Au, Pt, Ir, PtIr, stainless steel, tin-doped indium oxide (ITO) [90,95,96]. Marzouk [8] in a valuable work investigated various substrate pure metals such as Au, Ag, Ti, Cu, Ni, W, Zr, and Co and some alloys such as nickel-chrome, Hastelloy and stainless steel. The blue layer of deposit, proper adhesion of deposit to surface, and stability of the cyclic voltammogram were the most important factor for substrates comparing. Mayorga *et al.* [63,96] described a simple pH sensor fabrication through IrO_2 electrodeposition on stainless steel substrate. The fabricated sensor had fast response time and good repeatability.

Most of researchers followed original Yamanaka solution [90], although some others attempted the modification of his solution [97,98]. Marzouk approved that using $(\text{NH}_4)_2[\text{IrCl}_6]$ instead of IrCl_4 was wrong since the solution did not develop to

dark greenish-blue color for up to 7 days at room temperature [8]. Marzouk was successful to reduce the development time of solution from 3 days to 10 minutes by heating the solution to 90 °C. Petit *et al.* [97] replaced IrCl₄ with K₃IrCl₆. The required time for solution development was 4 days at 35 °C. This solution did not offer any highlighted merit. Lu *et al.* [33] attempted to use H₂IrCl₆·6H₂O for electrodeposition solution. Their solution was developed from light yellow to dark blue after 5 days.

Table 2.1: Application and characterization of IrO₂ electrodes fabricated by electrodeposition technique[7].

Substrate	Precursor materials	Oxide thickness	Sensitivity (Nernstian behavior mV/pH)	Application	References
Platinum wire	-----	-----	70.2	Interfacial pH measurement	[98]
Au, Pt, Ir, PtIr, and 316LVM stainless steel wires	IrCl ₄ , oxalic acid, and K ₂ CO ₃	100 nm	-----	Neural stimulation and recording	[95]
Tin-doped indium oxide (ITO)	IrCl ₄ , oxalic acid, and K ₂ CO ₃	-----	-----	Electrochromic display devices	[90]
Platinum	IrCl ₄ , oxalic acid, and K ₂ CO ₃	-----	-68 to -77	Glucose sensor	[71]
Au, Ag, Ti, Cu, Ni, W, Zr, Co, nickel-chrome, Hastelloy and stainless steel	IrCl ₄ , oxalic acid, and K ₂ CO ₃	-----	-73	pH measurement as a detector in a flow injection analysis (FIA) system	[8,99]
Platinum	H ₂ IrCl ₆ ·6H ₂ O.	-----	-75.51	pH measurement as a	[33]

	oxalic acid, and K_2CO_3			Neural sensor	
Stainless steel	$IrCl_4$, oxalic acid, and K_2CO_3	20-30 nm	-----	pH measurement as a biosensor	[63,96]
SnO ₂ -coated glass	K_3IrCl_6 , oxalic acid, and K_2CO_3	-----	-----	-----	[97]
Polyimide-Cr-Au	$IrCl_4$, oxalic acid, and K_2CO_3	-----	77	pH measurement in brain tissues	[100]
ITO-coated glass	$IrCl_4$, oxalic acid, and K_2CO_3	-----	64.5	-----	[80]
Carbon fiber	Na_2IrCl_6 , HCl, NaOH	-----	-----	Scanning electrochemical microscope (SECM)	[30]
Sputtered Platinum on flexible Kapton films	$IrCl_4$, oxalic acid, and K_2CO_3	-----	-63.5	pH measurement of extracellular Myocardial Acidosis during Acute Ischemia	[99]
Platinum	$IrCl_4$, oxalic acid, and K_2CO_3	-----	-77.6	pH measurement of microfluidic-based microsystems	[93,101]
Sputtered Gold on Si wafer	$IrCl_4$, oxalic acid, and K_2CO_3	-----	-68	Monitoring of water quality	[82]
Stainless steel	$IrCl_4$, oxalic acid, and K_2CO_3	-----	-73	Corrosion monitoring	[9]

Nguyen *et al.* [100] observed a 12 mV/pH as drift of sensitivity after 8 days sensitivity test repeating. They explained that this change in sensitivity is due to dehydration phenomenon of hydrated iridium oxide, which can be minimized by keeping IrO_2 pH sensor in phosphate buffered saline (PBS) solution.

Wipf *et al.* [30] produced a pH microelectrode via electrodeposition of IrO₂ on carbon fiber. They used this pH sensor in development of the scanning electrochemical microscope (SECM). The fabricated pH sensor was able to measure pH near a surface.

As Lu *et al.* [33] reported there is an optimum thickness for IrO₂ electrodeposited coating. Coating electrochemical performance increase when its CSCc and thickness increase, but when CSCc approach to ~45mC/cm² delamination of IrO₂ coating was detected. Their demonstrated iridium oxide electrode showed a pH sensitivity -75.51 mV/pH in broad pH range of 1-13. More research works are presented in Table 1 with electrode application and other characterization.

Elsen *et al.* [102] in a valuable work compared four methods for electrodeposition of IrO_x which involved a constant current, single potential pulse, alternating potential pulse, or cyclic potential protocol. The maximum rate of pH response for sensors of the same thickness was found to be at least somewhat smaller for the sensors produced by the pulsed potential and cyclic potential methods relative to those produced by the other two methods examined in their project. However, because of the uniformity of the sensing layers produced by the pulsed potential and cyclic potential methods, the thickness necessary for stable sensor function was smaller. They postulated that this can be explained by a relatively smaller porosity of those films. Consistently with this postulate, the sensors produced by the pulsed potential and cyclic potential methods were also found to exhibit smaller intrinsic capacitance relative to those produced by the other two methods.

Based on their finding, cyclic voltammetry was chosen as electrodeposition method for our project.

2.9.1.5 Other methods

A surface renewable IrO₂ pH sensor or hydrogen ion-selective electrode can be made by using composite electrode technique. Quan *et al.* [86] used carbon black, polyvinyl chloride and ammonium hexachloroiridate to fabricate an IrO₂ based composite electrode. Increasing IrO₂ content up to 40 wt% showed an increasing on the pH response. They also investigated the effect of different ions on pH electrode efficiency that resulted Fe(CN)₆³⁻, Fe(CN)₆⁴⁻, I⁻, and H₂O₂ affected by electrode result. Similar results for IrO₂ pH sensor were also reported in other research [31].

Park *et al.* [103,104] fabricated an iridium oxide-glass composite electrode by mixing ammonium hexachloroiridate and glass powder, pressing, and sintering under oxygen atmosphere. The mention electrode was renewable by using 2000 grit SiC emery paper whenever it becomes fouled or deactivated. They observed many microscopic voids in the electrode surface after sintering at high temperature. pH response in these electrodes was dependent on the size and population of voids. Surface voids can be reduced by hot press sintering technique.

2.9.2 Applications of IrO₂ electrode

2.9.2.1 Biomedical and Biological applications

Marzouk *et al.* [105] in 2002 measured extracellular pH in ischemic rabbit papillary muscle for the first time. They used a pH sensor based on an IrO₂ film electrode deposited on a planar sputtered platinum electrode fabricated on a flexible Kapton substrate.

Fast response time of pH sensor is very important for biological application. Iridium oxide pH microsensors were used to measure the acidification rate of CHO and fibroblast cells in a cell culture with microfluidic control [93]. This approach can also be used in bioanalytical field or biosensor [93,101]. Iridium oxide sensors are widely used in neural stimulation and recording electrodes regarding to their low impedance, high charge storage capacity [95].

Iridium oxide based pH sensor is a reliable and robust approach for biological application. O'Hare *et al.* [74] investigated application of IrO₂ electrode fabricated by thermal oxidation and anodization as a pH sensor in the cultured intervertebral disc. Their electrodes were found to be unstable in physiological media and dissolution of the hydrated oxide film happened in higher concentrations of chloride. They reduced the effect of chloride by using thermally annealed Nafion films. Although Nafion film caused an increase in response time, it could protect iridium oxide film against the aggressive nature of biological media [93,99].

2.9.2.2 Industrial applications

Zhang *et al.* [98,106] used IrO₂ pH sensor for measuring pH in electrode/solution interface in electrodeposition process. They found that by increasing the applied potential, interfacial pH increased. Marzouk [8] fabricated a tubular IrO₂ pH sensor for using in a flow injection analysis (FIA) system as a detector.

The pH of a solution is one of the most important parameters used for characterizing an electrolyte during corrosion processes [29,75,78]. For this purpose, some researcher used iridium oxide microelectrode to study the effect of local pH near the surface on corrosion on steel surfaces [79,107].

2.10 Design of Experiments

Sir Ronald Fisher -father of modern experimental design- developed the fundamental concepts of Design of Experiments (DOE) in England through the 1920s [108]. The aim of DOE is usually to demonstrate the statistical significance of factors effect on the dependent variable; and determining the optimum settings the various factors affect the fabrication procedure [109].

In DOE we need a statistics-based approach to designed experiments. Experimental techniques are growing to optimize production process. Major approaches that are usually utilized in industrial experimentation are: factorial design, taguchi method, and response surface design and special procedures for creating experiments in controlled experimental regions.

2.10.1 Response Surface Methodology

Optimization techniques such as Response Surface Methodology (RSM) can be used considering that various parameters affect the quality of electrodeposition. Initially, RSM was proposed to model experimental responses and then migrated into the modelling of numerical experiments [110].

The most important applications of RSM are in the particular situations where several input variables potentially influence some performance measure or quality characteristic of the process. Thus performance measure or quality characteristic is called the response. The input variables are sometimes called independent variables, and they are subject to the control of the scientist or engineer. The field of response surface methodology consists of the experimental strategy for exploring the space of the process or independent variables, empirical statistical modeling to develop an appropriate approximating relationship between the yield and the process variables,

and optimization methods for finding the values of the process variables that reduce desirable values of the response [111].

RSM has recently been applied to optimize electrodeposition involving various alloys [11,112,113]. However, no statistical studies have been reported on the fabrication of an IrO_x pH sensor by electrodeposition. The use of RSM in statistical analysis elucidates the aforementioned process. RSM also decreases the number of required experimental runs to create statistically valid results [109] and saves time and resources. The first step in RSM involves the Design of Experiments (DOE), which determines the number of experiments that provide reliable and acceptable measurements of the chosen response. Central Composite Design (CCD) can be employed by RSM as an experimental design to fit a model by the least-squares technique [114]. CCD requires a minimum number of experiments as the standard 2ⁿ factorial with its origin at the center and 2ⁿ axial points fixed axially at a distance, say α , from the center and replicate experiments at the center [115]. RSM helps investigate the effects of interactions among independent variables on a selected response.

2.10.2 Central Composite Design

Central Composite Design (CCD) is popular technique among researchers to examine the effect of variables. CCD allowed us to demonstrate which variables considerably affect every response and optimize the value of variables that were created significant [114]. CCD with three experimental factors employed sixteen experiments. These experiments have eight runs at two level, six star points and two center points to permit estimation of error and supply a check on linearity.

2.10.3 Analysis of Variance

Analysis of Variance (ANOVA) is a more effective method to survey the result more significantly. ANOVA studies all means and models them together. Principally, it is an easy mathematical method of classification the mechanism of difference in a known set of data and given test of significance [116]. The two principals complicated are partition of sums of the squares and estimating the variance of population by various techniques and evaluating these estimates.

The result of modeling and analysis of designed experiment data can be demonstrated in table recognized as the ANOVA. The table will show the relationship between the predicted data and observed data. ANOVA table also display the calculation on sum of square that provides the output for ANOVA [117].

CHAPTER 3

METHODOLOGY AND CHARACTERIZATION TOOLS

3.1 Methodology Overview

This chapter describes methods which are used for the fabrication and characterization of IrO₂ pH sensor. The application of fabricated pH sensor for surface pH measurement without and under deposit will be mentioned. In order to fabricate an IrO_x pH sensor, electrodeposition method was used. The fabricated pH sensor was then used in electrochemical system to investigate and monitor pH in metal surface and under artificial deposit layer. Electrochemical experiments were conducted in pH sensor fabrication phase to investigate characterization of IrO₂ coating versus various fabrication variable factors. Electrochemical experiments were used in next step to monitor corrosion of carbon steel by using fabricated pH sensor. The electrochemical techniques used were cyclic voltammetry (CV), electrochemical impedance spectroscopy (EIS), linear polarization resistance (LPR) and open circuit potential (OCP). Surface characterization analyses were performed to investigate the film morphology formed from corrosion process by using FESEM, EDAX and AFM.

3.2 Design of experiments, analysis, and model fitting

This study aims to define the functional relationship among scan rate, temperature, number of cycles, pH sensitivity, and IrO_x coating thickness by RSM with CCD. Design-Expert version 6.0.6 (Stat-Ease, Inc., USA) was used to generate the regression model as well as perform statistical and data analyses. The variables in this study included three numerical factors: scan rate (X1), temperature (X2), and

number of cycles (X3). The three independent variables and experimental design levels are shown in Table 3.1. Twenty experimental runs were determined from CCD, including eight factorial points, six axial points, and six center points. The axial distance (α) from the center point was set at 0.5 in coded units. Table 3.2 indicates the complete design matrix of the applied experiments and actual responses in this study. The two-factor interaction model (2FI) to predict the optimal point can be written as follows:

$$Y = \gamma_0 + \sum_{i=1}^k \gamma_i X_i + \sum_{i<j} \gamma_{ij} X_i X_j + \varepsilon_\alpha \quad (3-1)$$

where Y represents the response (pH sensitivity and IrO_x coating thickness), and γ_0 , γ_i , denote the constant coefficient and the first linear coefficient, respectively. γ_{ij} is the linear model coefficient. X_i and X_j are the coded independent variables, and ε is the standard error. Statistical “p” values less than 0.0500 were used to indicate the significant factors of the model.

Table 3.1: Codified and normal values of the experimental design levels

Parameters	Levels				
	-1	-0.5	0	0.5	1
Scan Rate (mV/s) :A	50	87.5	125	162.5	200
Temperature (°C) :B	25	35	45	55	65
Cycles (cycle) :C	100	200	300	400	500

Table 3.2: Experimental design and actual response of the thickness and pH sensitivity of pH electrode.

Design points	Point type	Variables in coded levels		
		A:Scan Rate (mV/s)	B:T (°C)	C:Cycle (cycle)
1	Center	0	0	0
2	Center	0	0	0
3	Center	0	0	0
4	Center	0	0	0
5	Center	0	0	0
6	Center	0	0	0
7	Axial	0	-0.5	0
8	Axial	0	0.5	0
9	Axial	0	0	-0.5
10	Axial	0	0	0.5
11	Axial	0.5	0	0
12	Axial	-0.5	0	0
13	Fact	-1	-1	1
14	Fact	-1	1	1
15	Fact	1	1	1
16	Fact	-1	1	-1
17	Fact	1	1	-1
18	Fact	1	-1	1
19	Fact	-1	-1	-1
20	Fact	1	-1	-1

3.3 Design and Fabrication of pH Sensor

3.3.1 Chemicals and Materials

For fabrication of iridium oxide pH sensor following material were used: Iridium(IV) chloride hydrate ($\text{IrCl}_4 \cdot x\text{H}_2\text{O}$) (Catalogue no. 516996); 30% hydrogen peroxide (Catalogue no. 216763); oxalic acid (Catalogue no. 75699); potassium carbonate K_2CO_3 (Catalogue no. P5833); stainless steel rods, 2.4 mm diameter; and standard pH solution buffer (4, 7, and 9) were used in this study. All chemicals were

analytical reagent grade and purchased from sigma-Aldrich, USA. Distilled water was used for preparing all solution. A commercial glass pH probe was used in electrochemical experiment and for calibration of IrO₂ pH sensor.

3.3.2 Preparation of Electrodeposition Solution

The electrodeposition solution was prepared by mixing 150 mg of IrCl₄.xH₂O in 100 mL of distilled water in a 200-mL glass beaker, and followed by stirring for 10 minutes for complete mixing. Then 360 mg oxalic acid was added to the solution and then stirred for another 10 minutes. Oxalic acid acts as the complex-forming agent to prevent precipitation in alkaline solutions. A 1-mL of 30% hydrogen peroxide was added, and then solution was left for 15 minutes stirring. The pH of the solution was increased slowly to pH 10.5 by adding anhydrous potassium carbonate [15]. Addition of hydrogen peroxide to the iridium tetrachloride solution before adding K₂CO₃ made the electrodeposited film smooth and lustrous. It also made it possible to deposit oxide films at lower current densities [118]. A light green solution was obtained. The solution was allowed to age for two days in an air-conditioned laboratory to achieve a dark blue stable solution. The iridium in iridium tetrachloride has the oxidation state 4 as is shown in Figure 3.1. The schematic of the electrodeposition solution preparation is shown in Figure 3.2.

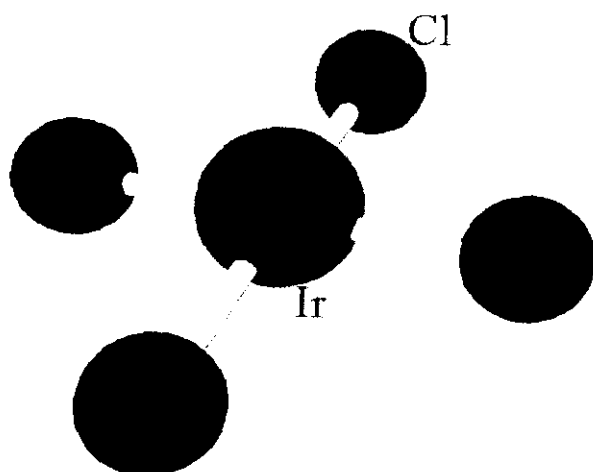


Figure 3.1: Four iridium oxidation state in iridium tetrachloride

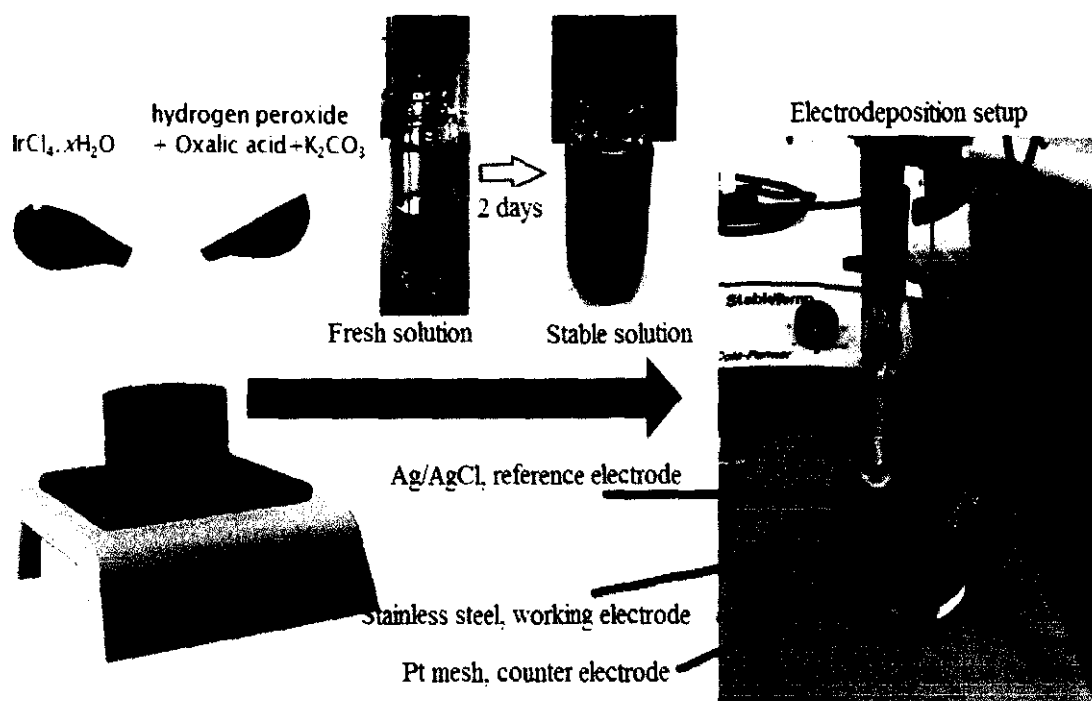


Figure 3.2: Solution preparation and electrodeposition setup

3.3.3 Preparation of IrO_x electrode for electrochemical experiments

Twenty sample of stainless steel rod with diameter of 2 mm and long of 20 mm were used as substrates for electrodeposition of IrO_x according to experimental design by DOE software. Electrodes were first polished with sandpaper and alumina dust to achieve a surface with 0.5 μm roughness. The electrodes were then ultrasonically cleaned with acetone and deionized water. For all electrochemical experiments, a three-electrode glass cell was used with a platinum mesh counter electrode and an Ag/AgCl (3M KCl) reference electrode for electrodeposition in CV, as shown in Figure 3.2. Schematic of fabricated samples is shown in Figure 3.3. A high-performance potentiostat/galvanostat (Autolab/PGSTAT128N) as shown in Figure 3.4 was used for electrodeposition and electrochemical experiments. CV as shown in Figure 3.5 was applied for electrodeposition in a potential range of -0.5 V to 0.65 V versus Ag/AgCl (3M KCl) at various scan rates, temperatures, and cycles, as indicated in Table 3.1. A mesh Pt electrode was employed as counter electrode

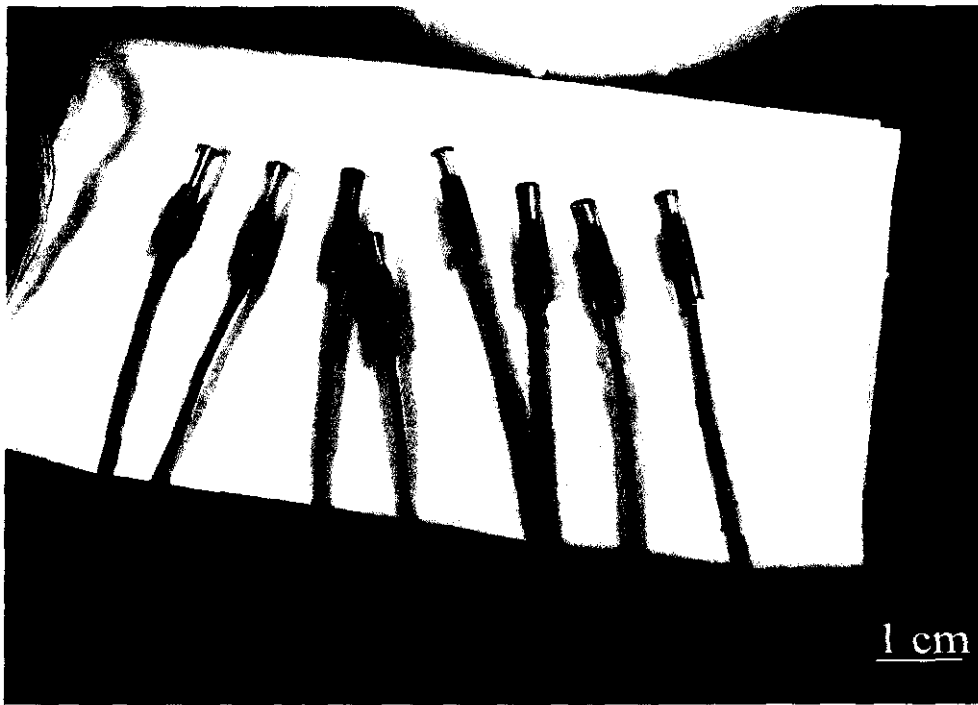


Figure 3.3: IrO_x electrodeposited on stainless steel substrate for electrochemical investigations.

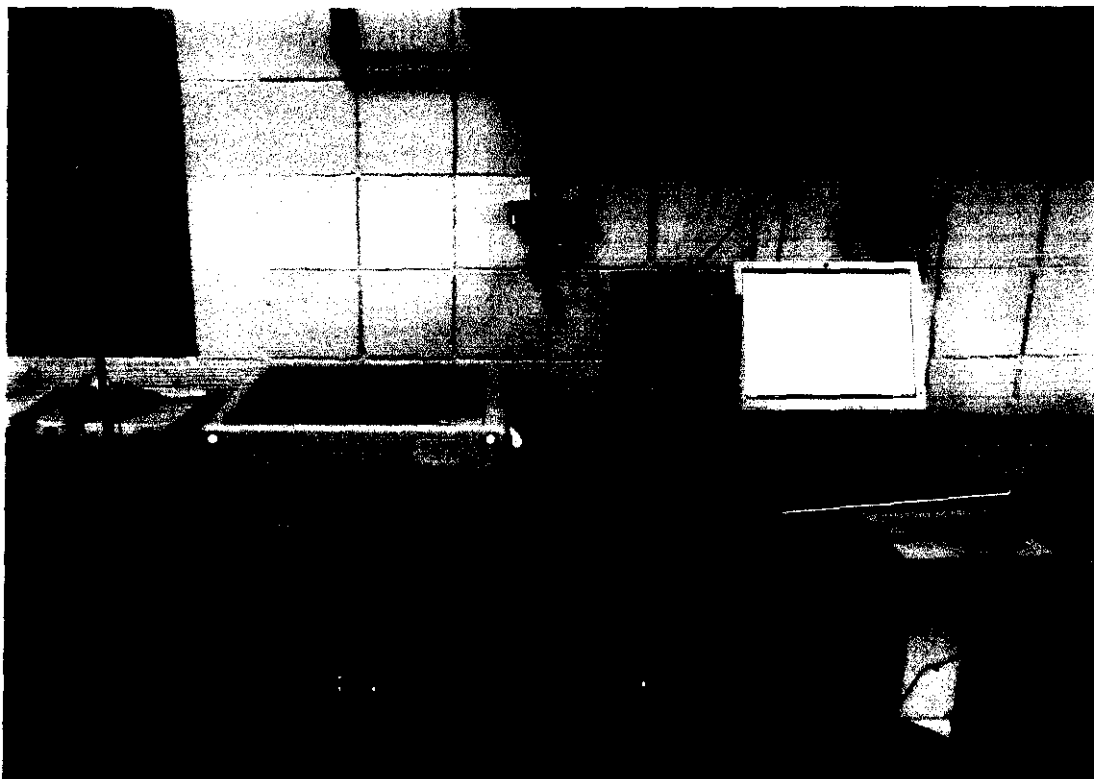


Figure3.4: A high-performance potentiostat/galvanostat (Autolab/PGSTAT128N, the Netherlands) used for pH sensor fabrication, calibration and all electrochemical investigations.

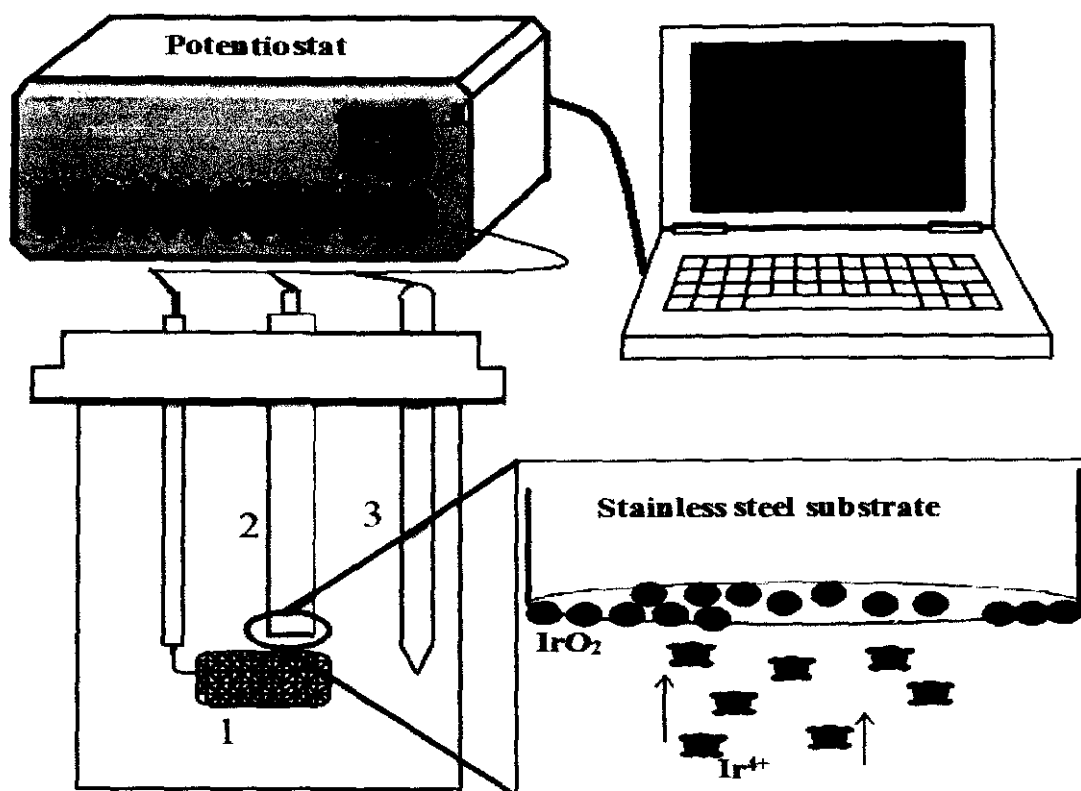


Figure 3.5: Schematic diagram of an electrodeposition setup: (1) Pt mesh counter electrode, (2) stainless steel (working electrode), (3) Ag/AgCl (3M KCl) reference electrode.

3.3.4 Preparation of IrO_x pH sensor for surface pH measurements

Three stainless steel rod (2 mm in diameter and 20 mm long) were used as substrates for electrodeposition of IrO_x. Electrodes were connected to a copper wire, and then covered in Teflon tube to insulate all area except a circular exposed area of 3.14 mm² for electrodeposition. These electrodes embedded in a carbon steel sample which will play role of working electrode later. All assembled parts that is shown in Figure 3.6 are polished by using sandpaper of different grit sizes, diamond paste and alumina powder to achieve a surface roughness of 0.5 μm. The electrodes were then rinsed and ultrasonically cleaned in acetone and deionized water. Electrodeposition of IrO_x on stainless steel substrates was done as described in section 3.3.3.

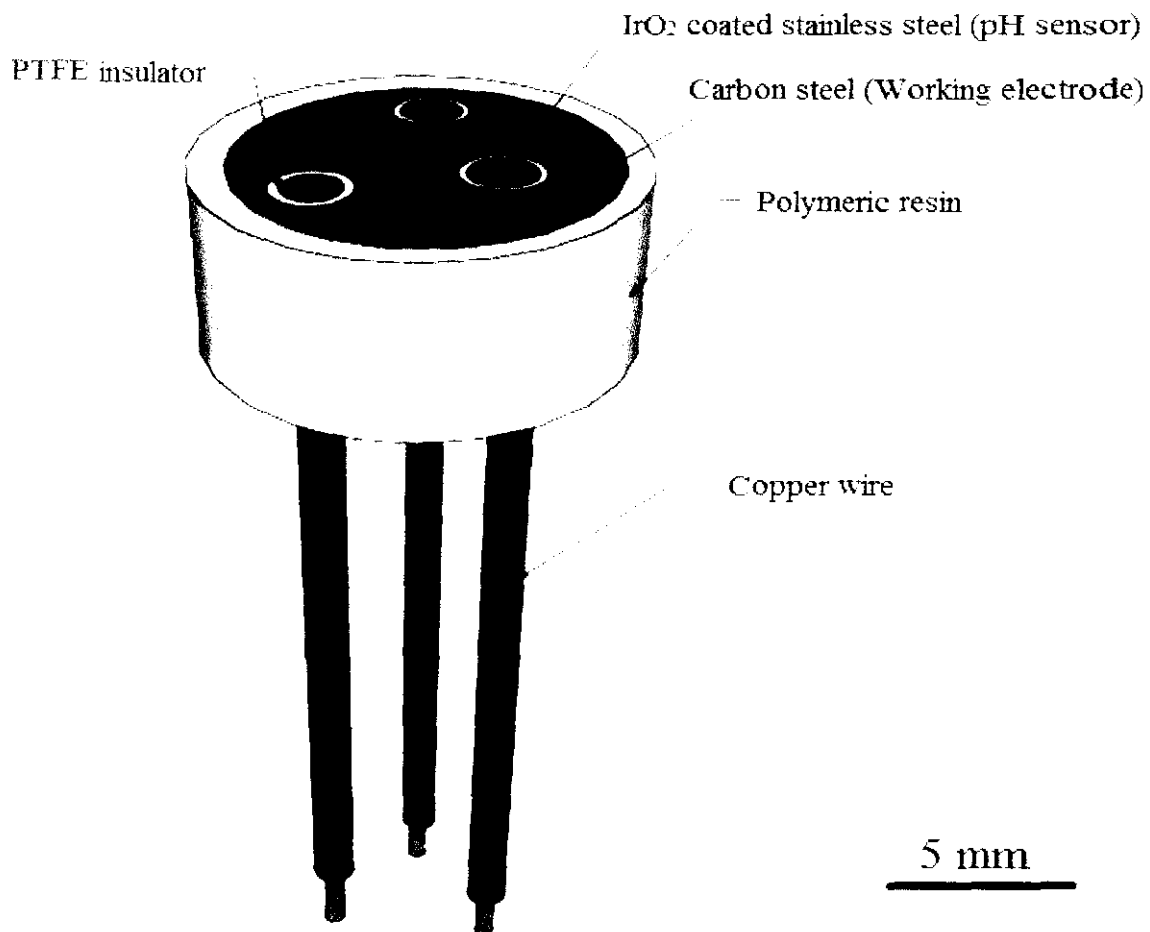


Figure 3.6: Schematic Design of pH probe for surface pH measurement of corroding carbon steel

3.3.5 Preparation of IrO_x pH sensor for under deposit pH measurement

Fabrication of IrO_x pH sensor for under deposit pH measurement was same as mentioned in section 3.3.3 and 3.3.4, except one extra copper wire was connected to carbon steel for doing LPR test simultaneously with pH measurement. Also a cap and tube were used for holding deposit as shown in Figure 3.7. A tube as is shown in this figure filled with 5mm deposit (Agar). The assembled probe was exposed to CO₂ containing 3% NaCl solution.

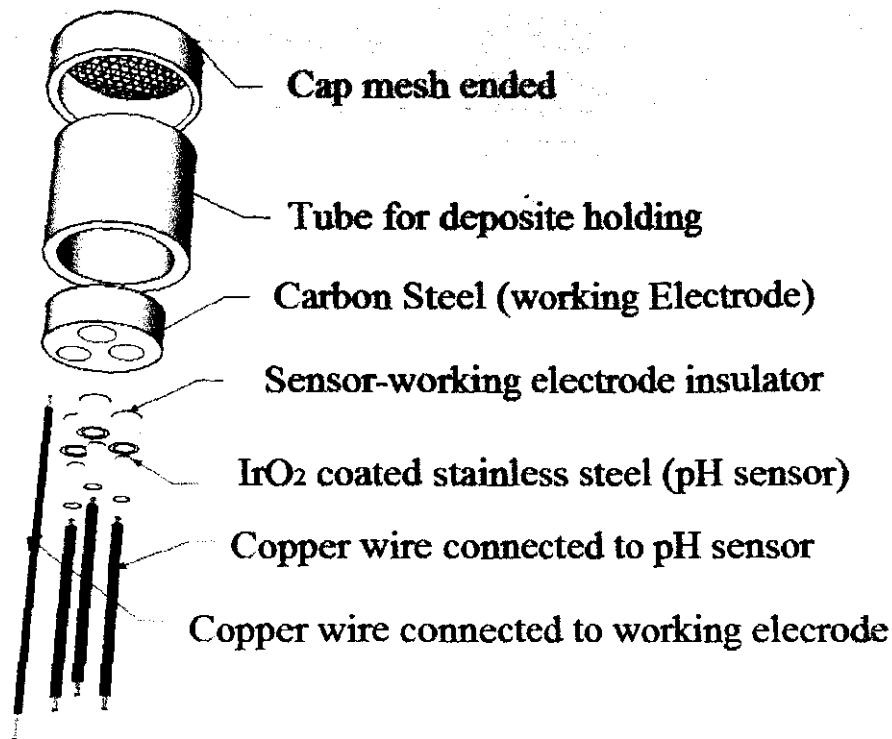


Figure3.7: Schematic Design of pH measurement probe for monitoring of pH and corrosion under deposit (Agar).

3.4 Research Test matrix of pH sensor application

The working electrode of this study was prepared from commercial X52 carbon steel. The chemical composition of X52 is shown in Table 3.2. A test matrix shown in Table 3.1 was design for conducting corrosion monitoring by surface pH measurement of working electrode. An SEM image of polished X52 carbon steel before testing is shown in Figure 3.8.

All experiments were conducted in the glass cell equipped with Ag/AgCl (3M KCl) reference electrode and stainless steel as a counter electrode.

LPR and OCP techniques were used simultaneously for measuring of corrosion rate and pH, respectively.

Table 3.3: Composition of X52 carbon steel

C (%)	Si (%)	Mn (%)	S (%)	P (%)	Cr (%)	Ni (%)	Mo (%)	Fe (%)
0.064	0.26	1.55	0.001	0.012	0.05	0.04	0.01	Balance

Table 3.4: Test matrix for surface pH measurement and under deposit pH measurement

Steel type	X52
Solution	3 wt% NaCl
T (°C)	25, 50, 80
De-oxygenation gas	CO ₂
Pco2(bar)	1
Technique	LPR, OCP
Time (hours)	24
pH	4, 6
Deposit	Agar
Deposit thickness (mm)	5

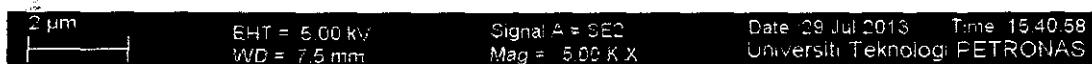


Figure 3.8: SEM image of polished X52 carbon steel before testing

A 1 liter 3 wt% NaCl solution was prepared in the glass cell by mixing 30 gr NaCl in 1 liter distilled water. Prior to samples immersing, the solution was purged with 1 bar CO₂ gas for two hours. After the solution was deoxygenated, the pH was recorded by using a glass pH sensor. It was 4 to 4.3 during experimental. After that, the working electrode is put into test solution. CO₂ gas purging was continued till end of experiment. The pH measurement was done by means of OCP method contributed with an Ag/AgCl reference electrode. Also, the corrosion rate measurements were taken for samples under Agar deposit. All experiments were conducted for 24 hours. All working electrodes and stainless steel substrates were ground with silicon carbide paper grid #240 to #600, and 0.5 μm diamond pastes and rinsed with alcohol before electrodeposition and pH measurement experiment.

3.5 Electrochemical investigation

Electrical circuits and commercial instrumentation have been employed to measure electrode properties very effectively. This section describes the electrochemical cells and measurement equipment that were used in the thesis.

3.5.1 Linear polarization resistance (LPR)

LPR technique is used to monitor the corrosion rate sweeping from -10 mV to +10 mV with the sweep rate 10 mV/ min. This method is based on ASTM standard G 102-89 [119]. The equations used to calculate the corrosion rate using LPR are shown in Equation 3.1 – 3.3 whereby polarization resistance (R_p) is given by Stern and Geary equation [120]:

$$R_p = \frac{B}{i_{corr}} = \frac{\Delta E}{\Delta I} \quad (3.1)$$

Where,

$$B = \frac{b_a b_c}{2.303(b_a + b_c)} \quad (3.2)$$

The corrosion current can be related directly to the corrosion rate from Faraday's law:

$$CR(\text{mm/year}) = \frac{315 \times Z \times i_{corr}}{\rho \times n \times F} \quad (3.3)$$

Where,

CR = Corrosion rate (mm/year)

i_{corr} = Corrosion current density, $\frac{\mu A}{cm^2}$

ρ = Density of iron, 7.8 g/cm³

F = Faraday's constant, 96,500 C/mole

Z = Atomic weight (g/mol)

n = Number of electron

b_a, b_c = The slopes of the logarithmic local anodic and cathodic polarization curves respectively.

R_p = Resistance polarization (ohm)

3.5.2 Electrochemical impedance spectroscopy (EIS)

Electrochemical impedance spectroscopy (EIS) was conducted measuring the electrical impedance and phase angle obtained with sinusoidal voltage or current excitation of the electrode. The measurement can be done over a broad frequency range, typically 0.01 Hz to 10⁵ Hz, and the magnitude of the excitation is sufficiently small that a linear current-voltage response is obtained at each frequency. For voltage excitation, the root-mean-square magnitude of the excitation source is typically 10 mV, and generally not more than 50 mV. EIS spectra are probably most valuable in assessing the recording capabilities of micro electrodes.

An Autolab/PGSTAT128N potentiostat was used for EIS measurement. The frequency used for the impedance measurements ranged from 0.01 Hz to 10 kHz. A software, NOVA-1.8, was used for the EIS measurements and curve fitting analysis.

3.5.3 Open Circuit Potential (OCP)

IrO_x pH sensor works as potentiometric sensor. For this purpose, potential changes between pH sensor and a reference electrode should be measured. Open Circuit Potential (OCP) is a technique which measures potential of working electrode

regarding to reference electrode when no potential or current is being applied to the cell. OCP were conducted using an Autolab/PGSTAT128N potentiostat.

3.5.4 Cyclic Voltammetry (CV)

Cyclic voltammetry (CV) is one of the key techniques of modern electrochemistry. Almost every electrochemical investigation begins with a number of voltammograms. Under the right conditions, cyclic voltammetry can be used in quantitative investigations of equilibrium potentials, reaction rates, and absorption processes. Often, however, cyclic voltammetry is used qualitatively to get a general idea of what reactions and electrode processes are occurring in an electrochemical system. Cyclic voltammetry has a number of other uses.

One is to measure the effective charge storage and charge transfer capabilities of an electrode. Another is to deposit materials onto an electrode surface and characterize the extent of such deposition. Repeated CV testing can also be used as a simple means of checking electrode stability.

Cyclic Voltammetry (CV) is the most widely method used for investigation of electrochemical reactions. CV at slow scan rate (50 mV/s) gives qualitative information about oxidation and reduction reaction of microelectrode. CV was done for all fabricated pH sensor in a pH 7 universal buffer solution at a scan rate of 50 mV/s. The potential range of CV was -0.6 V to 0.8 V (vs. Ag/AgCl) to prevent IrO₂ destruction at higher potentials.

3.6 Surface Morphology Characterization

Morphology of electrodeposited iridium oxide on stainless steel substrate and corroded carbon steel samples were investigated by using Field Emission Scanning Electron Microscope (FESEM), Energy Dispersive X-rays spectroscopy (EDX), Atomic Force Microscopy (AFM), and X-rays diffraction (XRD).

3.6.1 Field Emission Scanning Electron Microscope (FESEM)

Iridium oxide surfaces and cross-sections were characterized by Field-Emission Scanning Electron Microscope (FESEM) (Model: SUPRA 55VP from Carl Zeiss AG, Germany) with an accelerating voltage 0.2-30.0 kV. For surface SEM imaging, no gold/carbon coating was applied. Samples were fixed to a microscope stage with double sided adhesive and partially painted with conductive silver paint to avoid using the gold coating. FESEM used in our work is shown in Figure 3.9.

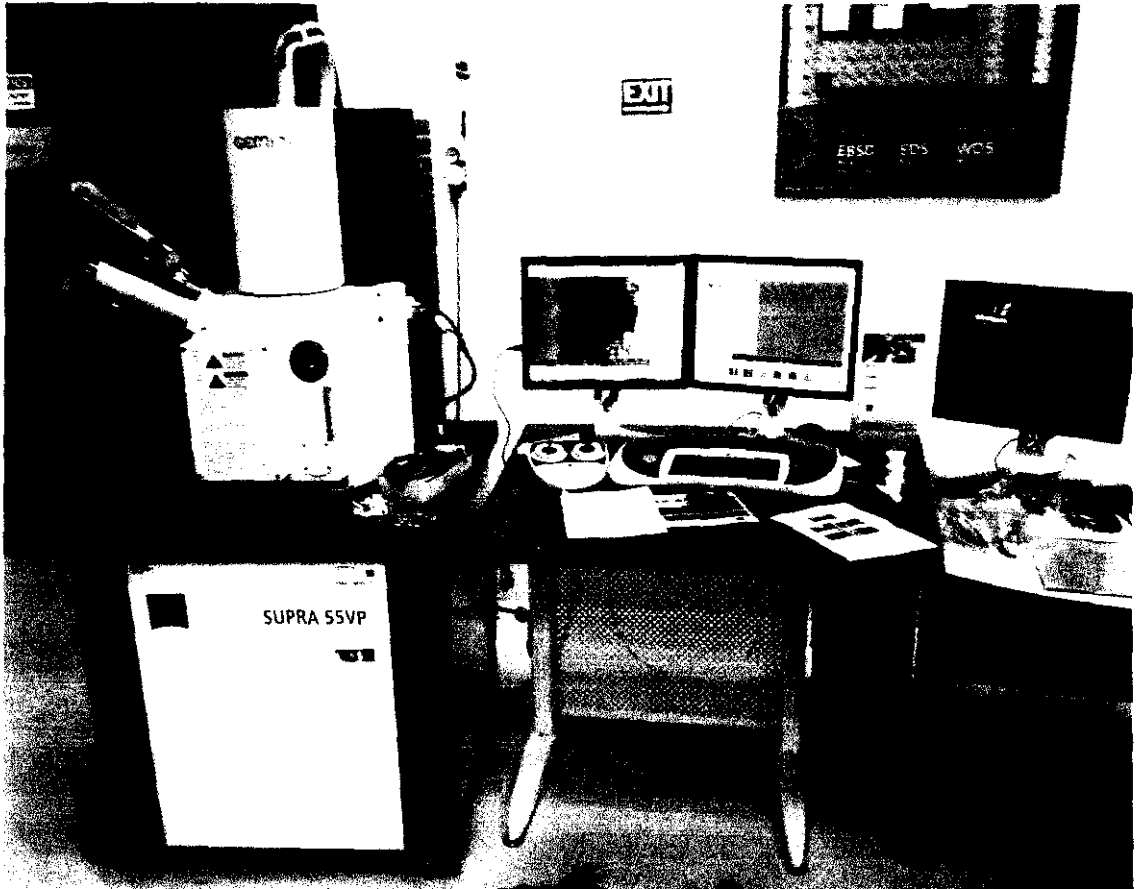


Figure 3.9: Field Emission Scanning electron microscopy (FESEM) system

3.6.2 Energy Dispersive X-rays Analysis (EDX)

Energy Dispersive X-Ray Spectroscopy (EDS) (Model: SUPRA 55VP from Carl Zeiss AG, Germany) is used in conjunction with Scanning Electron Microscopy (SEM).

3.6.3 Atomic force microscopy (AFM)

A 3D investigation of IrO_x film morphology was done by Atomic force microscopy (AFM) [Universal Scanning Probe Microscope (USPM), Model: Nano Navi (E-Sweep)]. Figure 3.10 shows a schematic diagram of the AFM operation.

Atomic force microscopy is a three dimensional imaging technique determining the topography of the measured sample with a very high resolution. The AFM works by detection of atomic forces acting between the sample and a cantilever with a sharp tip as it moves across the sample surface [121].

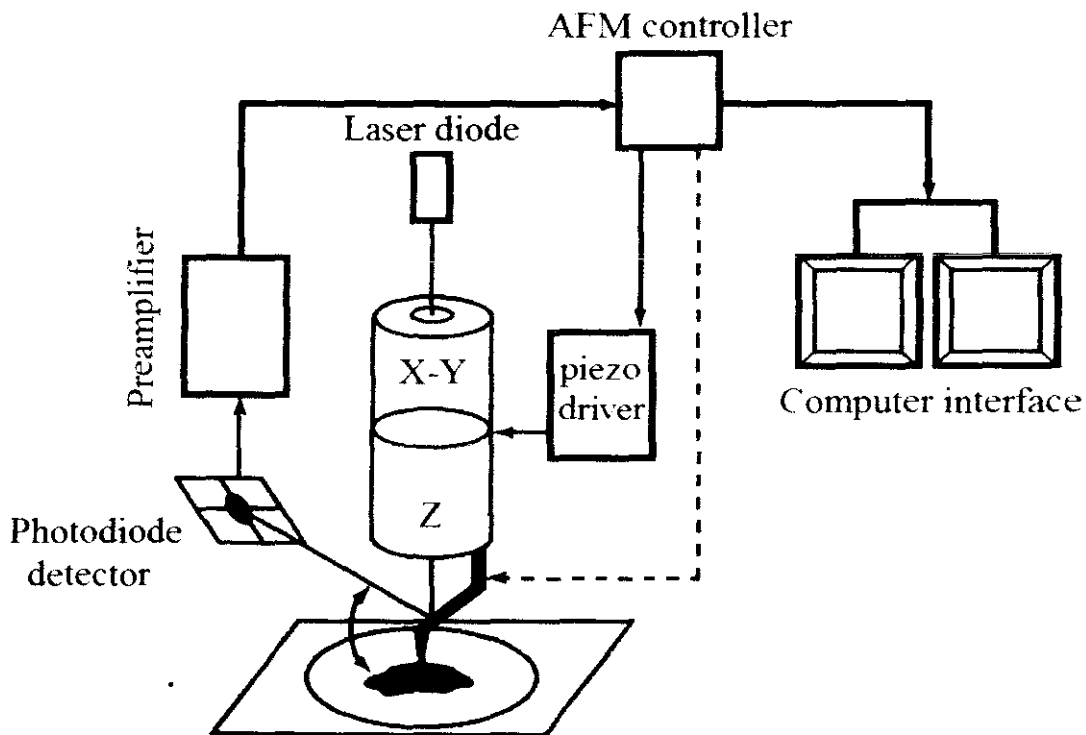


Figure 3.10: A schematic diagram of the AFM operation [121].

3.6.4 X-rays diffraction (XRD)

X-rays diffraction (XRD) (Model: Bruker AXS D8 Advance X-ray powder Diffractometer) was employed for crystalline investigation of IrO_x electrodeposited on stainless steel.

3.6.5 Infinite Focus Microscope (IFM)

Thickness of IrO_x films were measured by Infinite Focus Microscope (IFM). The IFM is a rapid non-contact optical 3D measurement device, which combines the low depth of field of an optical microscope with vertical scanning, traversing across the surface of the sample, to provide high resolution and high depth of field topographical images with a large field of view. An IFM is shown in Figure3.11.

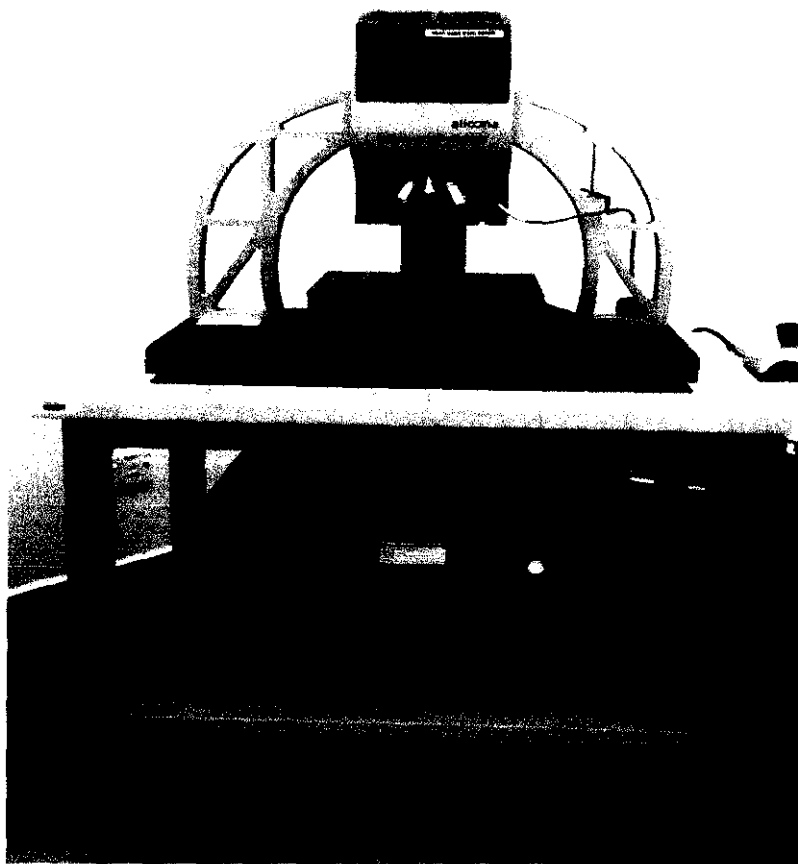


Figure 3.11: Infinite Focus Microscope (IFM) system

3.6.6 Transmission electron microscopy

Transmission electron microscope (TEM) is a powerful tool for investigation of the atomic structure of <100 nm thick samples. Micrographs in TEM are produced by the transmitted primary beam electrons while in SEM need to scan the electron beam. A TEM (model LIBRA 200FE, Carl Zeiss, Germany) with acceleration voltage of 200 kV was used to obtain visual images of samples of IrO_x powder deposited onto carbon covered copper grids to determine grain size and crystallinity.



Figure 3.12: Transmission electron microscope

3.6.7 Fourier Transform Infrared Analysis

Fourier Transform Infrared Analysis (FTIR) offers detailed information on the bond structures within compounds. FTIR depends upon the absorption of infra-red radiation arising from the vibrational and rotational characteristics of dipolar chemical compounds. The arrangement and strength of chemical bonds within a molecule have a direct effect on the characteristic modes of vibration and vibrational bond frequencies of a molecule, resulting in the formation of a series of characteristic mid-

infrared absorption bands ($4000\text{-}400\text{cm}^{-1}$) which can be used to characterise and quantify individual compounds.

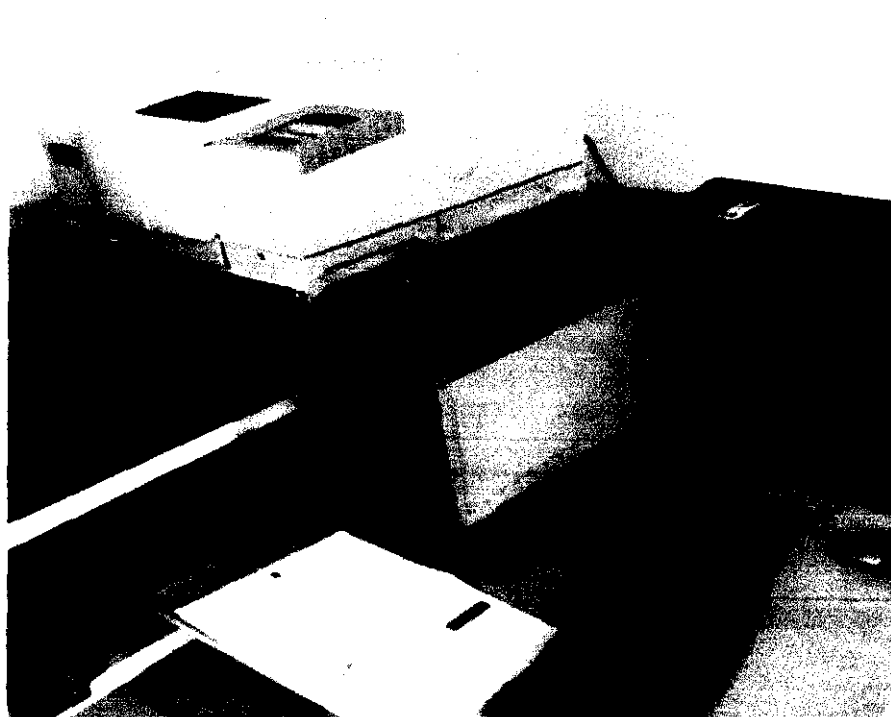


Figure 3.13: Fourier Transform Infrared Spectrometer

CHAPTER 4

RESULTS AND DISCUSSIONS

4.1 Chapter Overview

This chapter presents the most significant results in the design, fabrication and employment of iridium oxide pH sensor for pH measurement in CO₂ corrosion.

This chapter is divided into four parts. The first part of this chapter will show electrodeposition of iridium oxide on stainless steel which is one of the contributions of this study and then in the second part, the electrodeposition factors will be investigated by a statistical tool. In the third part, a novel design of pH probe will be proposed and its using result of measuring pH of carbon steel corroding surface will be presented. In the last part, fabricated pH probe will be customized to monitor pH under deposit for real-time monitoring of corrosion process.

4.2 Electrodeposition of Iridium Oxide on Stainless Steel

4.2.1 Preparation of the Deposition Solution

The deposition solution was aged for two days to an IrOx complex be created. UV-vis spectrophotometry was used for testing solution. The result is summarized in Figure 4.1. The of UV-vis spectrophotometry just was recorded after 400 nm wavelength since we expect a spectrum around 550 nm as mentioned in literature [33].

The result of UV–vis spectrophotometry showed the absorption at 580 nm indicates the formation of multinuclear iridium complexes as was reported in literature [33,122]. The solution was allowed to age for two days in an air-conditioned laboratory to achieve a dark blue stable solution as can be seen in Figure 4.1.

The anodic electrodeposition process can be described by the following equation [33,90]:

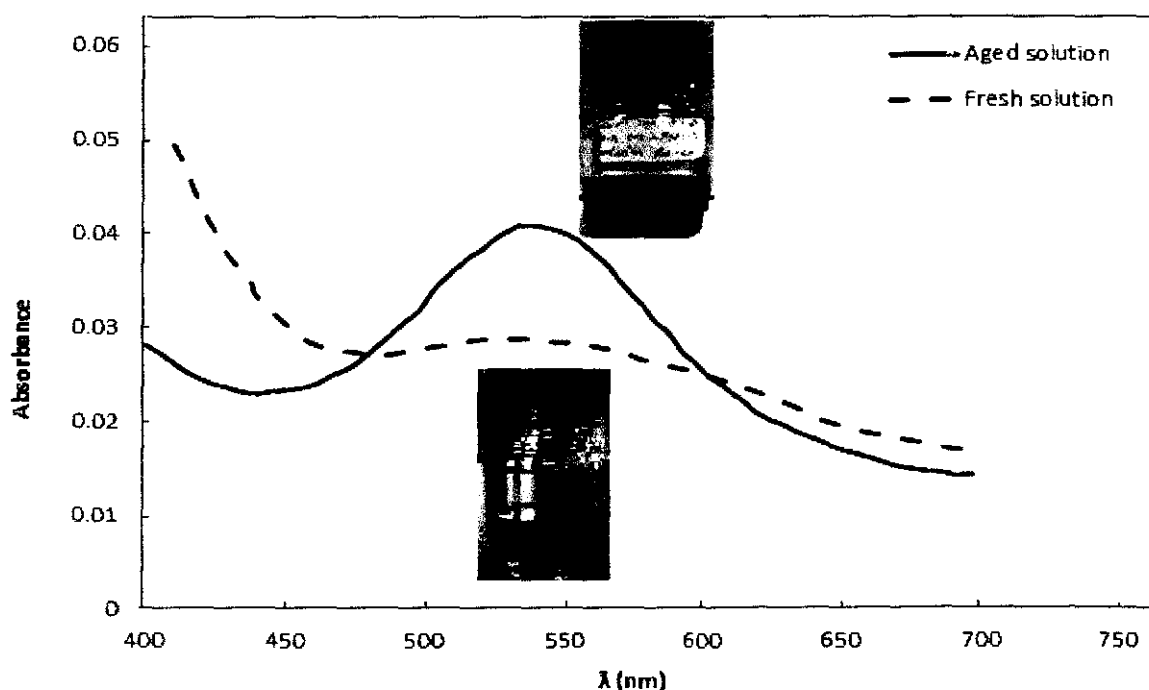
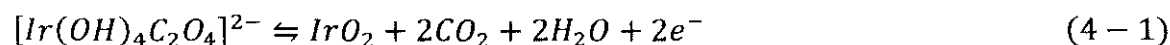


Figure 4.1: The UV–vis spectra of fresh and aged deposition solutions

4.2.2 Fabrication of Iridium Oxide Electrode

Initially, four electrodes were fabricated to check feasibility of electrodeposition technique and suitability of stainless steel as substrate. Method of fabrication is mentioned in the chapter 3 and shown in Figure 4.2. Several methods of electrodeposition were investigated and eventually cyclic voltammetry was selected

for this thesis as a result of visual inspection of electrodeposited IrO_x film on stainless steel substrate.

The electrochemical oxidation of iridium(III) oxide solution leads to the formation of the insoluble hydrous iridium(IV) oxide IrO₂ . xH₂O which has different degree of hydration. Accordingly, in the following the iridium(IV) oxide will be named IrO_x, which is the term usually used in most of the works related to this oxide [123-125].

According to Table 4.1, two scan rates (50 and 200 mV/s) and two numbers of cycles (100 and 500 cycles) were used in cyclic voltammetry method for deposition of iridium oxide layer.

Growing of iridium oxide layer on stainless steel with increasing cycles from 1 to 500 cycles is demonstrated in Figure 4.3. A significant result can be seen from this Figure, thickness of IrO_x layer increased by increasing cyclic number. The result is summarized in Table 4.1. All electrodeposited surfaces were blue in color and free of crack.

The thickness of IrO_x layer was measured by using IFM. As shown in Table 4.1, cathodic charge storage capacity (CSC_C) as a representative of IrO_x thickness is a function of cycle number and scan rate. IrO_x thickness increased with the increasing cycle number and decreasing scan rate.

Table 4.1: Experimental design for IrO_x electrodeposition on stainless steel

Sample code	Scan Rate (mV/s)	T(°C)	Cycle	CSC _C (mC/cm ²)	Sensitivity (mV/pH)
a	50	25	100	2.739 x 10 ⁻⁴	-73.84
b	200	25	100	1.162 x 10 ⁻⁴	-73.31
c	200	25	500	2.051 x 10 ⁻⁴	-74.5
d	50	25	500	10.385 x 10 ⁻⁴	-69.98

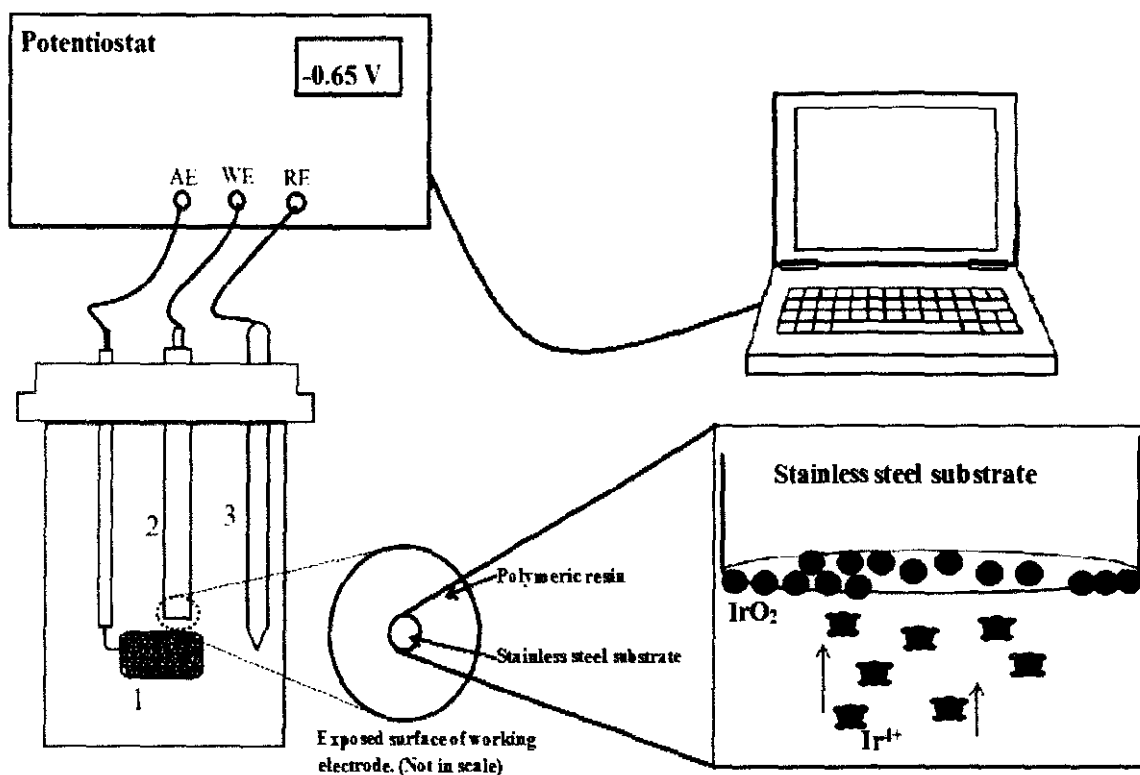


Figure 4.2: Schematic of an electrodeposition setup: (1) Pt mesh counter electrode, (2) stainless steel (working electrode), (3) Ag/AgCl reference electrode.

4.2.3 The Cyclic Voltammetry Growing of IrO_x Electrode

According to Figure 4.3, it is noted that with increasing cycles in the Cyclic Voltammetry method of IrO_x electrodeposition, CSC_C of electrodes will increase which is a critical characteristic in some application of IrO_x electrodes such as neural recording and stimulation. The CSC_C of the EIROF can be calculated using the time integral of the cathodic current during a potential sweep between 0.80 and $-0.60V$ (vs. Ag/AgCl) at a scan rate of 50 mV/s (Figure 4.4). According to literature, CSC_C is directly proportional to IrO_x thickness [95].

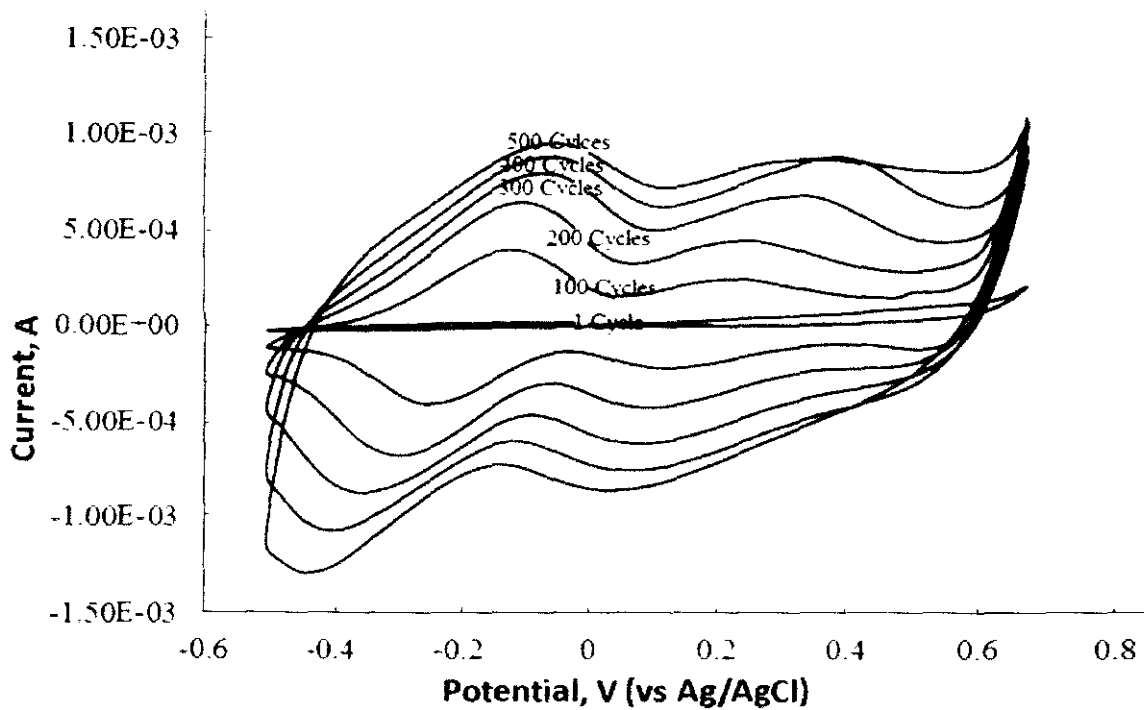


Figure 4.3: Growth of iridium oxide on stainless steel substrate by cyclic voltammetry method at a scan rate of 50 mV/s.

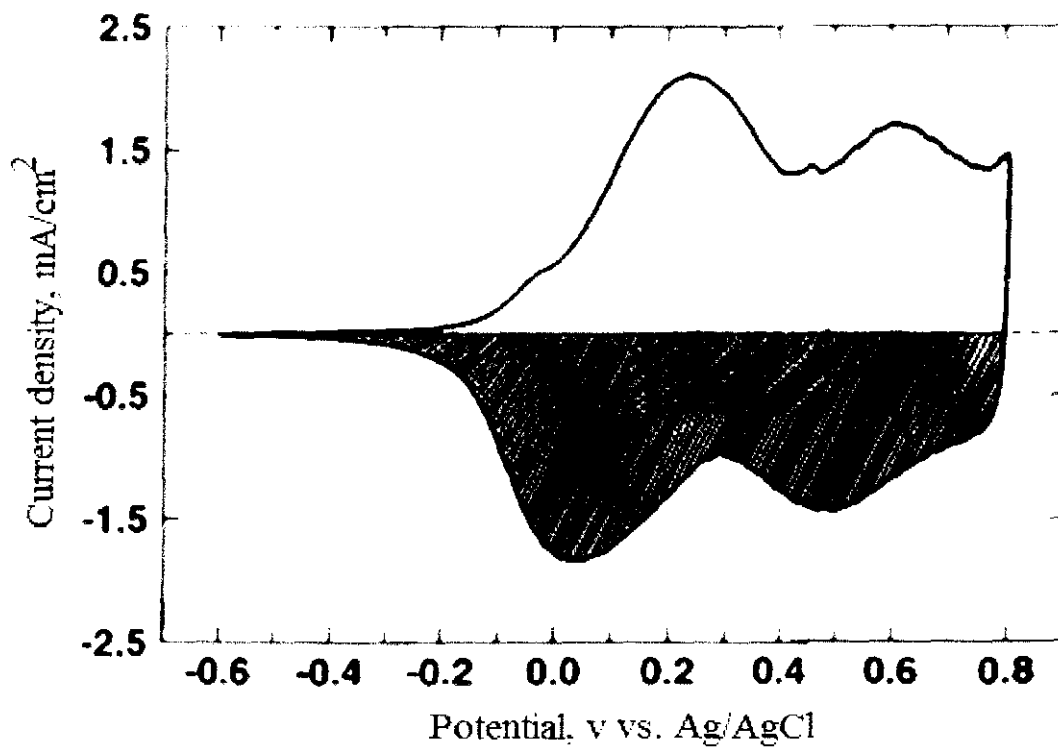


Figure 4.4: The area used to calculate CSC_c in EIROF electrode

4.2.4 The Sensitivity of IrO_x Electrode

The open circuit potential (OCP) of all fabricated pH sensors was measured versus three standard pH (4, 7, and 9) buffer solution. As shown in Figure 4.5, all sensors presented a good linear relation ($R^2=0.99$) and super-Nernstian response value in the range of -69.9 to -74.5 mg/pH unit. The different oxidation state is the main reason for the sensitivity deviations between sensors [87]. It can be concluded that pH response increased with either decreasing electrodeposition cycles or increasing scan rate. Sensor b had a faster response time due to its thinner IrO_x layer, although it was not very stable in pH 2 buffer solution. The sensitivity of the pH electrodes stayed almost constant during 6–7 weeks storage time in pH 7 buffer solution.

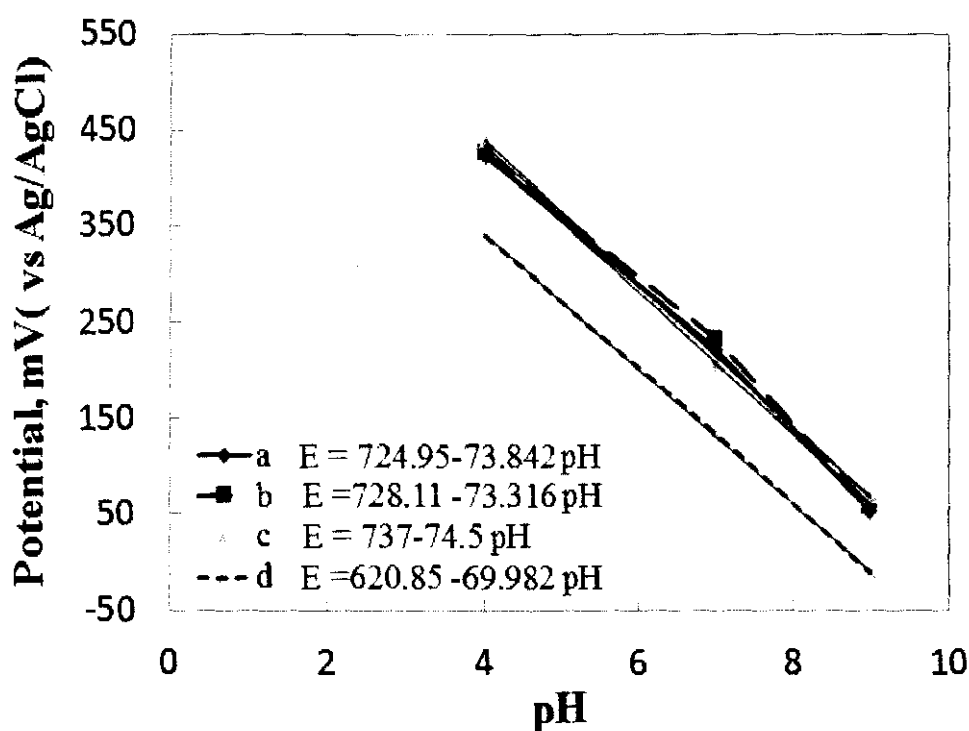


Figure 4.5: Typical potentiometric response of the EIROF electrode to a series of universal buffer solutions. . This response is in agreement with published reports for iridium oxide.(Please refer to Table 4.1 for detail of a, b, c, and d)

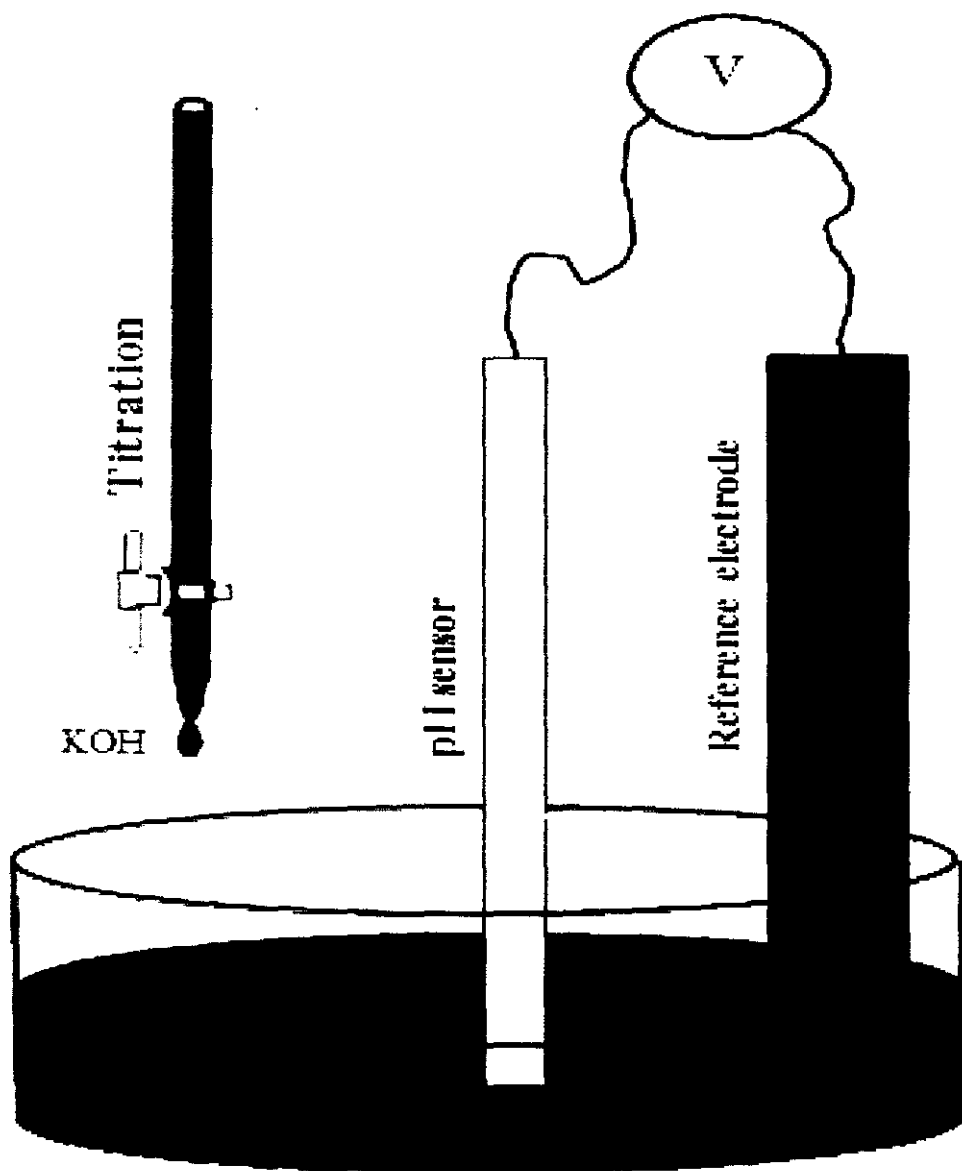


Figure 4.6: Schematic titration of IrO₂ pH sensor by adding 1M KOH to buffer solution.

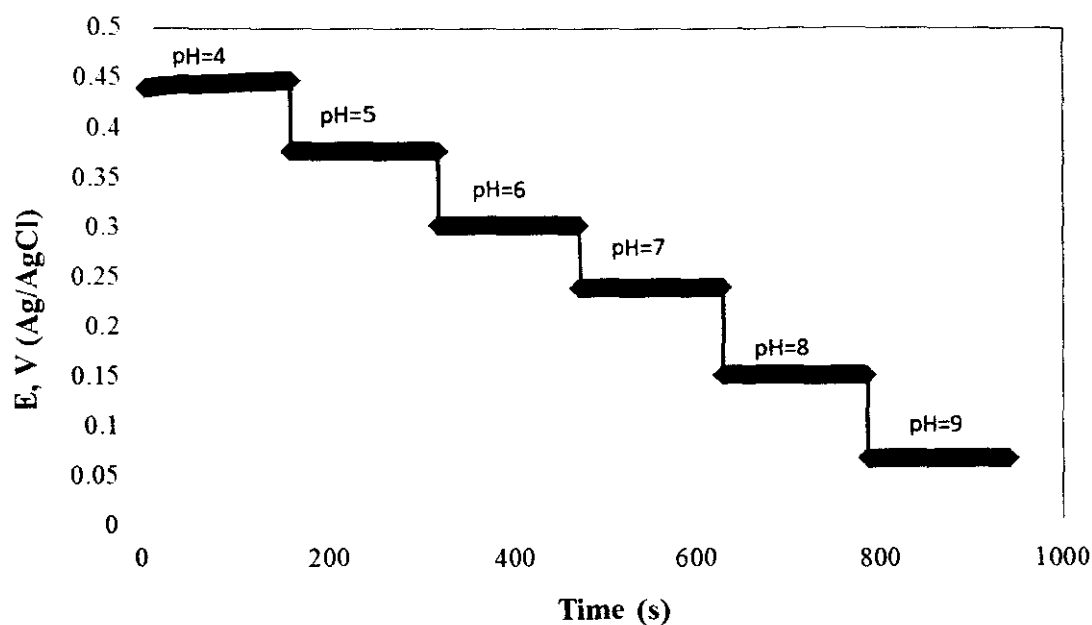


Figure 4.7: OCP response of an EIROF prepared by cyclic voltammetry on stainless steel in a universal buffer while it is titrated with KOH.

Titration experiment was done as shown in Figure 4.6. The result is depicted in Figure 4.7; OCP of iridium oxide electrode was plotted versus time with titration of 100 ml universal buffer solution with 1M KOH. The result shows a considerably constant buffer capacity in the mentioned pH range. The pH values of the buffer solution, showed in Figure 4.7, were recorded with a commercial glass electrode.

4.2.5 The Cyclic Voltammetry of IrO_x Electrode

Cyclic voltammograms of bare stainless steel and EIROF electrodes were given in Figure 4.8. The redox reactions peak of iridium oxides is indicated in CV of EIROF, which is included in the transfer of ions through the electrode/electrolyte interface. The CSC_C of the IrO₂ coated stainless steel electrodes is very larger than the bare stainless steel electrode. The CV result showed scan rate and number of cycles of CV electrodeposition method have a significant effect on cyclic voltammetry characteristics of EIROF.

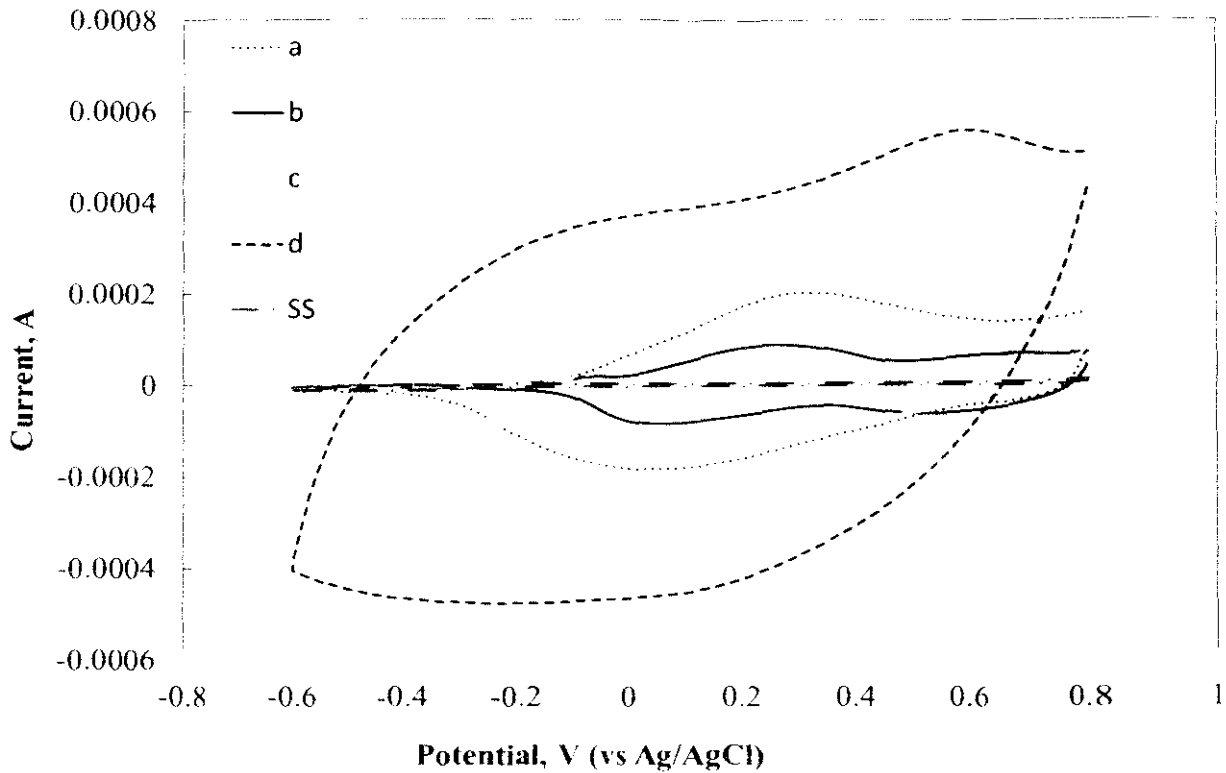


Figure 4.8: Cyclic voltammety of bare stainless steel and EIROF electrodes in pH 7 standard buffer solution at a scan rate of 50 mV/s. (Please refer to Table 4.1 for detail of a, b, c, and d)

4.2.6 The electrochemical impedances and Equivalent circuit models of IrO_x Electrode

The electrochemical impedances of bare stainless steel and EIROF electrodes in pH 7 standard buffer solution are illustrated in Figure 4.9 and 4.11. The impedance data are presented as a Nyquist plot (Figure 4.9) and Bode plots of $\log_{10}^{\text{Impedance modulus}}$ $|Z(\Omega)|$ versus $\log_{10}^{\text{Frequency (Hz)}}$ (Figure 4.11). Equivalent circuit model of fitting EIS data of Figure 4.9 is illustrated in Figure 4.10. The low coating resistor of IrO_x coating is because of its high conductivity. The benefit of iridium oxide in lowering electrode impedance is shown in these Figures.

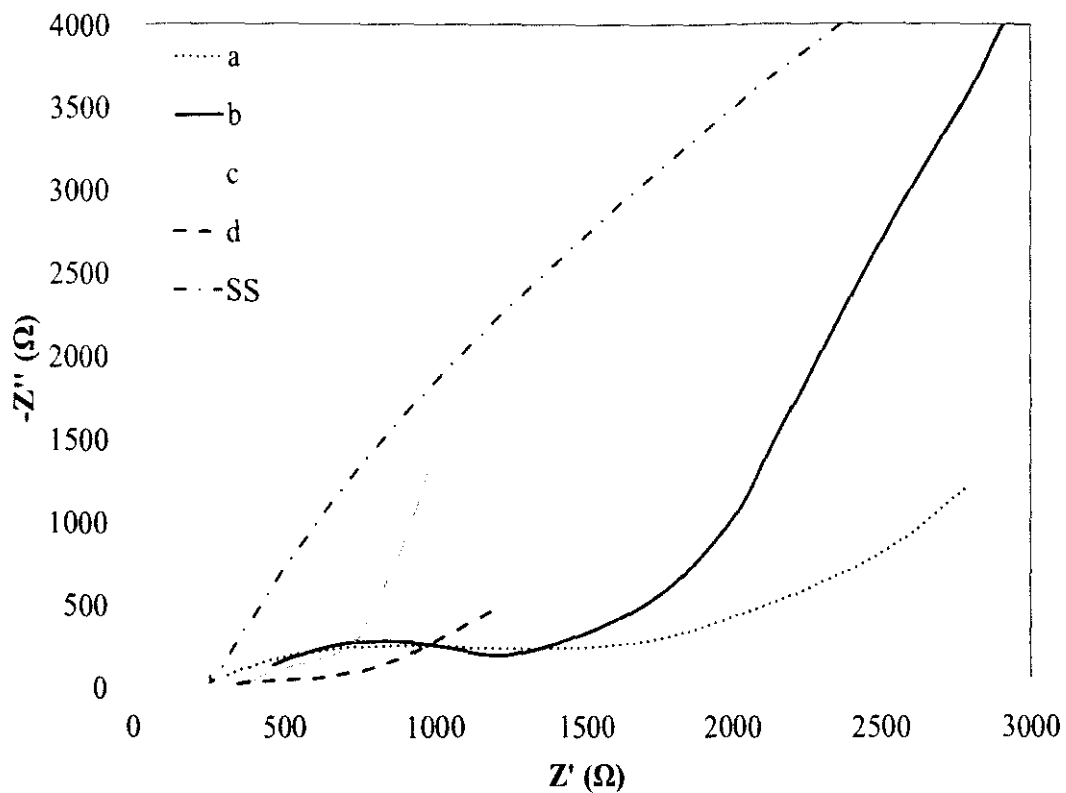


Figure 4.9: Nyquist plot of EIROF electrode on stainless steel (Please refer to Table 4.1 for detail of a, b, c, and d)

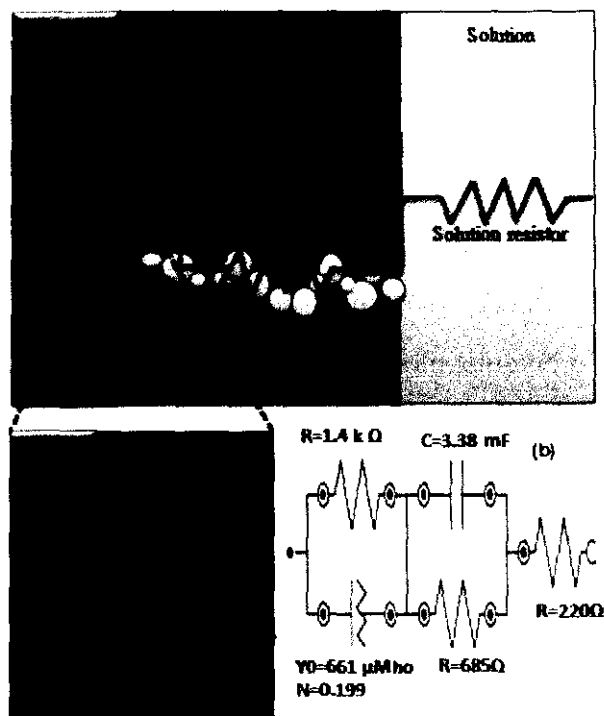


Figure 4.10: Equivalent circuit models; (a) circuit model of IrO_x coated stainless steel physical properties, (b) representing an equivalent circuit model of fitting EIS data

A constant phase element (CPE) was selected in the equivalent circuit model which shows a dispersive double layer capacitance. CPE is a substitute for normal capacitor when electrode surface is non-homogenous. The CPE impedance is represented as the following equation [9,33,65]:

$$Z_{CPE} = \frac{1}{Q(i\omega)^\alpha} \quad (4 - 2)$$

Where Q is a constant, i is the imaginary number, ω is the angular frequency and α is a parameter that has a value between 0 and 1. EIS result shows that increasing cycles have more effect on lowering impedance than increasing scan rate. Electrodes which were coated by electrodeposition at different scan rate demonstrated similar behavior in impedance recording. It is worthy to mention that at frequencies below 104 Hz, the impedance decreases with increasing film thickness.

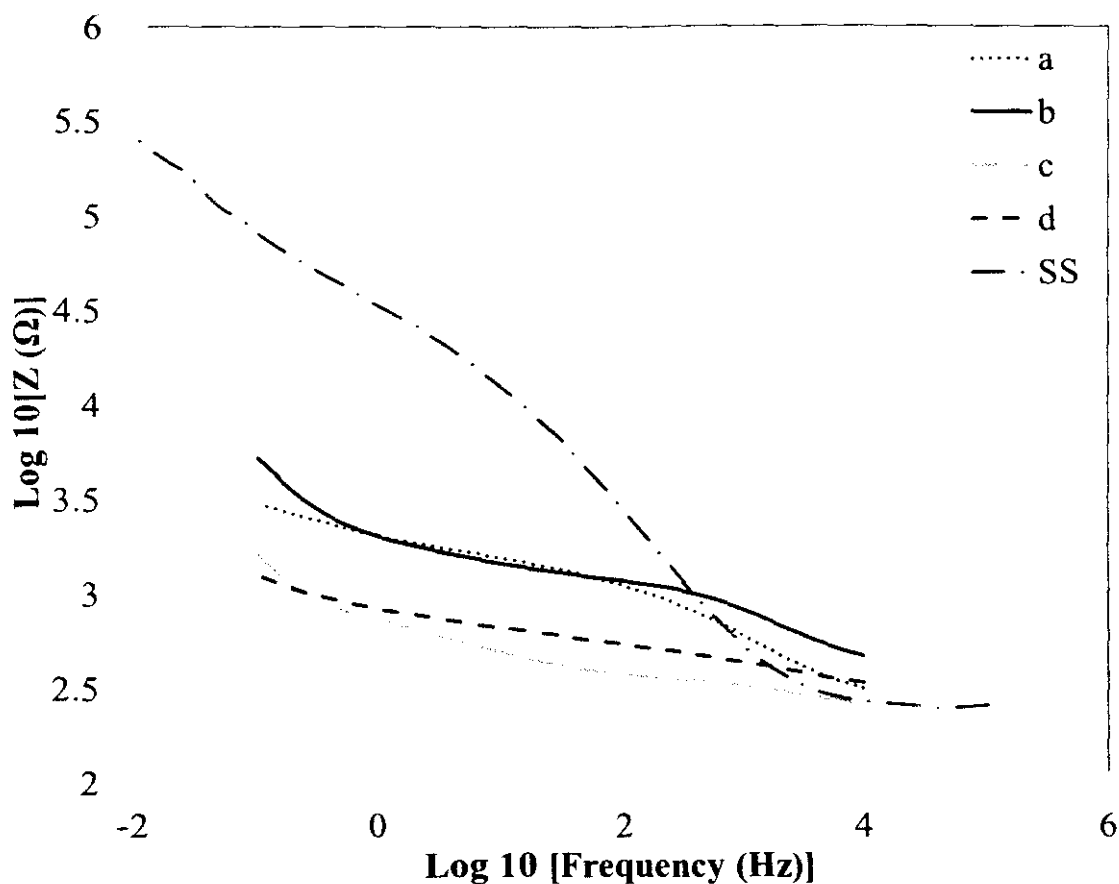


Figure 4.11: AC Impedance of bare stainless steel and EIROF electrodes as a function of cycles and scan rate (Please refer to Table 4.1 for detail of a, b, c, and d).

Surface roughness is less important for electrode materials like iridium oxide that rely on redox pseudocapacitance. The effective capacitance is determined primarily by the number and accessibility of the redox centers, not the surface area. The simplest model is to assume that charge moves rapidly through the film and that all of the centers are uniformly and easily available. If each electrode has the same thickness of deposited oxide, then the capacitance should once again scale with the geometric area.

This simple model has several important limitations. First, achieving a uniform oxide layer with a known thickness is by no means an easy task. Oxide deposition is almost certainly not uniform between electrodes or even across a single electrode. Predicting the distributions would be very difficult without careful studies using an electron microscope.

Second, the film resistivity is significant and depends on the redox state of the oxide. Some regions of the film will be much more accessible than others. The pattern of accessibility will be complex and state dependent. Third, mass transport and chemical reaction rates will play an important but difficult to model role. Despite this, it should be possible to develop models for the redox pseudocapacitance by adapting experimental and theoretical results from porous electrode theory [53,126,127].

4.2.7 The Surface Morphology of IrO_x Electrode (SEM, EDX, AFM, TEM, and XRD)

Figure 4.12 shows element maps and EDX analysis of EIROF electrodes. Iridium and Oxygen elements are shown clearly in element maps figure. A table indicating the element value is demonstrated in this Figure which shows iridium and oxygen has more weight percent in EIROF component.

FESEM images of EIROF surface are shown in Figure 4.13. The cracks that are indicated in FESEM images result from layer dehydration in the SEM vacuum chamber [128]. A cauliflower appearance was achieved in thicker films. More roughness of EIROF lead to higher surface area which results in more surface exposure to test environment and better response to pH changes.

A morphology feature of IrO_x layer taken by atomic force microscopy is shown in Figure 4.14. 3D image of the pH sensitive IrO_x layer shows that it was a unique and free of crack coating.

Micrograph of TEM in Figure 4.15 clearly shows an amorphous structure of IrO_x electrodeposited on stainless steel. As mentioned before, IrO_x are able to change its nature from amorphous oxide to crystalline oxide reversibly.

Result of XRD in Figure 4.16 confirms amorphous structure of IrO_x which was detected by TEM.

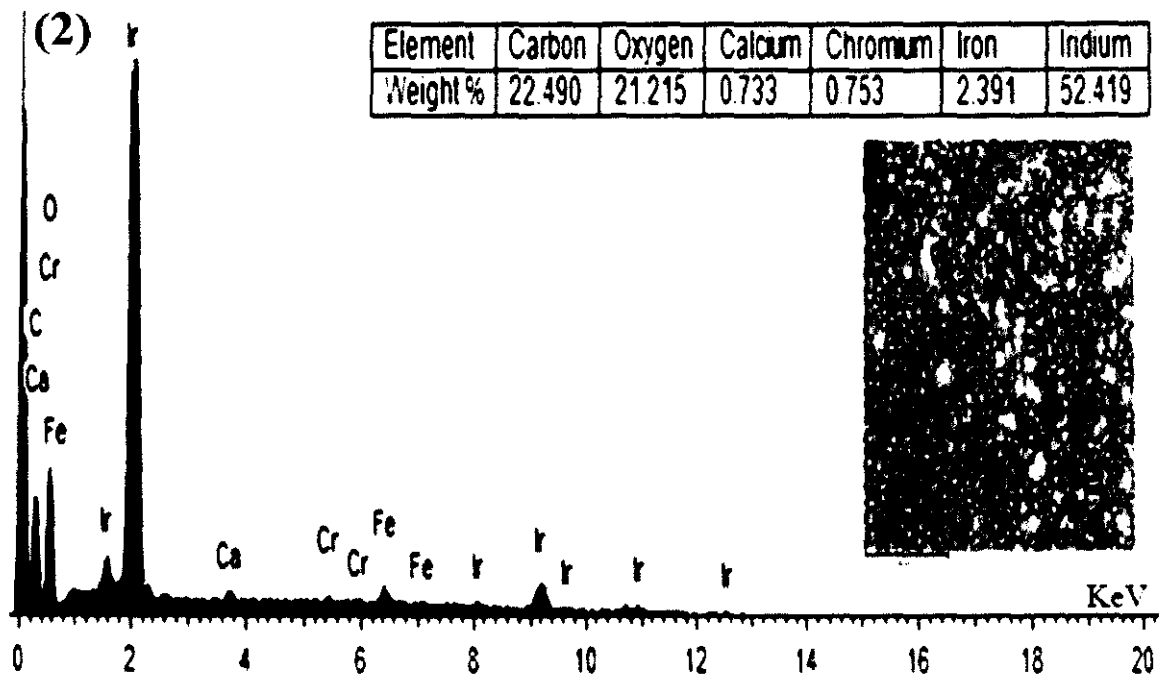
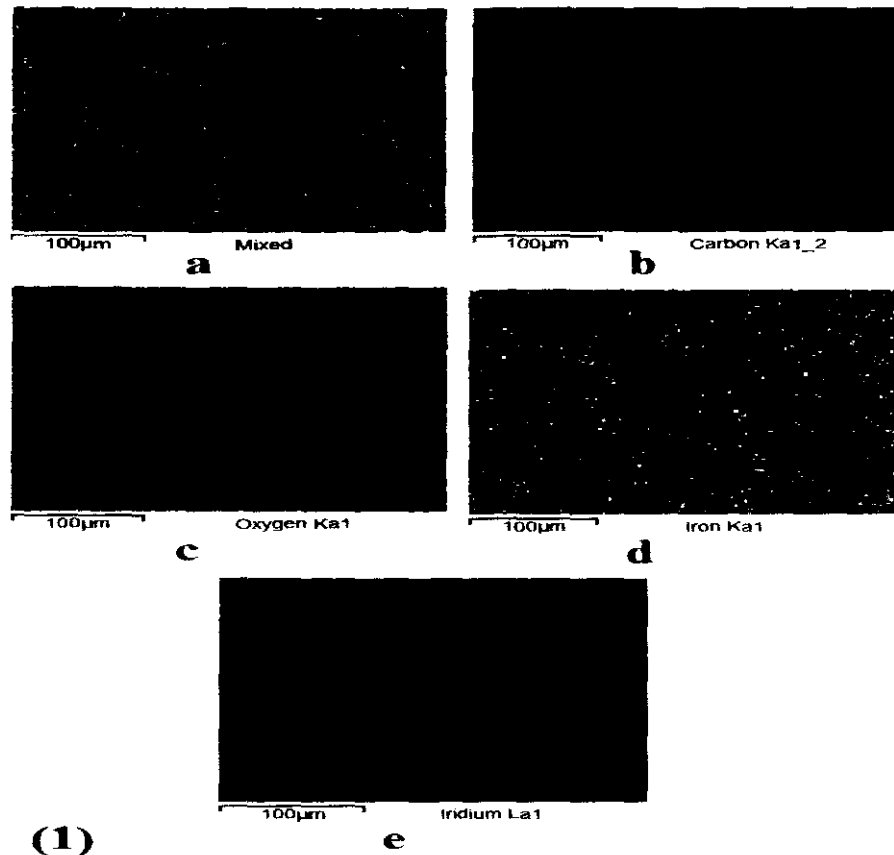


Figure4.12: (1) Element Maps of IrO₂ coated stainless steel ((a) Mixed map, (b) Carbon Ka1_2(blue), (c) Oxygen Ka1(green), (d) Iron Ka1 (black), (e) Iridium La1(red)); (2)EDX spectra of iridium oxide electrodeposited on stainless steel substrate

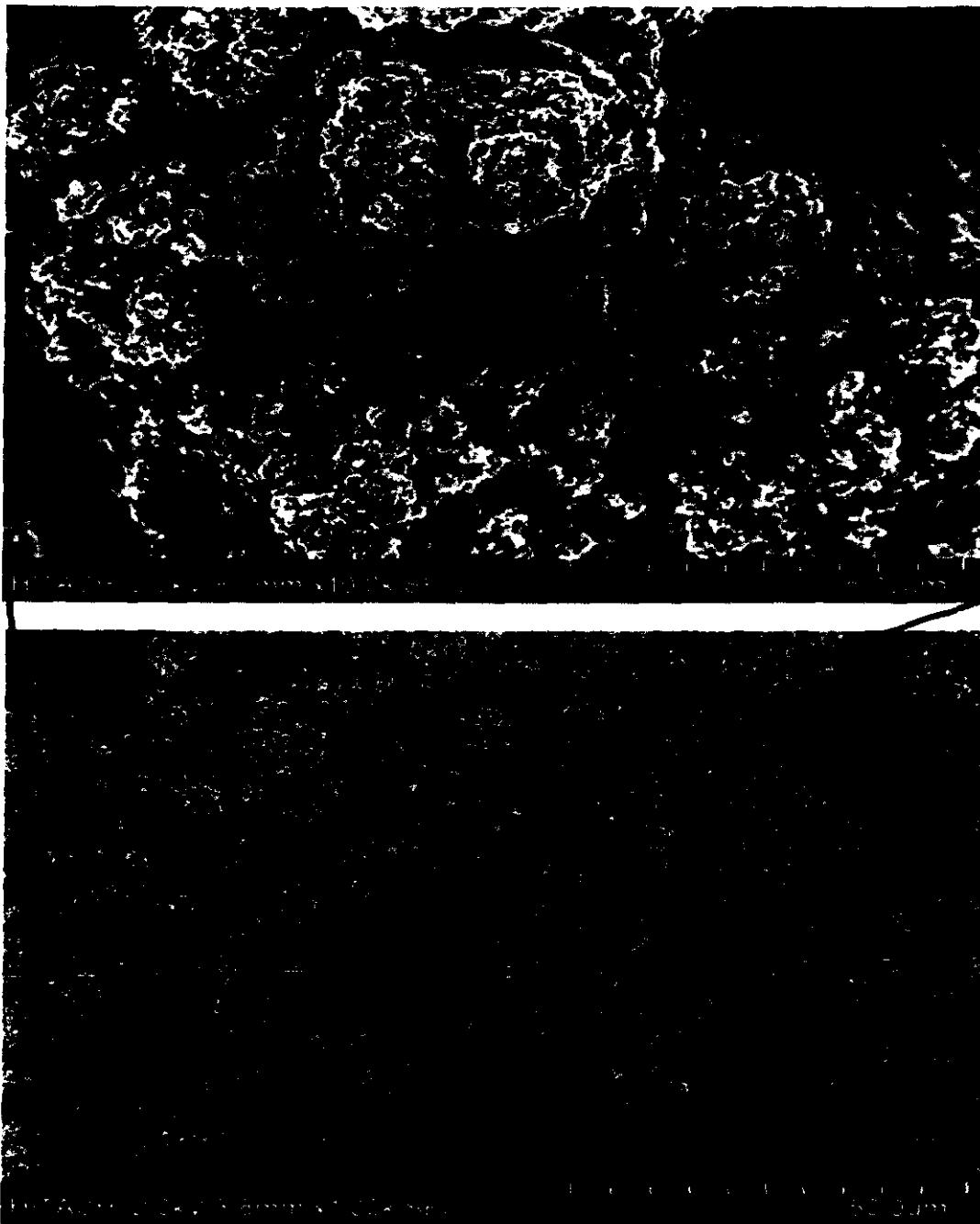


Figure 4.13: FESEM images of EIROF electrode

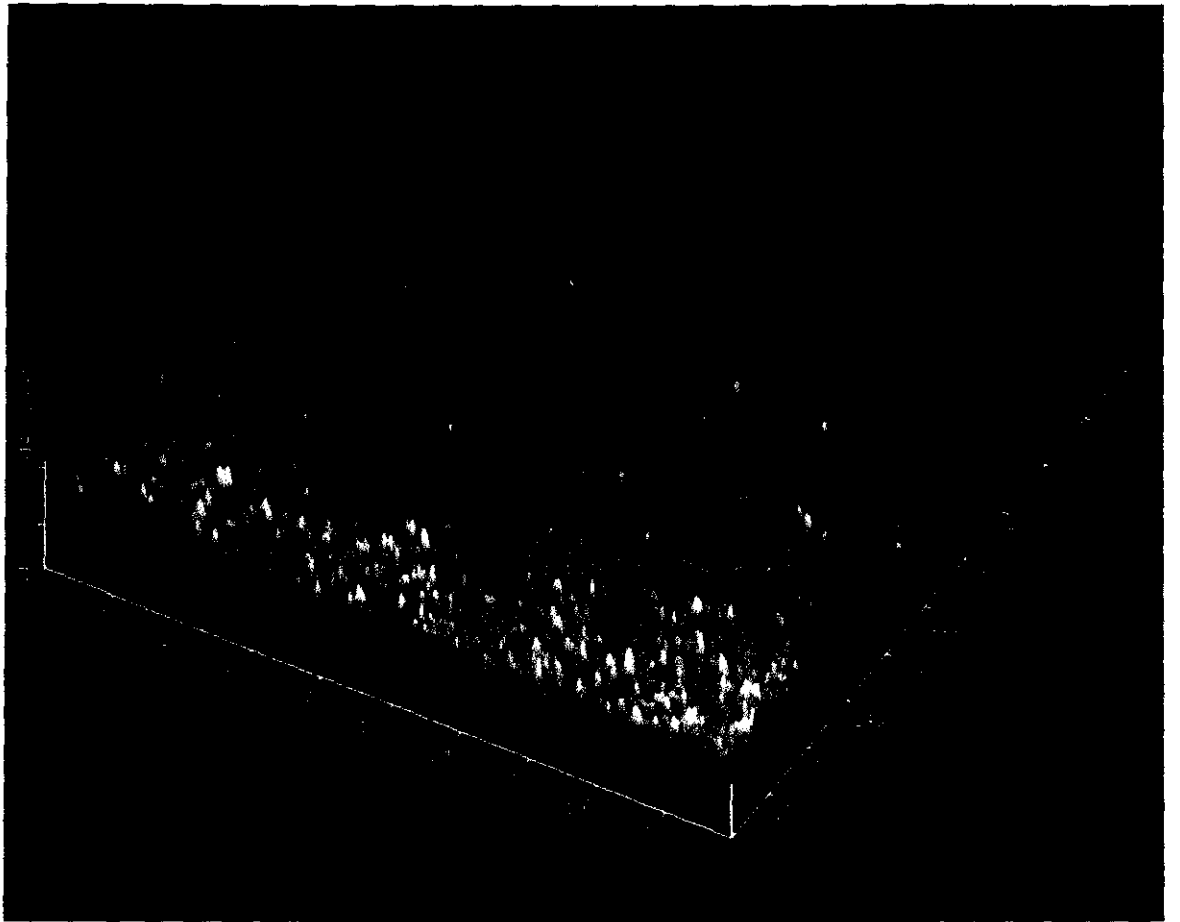


Figure 4.14: AFM image of iridium oxide fabricated by CV.



Figure 4.15: TEM images of iridium oxide electrodeposited by cyclic voltammetry

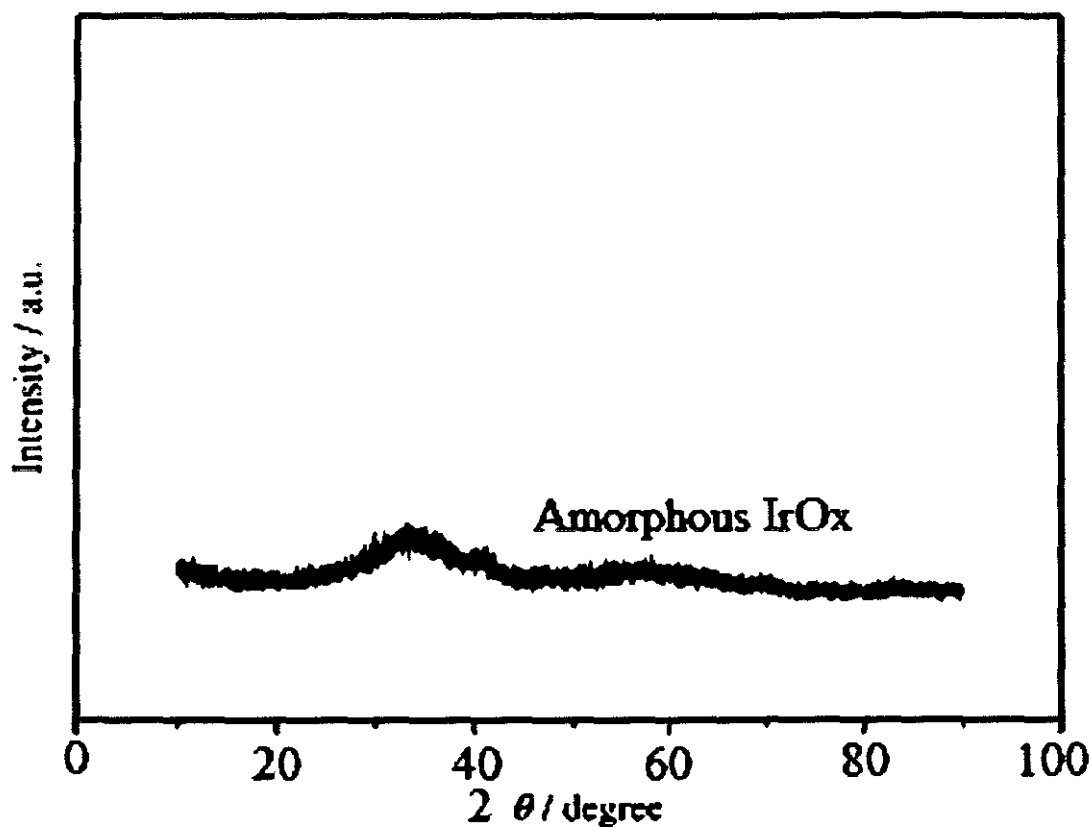


Figure 4.16: XRD result of iridium oxide electrodeposited by cyclic voltammetry

4.2.8 Stability of IrO_x Electrode

Stability is one of the essential characteristics of pH sensors. The fabricated IrO_x electrode exhibited both good mechanical stability as well as electrochemical stability. The cyclic voltammograms of the IrO_x electrode stayed almost unchanged before and after mechanical stability tests. A small change cyclic voltammetry was detected after ultrasonic bath. The result of ultrasonic test is depicted in Figure 4.17.

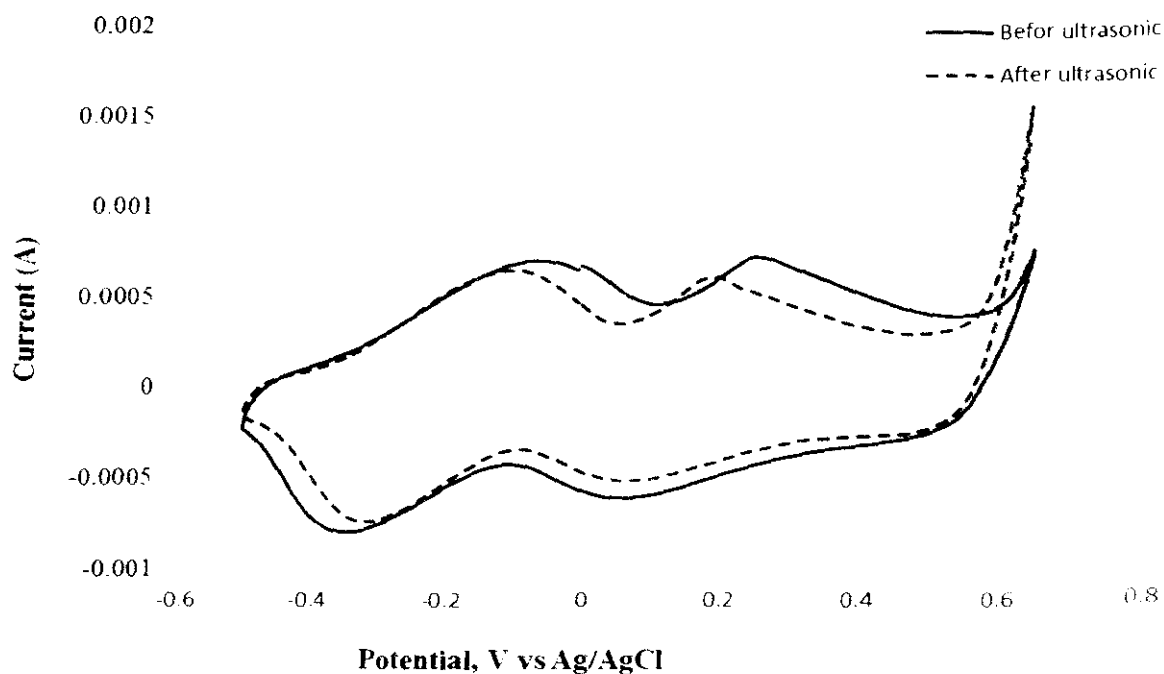


Figure 4.17: Cyclic voltammograms of IrO_x electrode before and after ultrasonic test

4.2.9 Conclusion

Iridium oxide was electrodeposited on a stainless steel substrate by the cyclic voltammetry method. The effect of cycle number and scan rates on iridium oxide characterization was investigated. A blue and homogeneous surface was observed after electrodeposition in all cases.

All fabricated pH sensor had a super-Nernstian response value in the range of -69.9 to -74.5 mV/pH unit. Thinner pH sensors showed faster pH response.

Electrochemical results indicated iridium oxide decreased electrode impedance which was in direct relation with its thickness. Cycle numbers have more effect on EIROF electrode characteristics than scan rate. Low resistance of IrO_x in the equivalent circuit models is an evidence for high electrical conductivity of EIROF.

The result of this part convinced us we need to pay more attention on variable factors such as scan rate, number of cycle and temperature which have effect on electrodeposition of IrO_x on stainless steel. We investigated these factors by an statistical tool in next part.

4.3 Statistical investigation of iridium oxide electrodeposition on stainless steel

4.3.1 Fabrication of pH electrodes

In this part, twenty IrO_x electrodes were fabricated according to experimental design proposed in Table 4.2. Method and material of fabrication these electrodes are mentioned in section 4.2. Electrochemical, morphological, and statistical characterization were done as discussed in follows.

4.3.2 Open-Circuit Potential Response

A typical open-circuit potential response of the electrodeposited IrO_x electrodes to the standard buffer solutions is shown in Figure 4.18. The potential response is measured at three universal pH values (4, 7, and 9). Electrodes no. 1 to no. 20 are indicated by the numbers 1 to 20, respectively. Graph 1 in figure (a) presents electrodes No. 1 to No. 6 placed under similar experimental conditions. Tables 3.1 and 4.2 provide additional information on the experimental conditions of each electrode. For all electrodes, a straight line is fitted through the measurement data with a slope ranging from -49 mV/pH to -81 mV/pH and a correlation coefficient > 0.9. Electrodes No. 19 and 10 showed deviation from a straight line which issued due to coating delamination in order to experimental error in electrode fabrication or preparation process.

Runs from 1 to 6 were performed to determine the reproducibility of the fabricated electrode in this study. As shown in Figure 4.18, all electrodes show the same super-Nernstian response values ranging from 78 mV/pH to 81 mV/pH. Table 4.2 also reveals that all electrodes exhibit the same coating thicknesses.

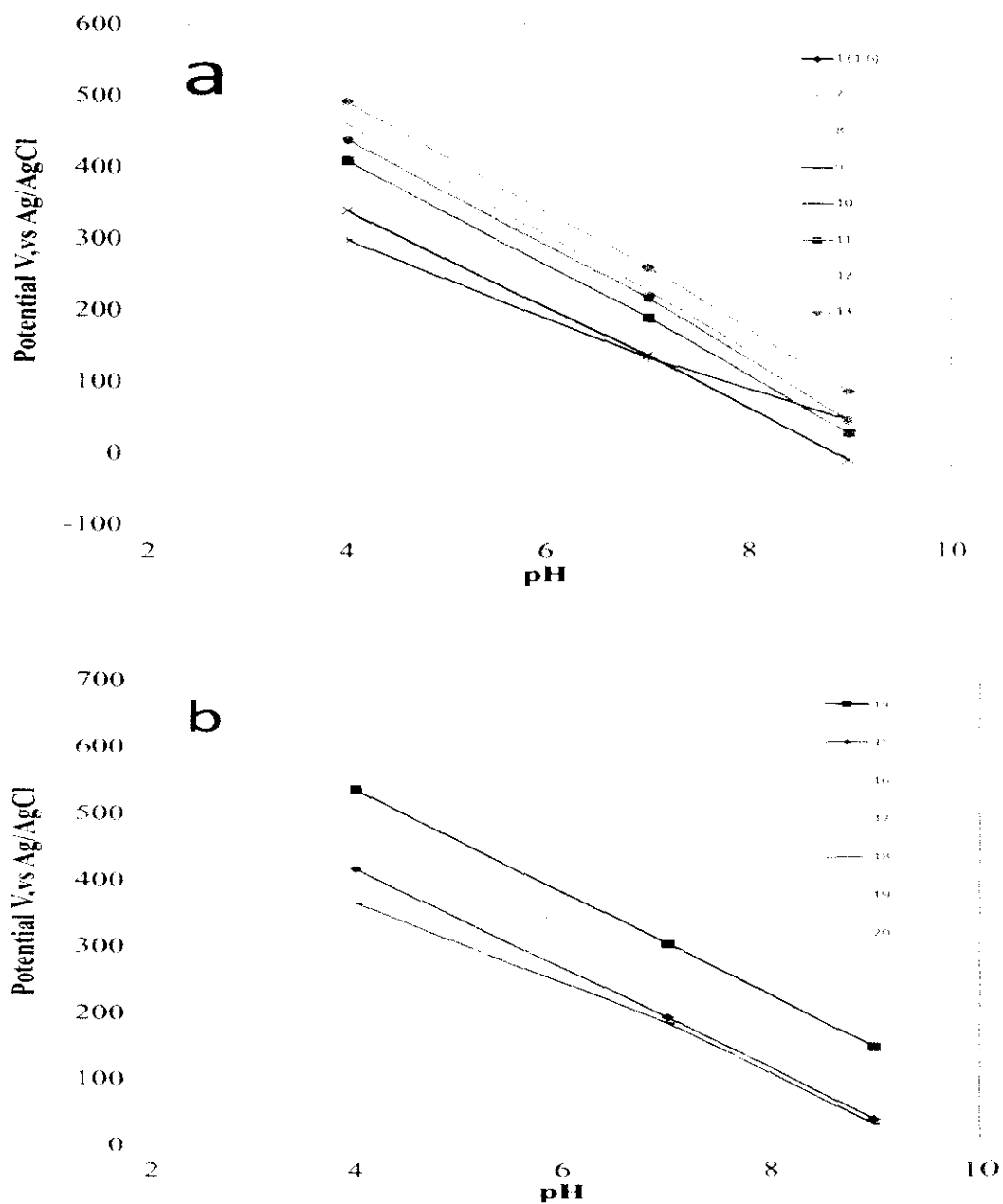


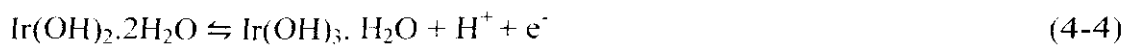
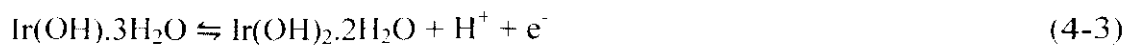
Figure 4.18: (a) and (b). Equilibrium potential as a function of pH for electrodeposited IrO_x films on stainless steel substrates deposited at different scan rates, temperatures, and number of cycles by cyclic voltammetry (CV).

Table 4.2: Experimental design and actual response of the thickness and pH sensitivity of pH electrode.

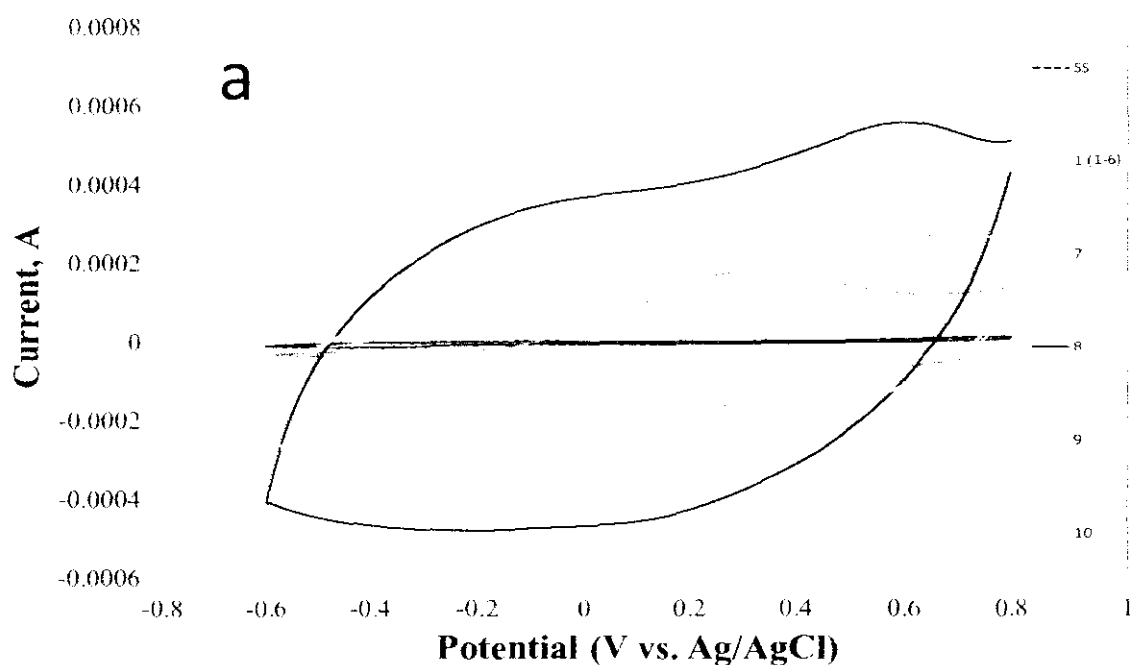
Design points	Point type	Variables in coded levels			H: Thickness (nm)	Sensitivity (mV/pH)	CSC _C (mC/cm ²) x10 ⁻⁴
		A:Scan Rate (mV/s)	B:T (°C)	C:Cycle (cycle)			
1	Center	0	0	0	815	-73.02	5.05
2	Center	0	0	0	815	-73.02	5.05
3	Center	0	0	0	815	-73.02	5.05
4	Center	0	0	0	815	-73.02	5.05
5	Center	0	0	0	815	-73.02	5.05
6	Center	0	0	0	815	-73.02	5.05
7	Axial	0	-0.5	0	500	-70.32	2.9
8	Axial	0	0.5	0	1380	-75.25	14.8
9	Axial	0	0	-0.5	810	-80.81	6.33
10	Axial	0	0	0.5	1180	-80.39	7.3
11	Axial	0.5	0	0	663	-79.76	4.1
12	Axial	-0.5	0	0	918	-71.71	5.67
13	Fact	-1	-1	1	1780	-69.98	10.385
14	Fact	-1	1	1	3025	-49.38	18.74
15	Fact	1	1	1	640	-68.73	3.95
16	Fact	-1	1	-1	1010	-69.56	6.25
17	Fact	1	1	-1	890	-76.51	5.5
18	Fact	1	-1	1	320	-74.5	2.05
19	Fact	-1	-1	-1	437	-73.84	2.7
20	Fact	1	-1	-1	181	-73.31	1.16

4.3.3 Cyclic voltammetry of IrO_x electrodes

Figure 4.19 demonstrates the CV results of bare stainless steel and electrodeposited IrO_x film (EIROF) electrodes in a pH 7 universal buffer solution at a scan rate of 50 mV/s. Electrodes No. 1 to No. 20 are indicated by the numbers 1 to 20, respectively. Graph 1 in Figure 4.19 (a) presents electrodes no.1 to no. 6 placed under similar experimental conditions. Tables 3.1 and 4.2 provide additional information on the experimental conditions of each electrode. The CV experiments were performed in the potential range of -0.6 V to 0.8 V (vs. Ag/AgCl) to prevent IrO₂ destruction at higher potentials. The indicated peaks of the CV curves are related to the successive monoelectronic oxidation of iridium from Ir^I to Ir^{IV}, as expressed in the following reactions [61]:



The area under the EIROF CV was significantly larger than the area under the stainless steel substrate CV, which is related to the significant charge storage capacity after electrodeposition [33]. Despite the superior charge storage capacity resulting from the decrease in scan rate and the increase in the number of cycles, an unstable electrochemical behavior was observed for some electrodes with thick IrO_x (refer to electrodes No. 8 and 13). Electrode no. 14 was not used in the CV experiment because of its very thick layer, which is prone to coating delamination.



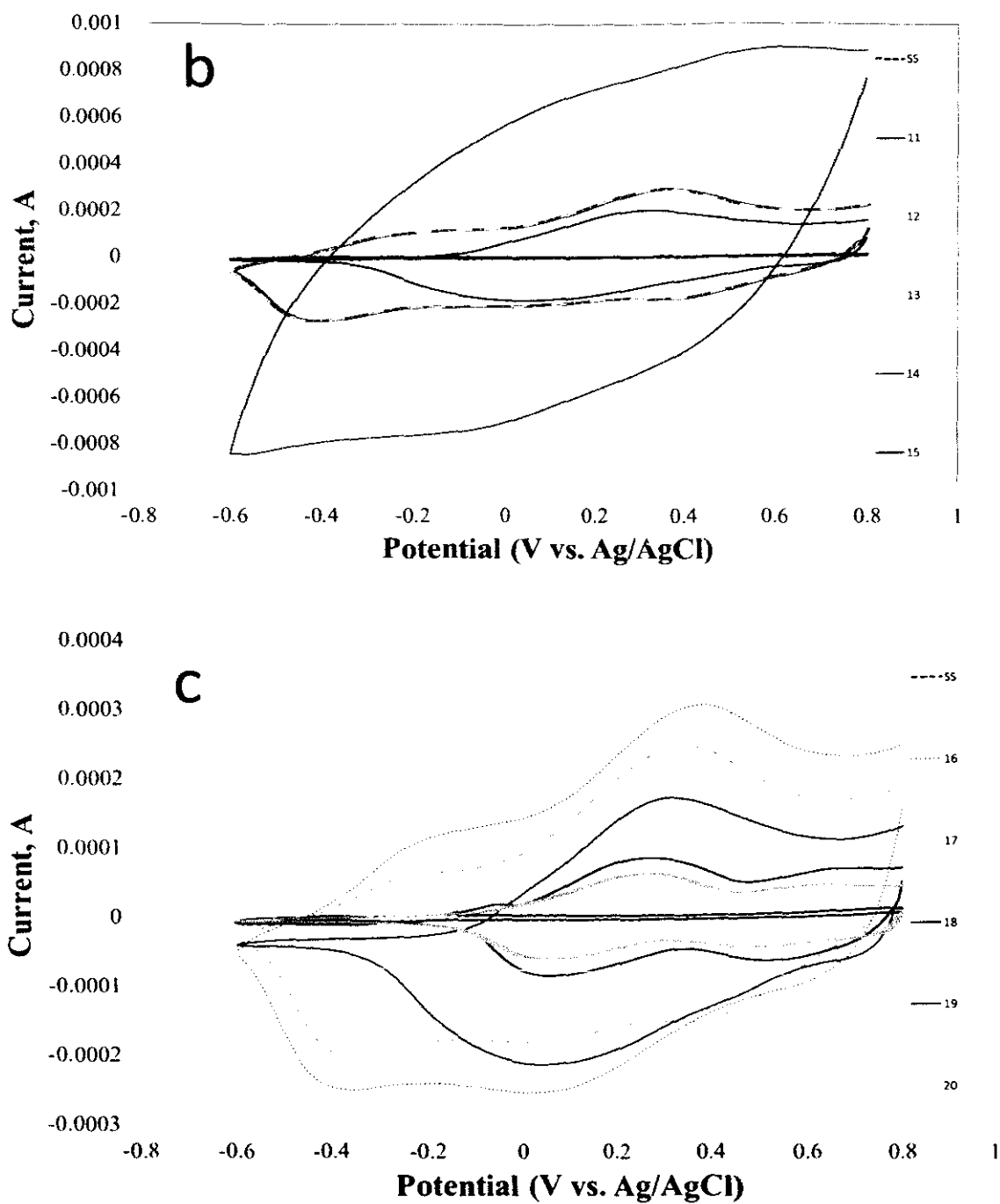
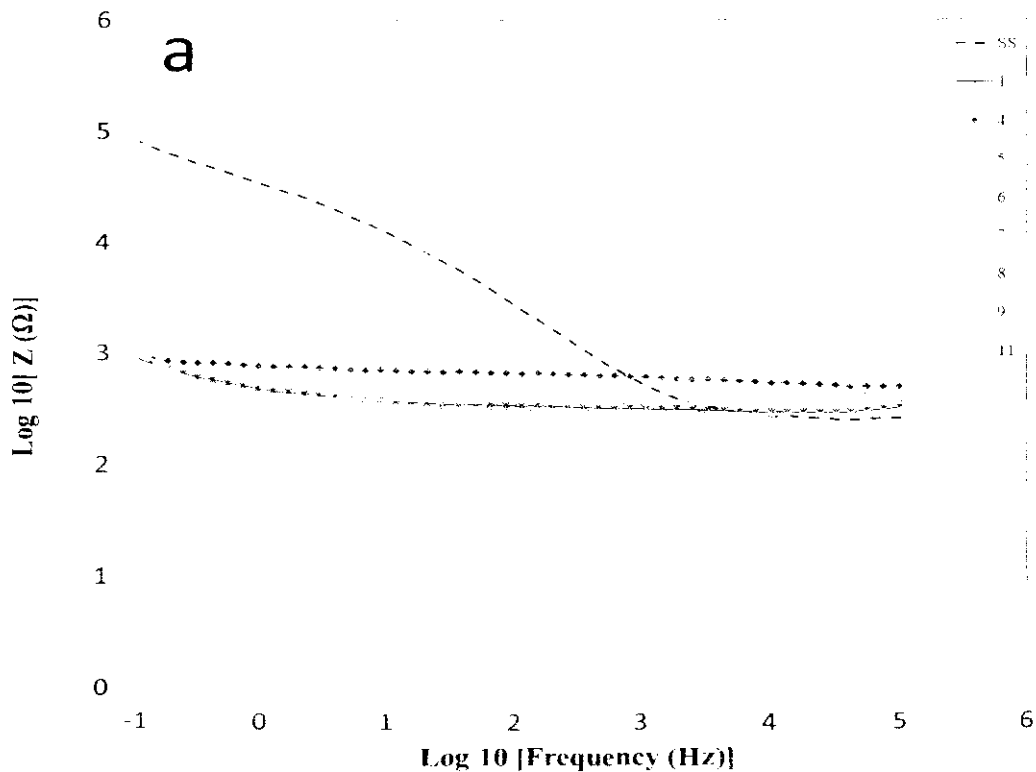


Figure 4.19: Cyclic voltammetry results of bare stainless steel and EIROF electrodes in a pH 7 universal buffer solution at a scan rate of 50 mV/s are shown in a, b, and c. SS = stainless steel electrode without coating.

4.3.4 Electrochemical Impedance Spectroscopy of IrO_x electrodes

Figure 4.20 shows the impedance module with respect to the frequency of bare stainless steel and IrO_x electrodeposited electrodes. Electrodes no. 1 to no. 20 is indicated by the numbers 1 to 20, respectively. Graph 1 in Figure 4.20 (a) presents electrodes no. 1 to no. 6 placed under similar experimental conditions. Tables 3.1 and 3.2 provide additional information on the experimental condition of each electrode. As indicated, the impedance of stainless steel decreased after IrO_x accumulation on the electrode surface for all IrO_x electrodes. Therefore, highly accessible redox sites are observed in the film because of the effective development of the film structure [68]. Lowest impedance is related to oxide film thickness [129], which is in agreement with the CV and RSM results.

More detail regarding to EIS properties and equivalent circuit of IrO_x is discussed in section 4.2.6.



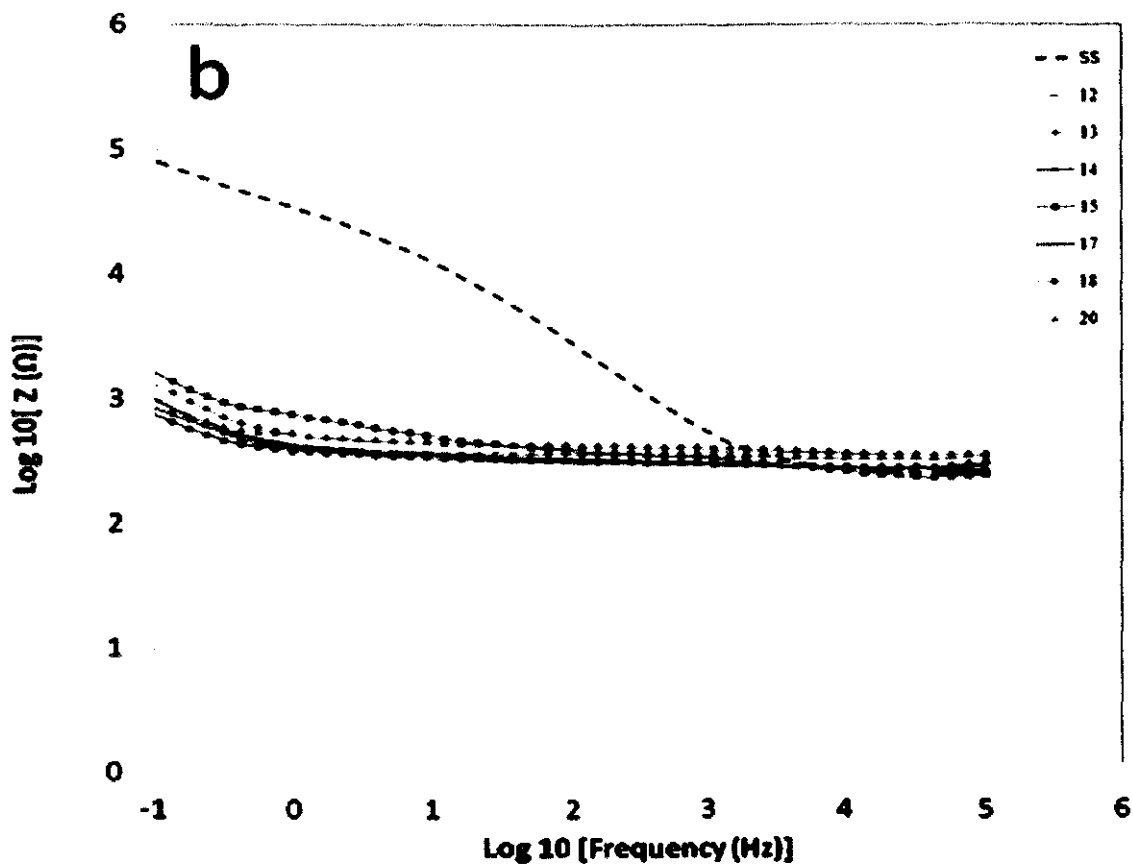


Figure 4.20: (a) and (b), A Bode plot showing the total impedance module versus the frequency of bare stainless steel and IrO_x electrodeposited on stainless steel electrodes. SS = stainless steel electrode without coating.

4.3.5 SEM and EDX of IrO_x electrodes

Figure 4.21 shows EDX result of one of IrO_x electrode which approve IrO_x coating on stainless steel substrate.

The FESEM images in Figure 4.22 reveal that the electrodeposited layer becomes more prone to cracking as the number of cycles increases, leading to thicker IrO_x film. It was not observed any significant changes in SEM image of different electrode. Just a cauli flower appearance was achieved in thicker films. Thicker IrO_x film also shown some crack due to fast drying and dehydration of IrO_x film in SEM vacuum chamber which this effect can be reduced by slow drying process in room temperature [128].

This phenomenon clearly indicates that dehydration occurs more slowly in thicker layers than in thinner layers. Thus, more cracks are observed under fast-drying high-vacuum FESEM conditions.

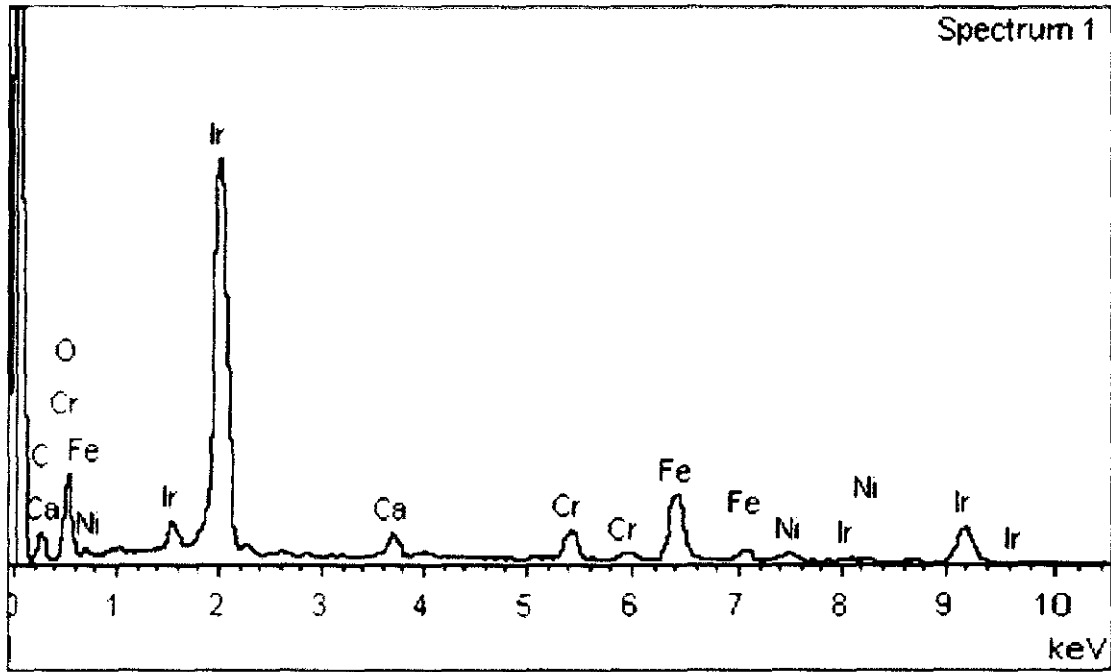


Figure 4.21: EDX result of IrO_x on stainless steel

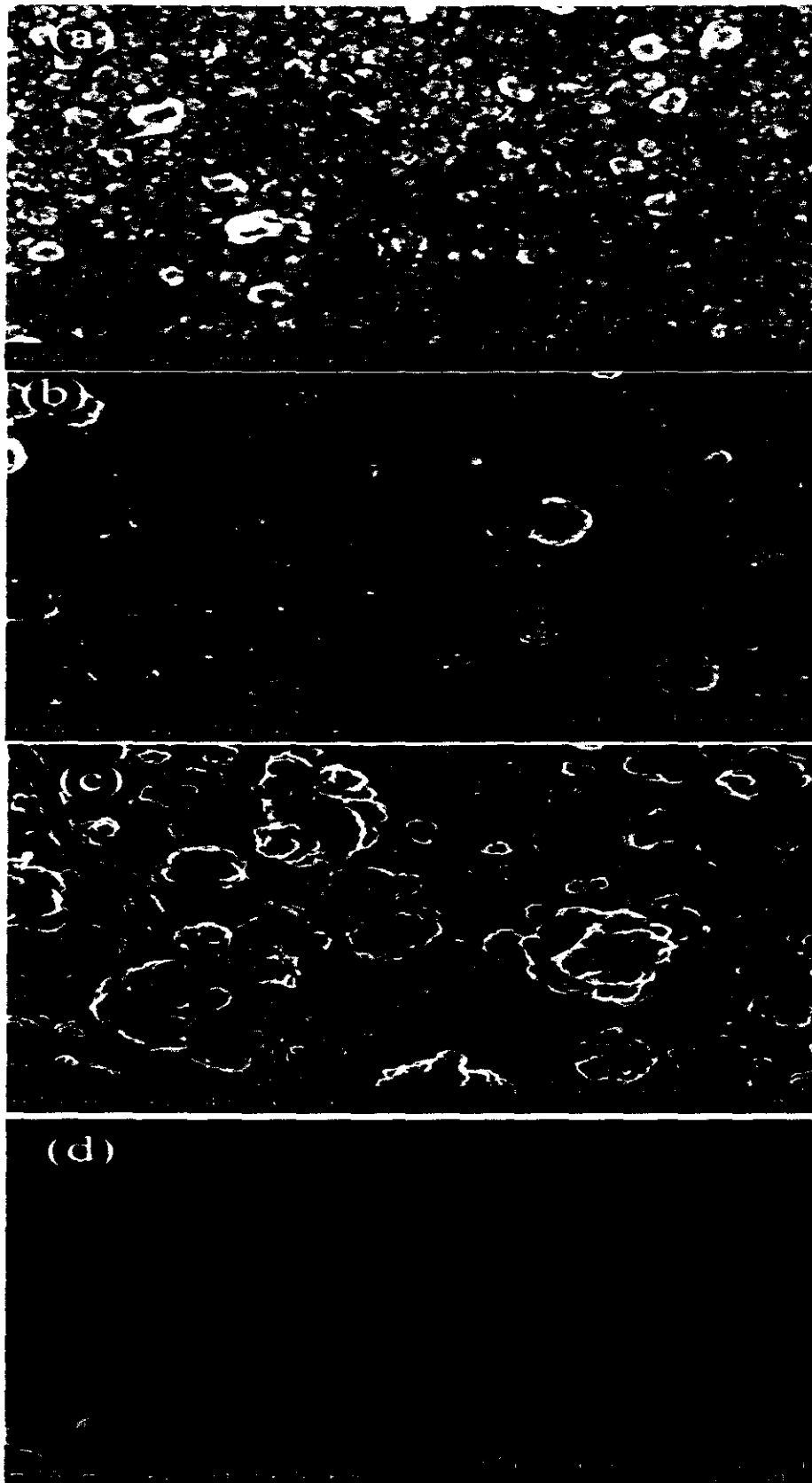


Figure 4.22: FESEM images of IrO_x electrodeposited layer with an increasing number of cycles. (a) 100, (b) 200, (c) 400, and (d) 500.

4.3.6 Response surface methodology model equations

In this study, RSM was used to design experiments and investigate the effect of independent variables such as scan rate, temperature, and cycles on three responses: IrO₂ coating thickness, pH electrode sensitivity, and Cathodic Storage Charge Capacity (CSC_C). The RSM result showed no significant relationship between the independent variables and pH electrode sensitivity, which is consistent with previous findings [102,129]. CSC_C is directly related to IrO_x thickness [129]; thus, the DOE software was solely used to examine coded experimental model equations of IrO_x thickness and the interaction of the significant terms in the proposed model.

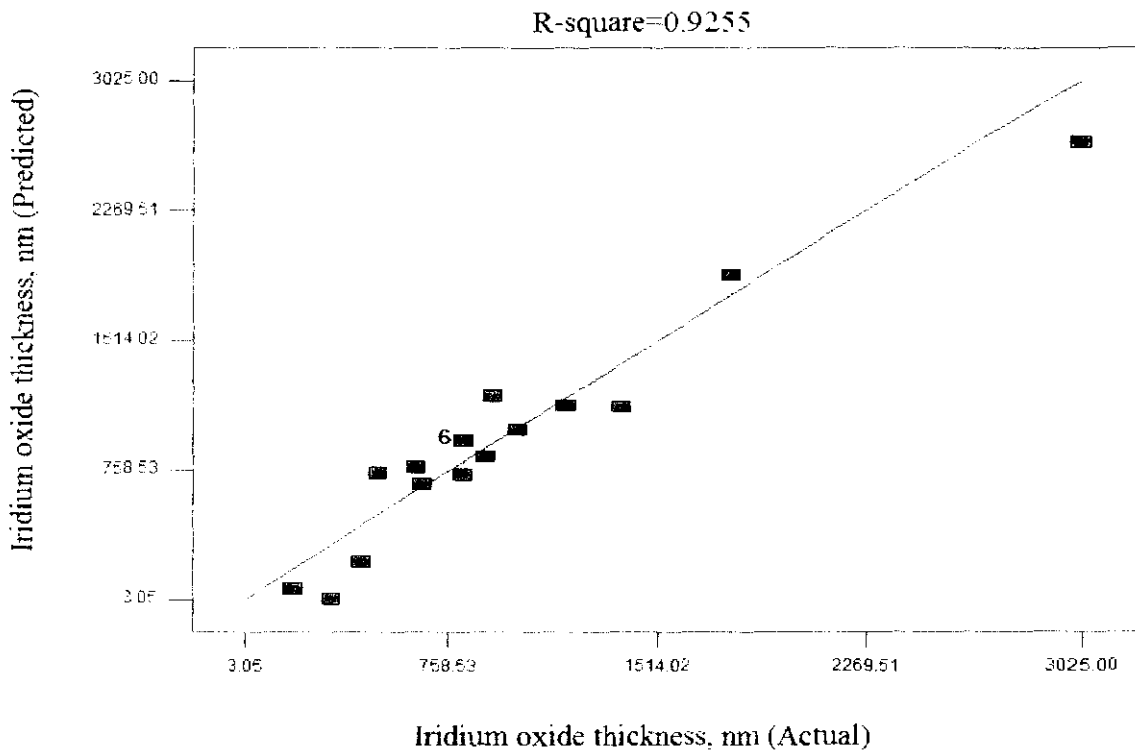


Figure4.23: Actual versus predicted response plot of the IrO_x coating thickness

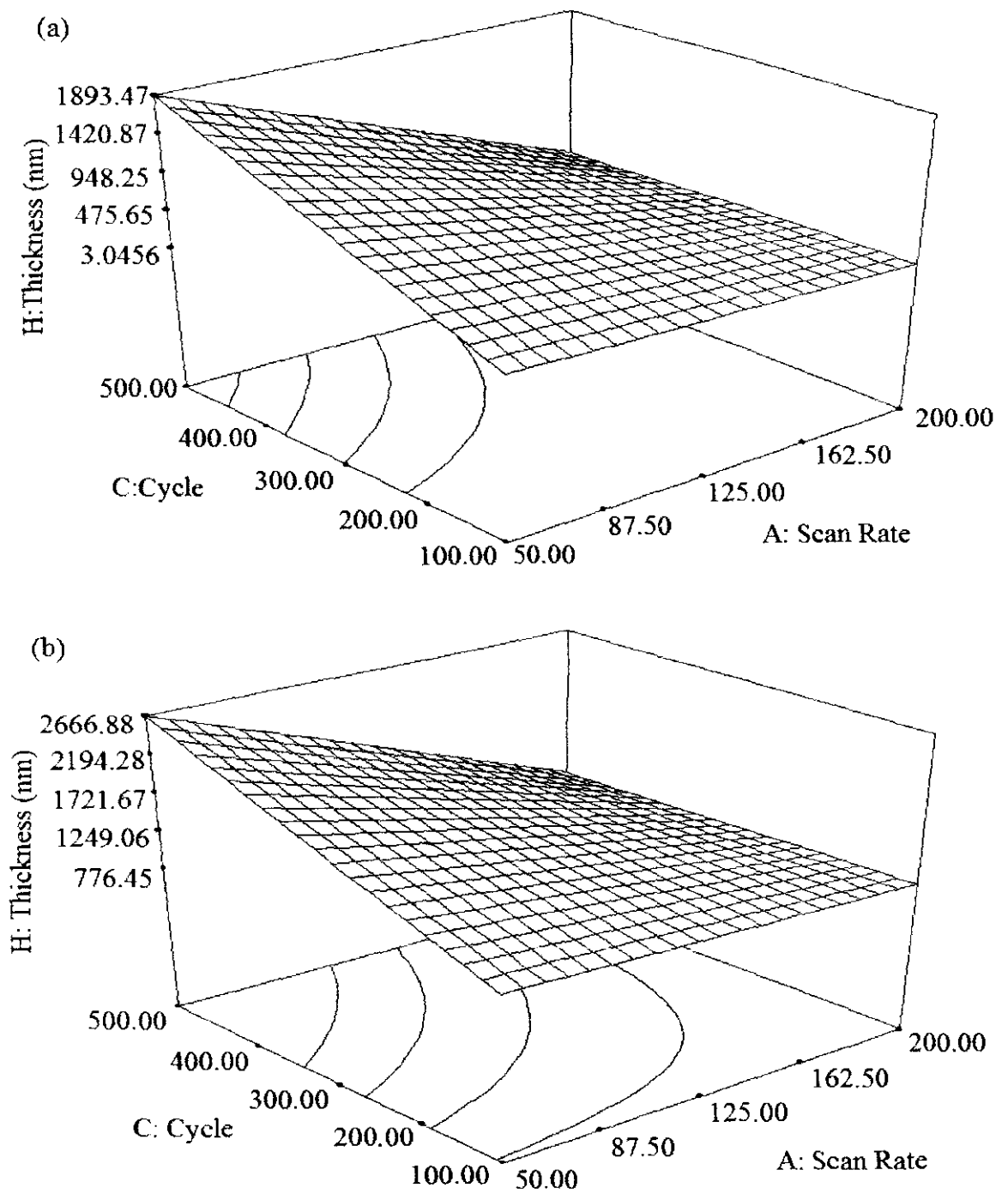
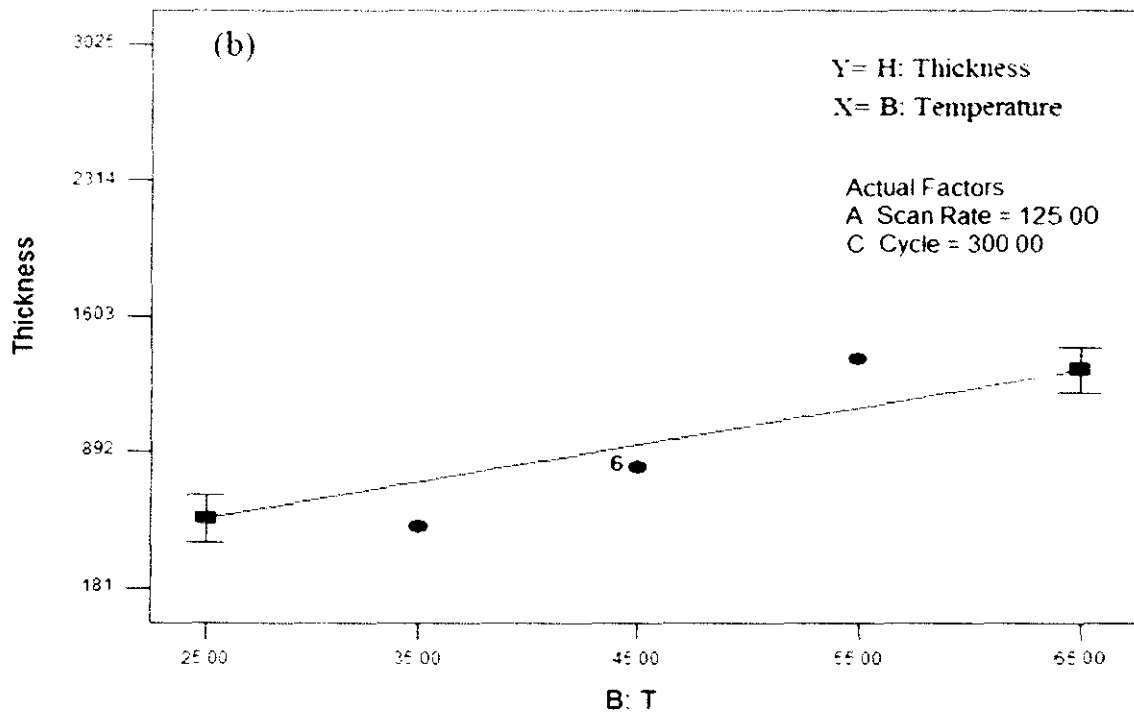
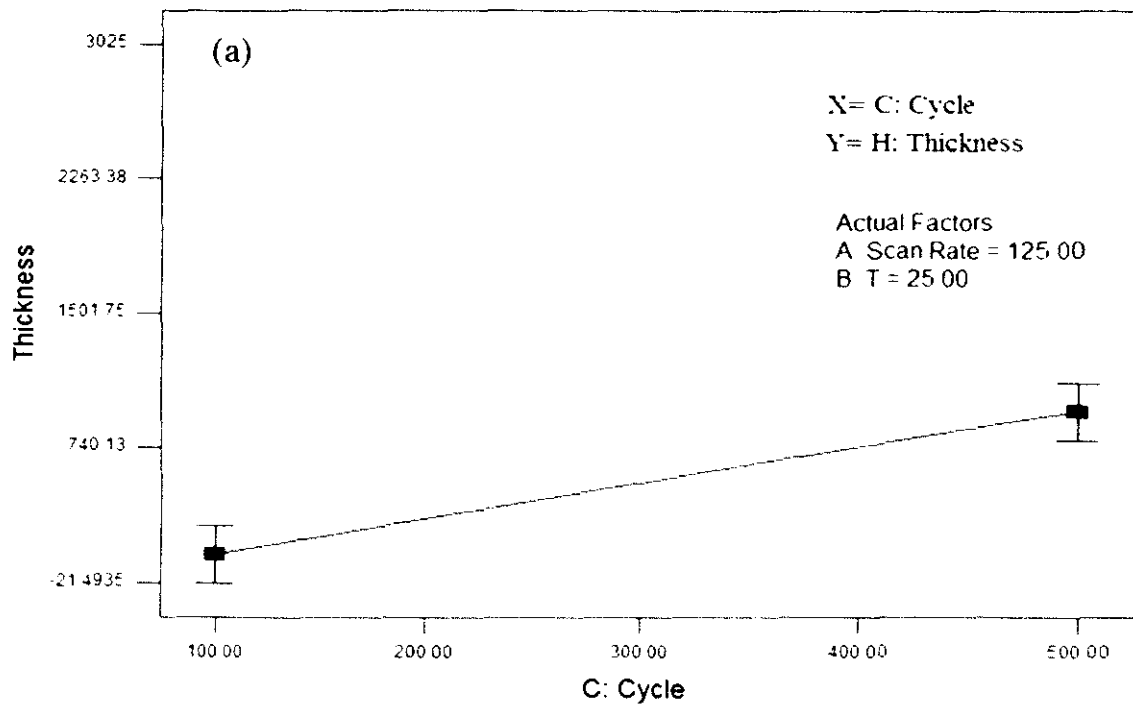


Figure 4.24: Response surface and contour plot of IrO_x coating thickness (nm) as a function of the number of cycles and scan rate (mV/s) at minimum and maximum temperatures: (a) 25 °C (b) 65 °C.



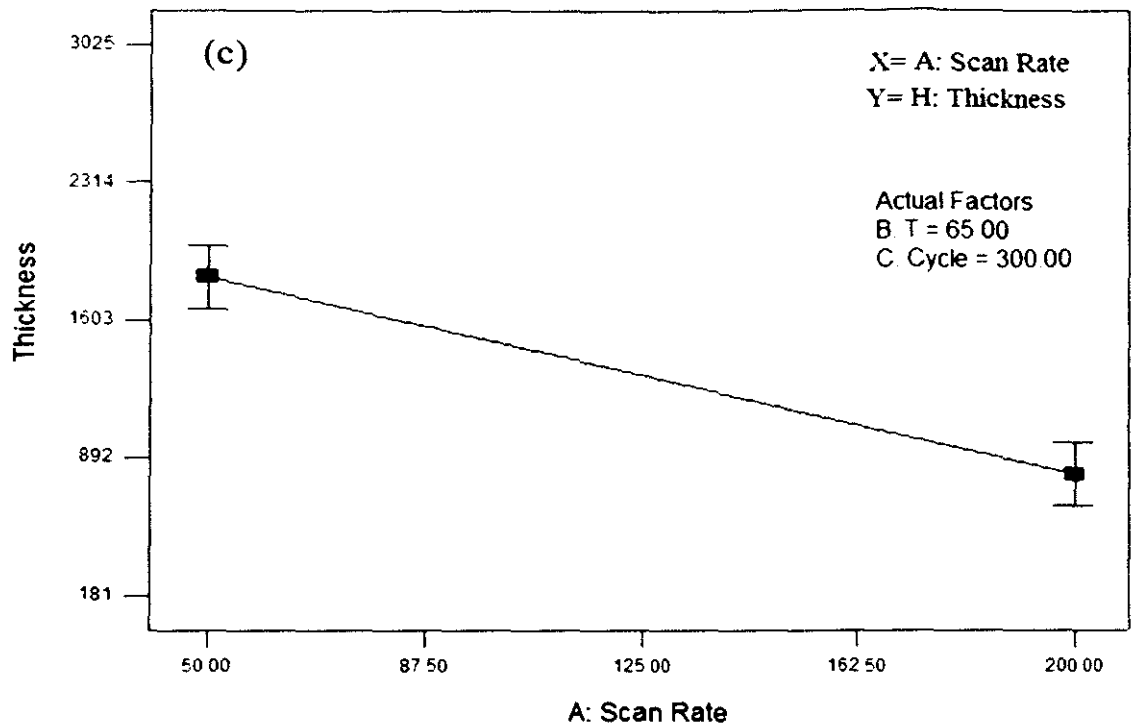


Figure 4.25: Changes in IrO_x coating thickness (nm) with different variables: (a) cycle (b) Temperature (°C) and (c) Scan rate (mV/s).

4.3.7 Coded experimental model equations for oxide thickness

The DOE software suggested a 2FI model considering the adjusted R-squared and the predicted R-squared rather than other models, as depicted in Table 4.3.

The regression model for IrO_x thickness, in coded factors, is shown by the following 2FI model equation:

$$H = 931.20 - (511.59A) + (386.71B) + (403.76C) - (98.63AB) - (433.63AC) + (35.37BC) \quad (4-6)$$

where H is the IrO_x thickness (nm). A, B, and C represent the scan rate, temperature, and number of cycles, respectively.

As shown in Table 4.4, the predicted R² of 0.2651 is not as close to the adjusted R² of 0.8911 as normally expected. This discrepancy suggests a large block effect or a problem with this model.

To address this problem, insignificant terms (AB and BC) should be removed from the proposed model to obtain an improved equation. The improved equation in terms of coded factors after removing the insignificant terms is shown as follows:

$$H = +931.20 - (511.59A) + (386.71B) + (403.76C) - (433.62AC) \quad (4-7)$$

According to Table 4.5, the predicted R^2 of 0.7444 is in agreement with the adjusted R^2 of 0.8897. Adequate precision measures the signal-to-noise ratio. A ratio greater than 4 is acceptable. The adequate precision ratio of 26.438 indicates an adequate signal. Therefore, this model can be used to navigate the design space.

As indicated in Eq. (4-7), the main effects of temperature and number of cycles correlate positively with the IrO_x thickness, which is in agreement with the CV result. The coefficients for scan rate (A) and number of cycles (C) are larger than the coefficients for temperature, indicating that parameters (A) and (B) have a more significant effect on the IrO_x thickness than the parameter (B).

Figure 4.21 shows the predicted result obtained from Eq. (4-7), which is in agreement with the experimental data, thereby indicating the reliability of the improved model for predicting IrO_x coating thicknesses under various electrodeposition conditions. An acceptable correlation-to- linear regression fit was also obtained, with an R^2 of 0.9255 for IrO_x thickness.

Table 4.3: Suggested Model Summary Statistics by DOE software

Source	Std. Dev.	R-Squared	Adjusted R-Squared	Predicted R-Squared	PRESS	Suggested model
Linear	363.44	0.6979	0.6412	0.2193	5.46E+06	
2FI	200.25	0.9255	0.8911	0.2651	5.14E+06	Suggested
Quadratic	179.98	0.9537	0.912	-0.0664	7.46E+06	
Cubic	55.31	0.9974	0.9917	-58.6796	4.17E+08	Aliased
"Model Summary Statistics": Focus on the model maximizing the Adjusted R-Squared" and the Predicted R-Squared".						

Table 4.4: 2FI Model summary statistics

Std. Dev.	200.25	R-Squared	0.9255
Mean	931.2	Adj R-Squared	0.8911
C.V.	21.5	Pred R-Squared	0.2651
PRESS	5.14E+06	Adeq Precision	23.083

Table 4.5: 2FI Model Summary Statistics Result after improvement

Std. Dev.	201.51	R-Squared	0.9129
Mean	931.2	Adj R-Squared	0.8897
C.V.	21.64	Pred R-Squared	0.7444
PRESS	1.79E+06	Adeq Precision	26.438

4.3.8 Interactions between independent variables

Three-dimensional response surface plots and two-dimensional contour plots are presented in Figure 4.24, which introduces the effects of the number of cycles and scan rate at minimum and maximum temperatures on IrO_x coating thickness (nm). These types of plot depict the effect of the interaction of two factors on the response at a time, which can demonstrate sensitivities with variable changes [130,131].

In the present study, increasing the number of cycles at low scan rates leads to an increase in deposit thickness. This enhancement in IrO_x thickness becomes more apparent at high temperatures, as indicated in Figures 4.22(a) and (b). Increase the number of cycles and decreasing the scan rate significantly affect the thickness of the electrodeposited layer.

Figure 4.25 illustrates the effect of each variable on the response. An increase in the scan rate negatively affects the growth of the IrO_x layer. The thickness of the electrodeposited layer increases with the increases in the number of cycles and temperature.

4.3.9 Conclusion

This work demonstrates the efficiency of response surface methodology in modeling and investigating the effect of various factors on IrO_x electrodeposition.

Statistical results showed that the significant effect of scan rate on the IrO_x layers is higher than those of temperature and number of cycles.

The results of the electrochemical experiment indicated that all fabricated electrodes were conductive and reduced the impedance of the stainless steel electrode. The CV result showed that CSC_C increased with an increase in the electrodeposited layer. However, the FESSEM images revealed that cracks in electrodeposited layer also increased with an increase in IrO_x thickness.

We have shown a stable and reproducible IrO_x film that can be used as an pH sensor electrode for amperometric sensing systems in corroding metal surface which will be discuss more in next parts.

4.4 Surface pH measurement in CO₂ corrosion with a novel microelectrode pH probe

Many electrochemical reactions taking place in corroding metal surface consume or produce protons. The pH in the near metal surface can therefore be significantly altered during the reaction and there is a need for in situ pH measurements tracing this near surface pH.

4.4.1 Design and fabrication of a novel microelectrode pH probe

The proposed surface pH probe is mentioned in section 3.3.4 and depicted in Figure 3.5. A combination of three IrO_x pH sensors was used in probe design to enhance accuracy of pH measurement.

The prepared electrodeposited IrO_x film showed good stability and fast response time. The electrochemical characteristics of IrO_x pH microelectrodes were

investigated before their application in surface pH monitoring. The response of electrodeposited IrO_x electrodes to exposure to a series of universal buffer solutions in the pH range between 4 and 9 is shown in Figure 4.26 depicts a linear super-Nernstian response resulting in a sensitivity of -73.421 mV/pH for combination of three IrO_x pH sensors. This value is in good agreement with results reported in the literature for the electrochemical deposition of IrO_x on metal substrates [8,90,100].

The OCP responses of the IrO_x films to varying pH were experienced for two weeks. After two weeks, visual inspection under a microscope indicated no obvious signs of film delamination or degradation. Also, the OCP response of the IrO_x film to varying pH remained at an average of =73 mV per pH unit with fluctuations of +/-5 mV per pH unit over the two week period.

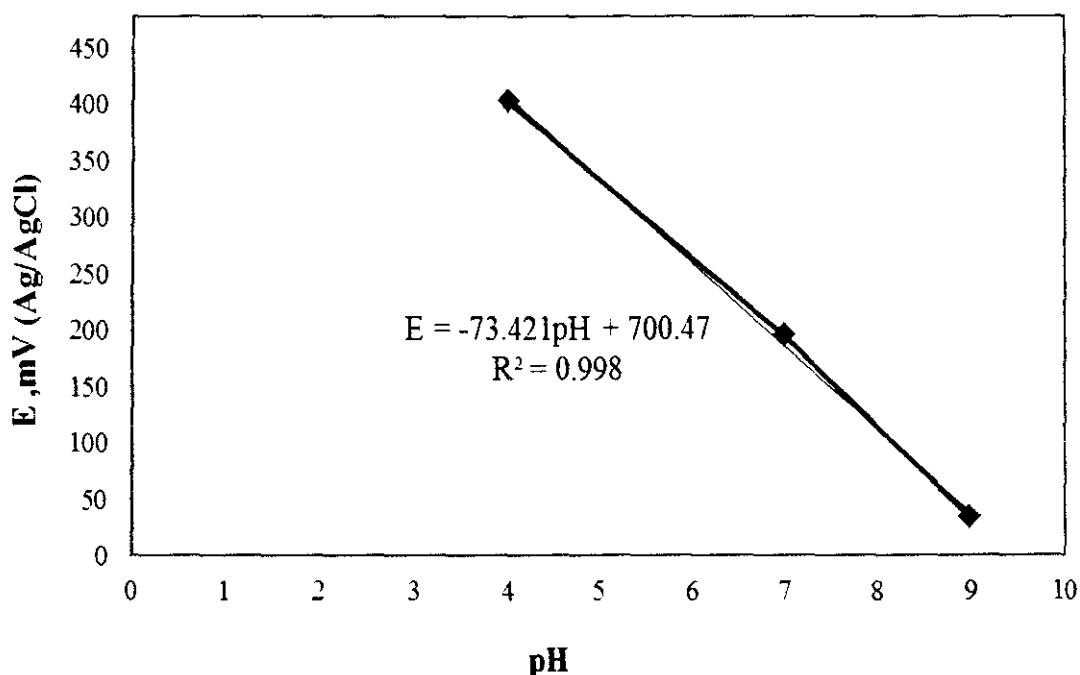


Figure 4.26: Potentiometric response of a IrO_x pH electrode in the pH range of 4–9 at a temperature of 25 °C.

4.4.2 Surface pH measurement in CO₂ corrosion at three different temperatures

Carbon steel electrode assembled with pH sensor was exposure to CO₂-saturated 3% NaCl solution as depicted in Figure 4.27. Chemical and electrochemical reaction

on the carbon steel surface changed pH on the surface. Experiment was done at three different temperatures; 25, 50, and 80 °C.

Generally, the following reactions are observed in CO₂ corrosion: (a) four chemical reactions occurring in a solution and (b) four electrochemical reactions — one anodic and three cathodic — occurring on metal surfaces [87-90]:

a) Chemical reactions:



b) Electrochemical reactions:



Cathodic Reactions:



FeCO₃, an insoluble corrosion product, can be formed at this stage, as follows:



Under certain conditions, the films can be very protective and offer great protection from corrosion by forming a barrier through blocking some parts of the metal surface which indirectly reduce the corrosion rate.

Result of surface pH measurement at 25 °C in bulk pH 4 and 6 are presented in Figures 4.28 and 4.29, respectively. After initial variation, a stable surface pH was measured after one hour which is approximately 2 pH units higher than the bulk pH. The pH of metal surface increased gradually up higher after exposure in CO₂-saturated 3% NaCl solution compared to the bulk solution pH. The pH of bulk

solution and metal surface were recorded every one hour for 24 hours with a normal pH probe and in-situ IrO_x pH sensor embedded in carbon steel.



Figure4.27: Set-up for measuring near surface pH on carbon steel corroding surface at three different temperatures; 25, 50, and 80 °C.

One of the important cathodic reactions in the CO_2 corrosion process as shown in Figure 4.34 is the reduction of H^+ ions, thus pH plays an important role in the cathodic reaction. Researchers found that there is a change in the pH immediately adjacent to the electrode surface in the electrolyte and it has a major effect on the physical properties of precipitates such as iron carbonate [132].

The achieved results correspond to steady state pH values. Result of surface pH measurement at 50 and 80 °C are shown in Figures 4.30 and 4.33, respectively. In all cases, considerably higher surface pH values were recorded with temperature increasing. This is due to the fact that the corrosion rate is higher at the higher temperature due to consumption of more protons which results in a higher surface pH measurement. Moreover, CO_2 dissolves less in the solution at higher temperatures and creates a weaker buffer solution. Water chemistry model calculation shows only half

of the CO_2 dissolves at 80 °C compared with 25 °C [5]. Both mechanisms contribute to a higher surface pH at higher temperature.

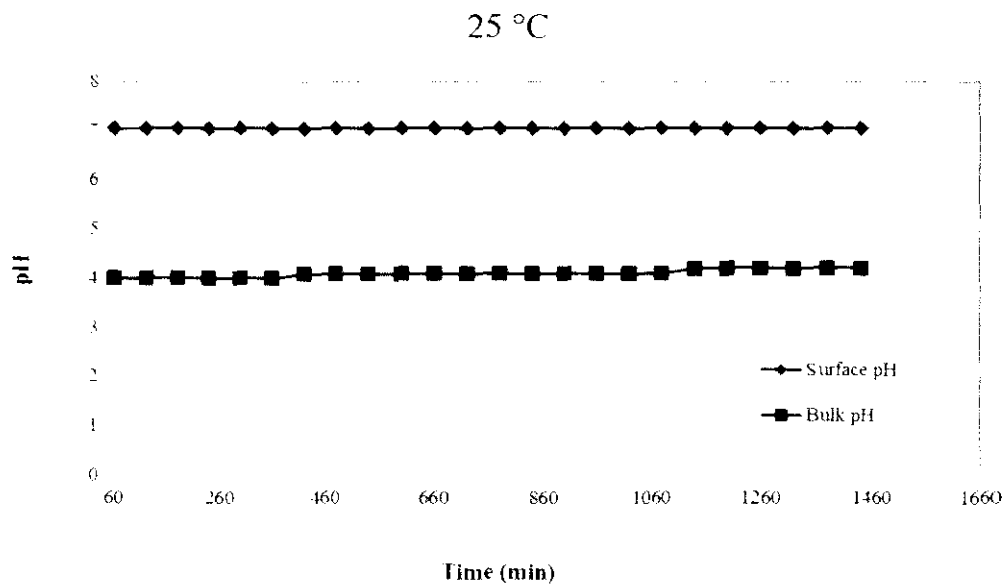


Figure 4.28: Surface pH measurement during X52 carbon steel corrosion under bulk pH 4.0; $p\text{CO}_2=0.97$ bar, temperature= 25 °C, and $[\text{NaCl}]= 3\text{wt}\%$.

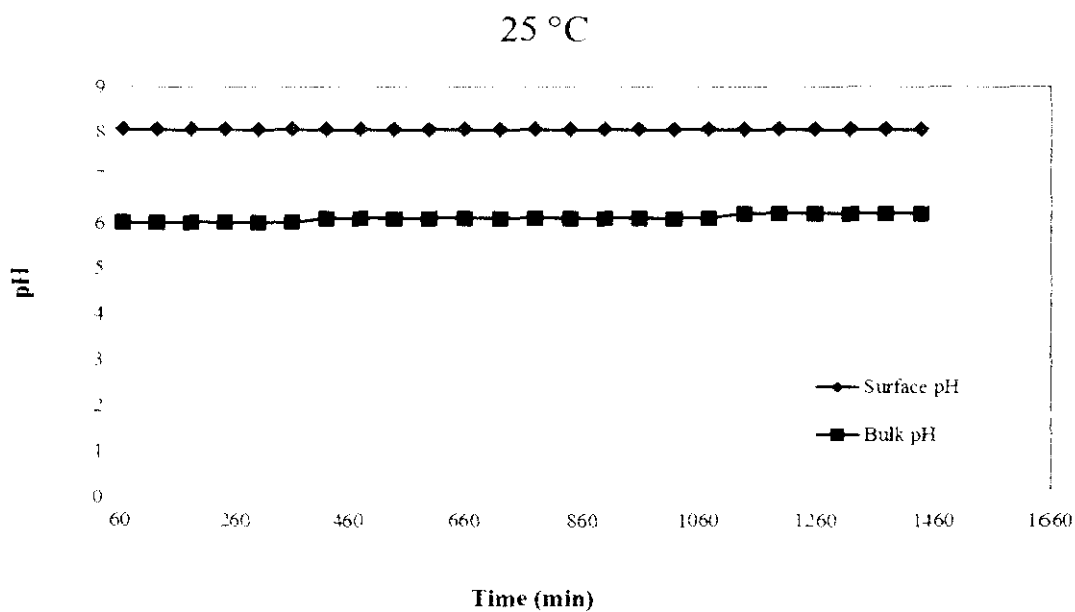


Figure 4.29: Surface pH measurement during X52 carbon steel corrosion under bulk pH 6.0; $p\text{CO}_2=0.97$ bar, temperature= 25 °C, and $[\text{NaCl}]= 3\text{wt}\%$.

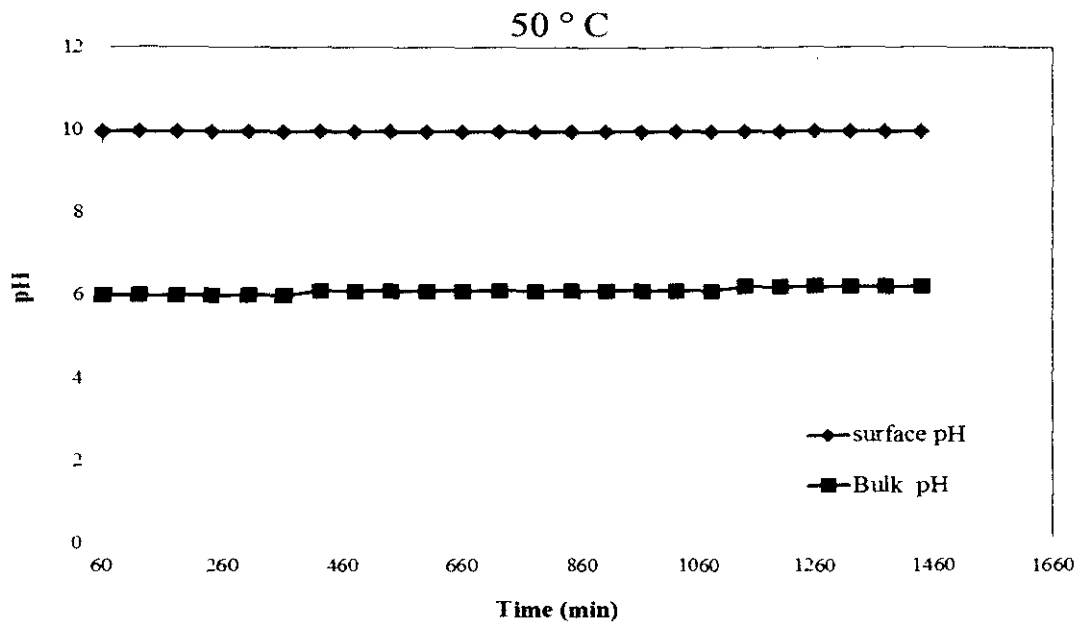


Figure 4.30: Surface pH measurement during X52 carbon steel corrosion under bulk pH 4.0; $p\text{CO}_2=0.88$ bar, temperature =50 °C, and $[\text{NaCl}] = 3\text{wt}\%$.

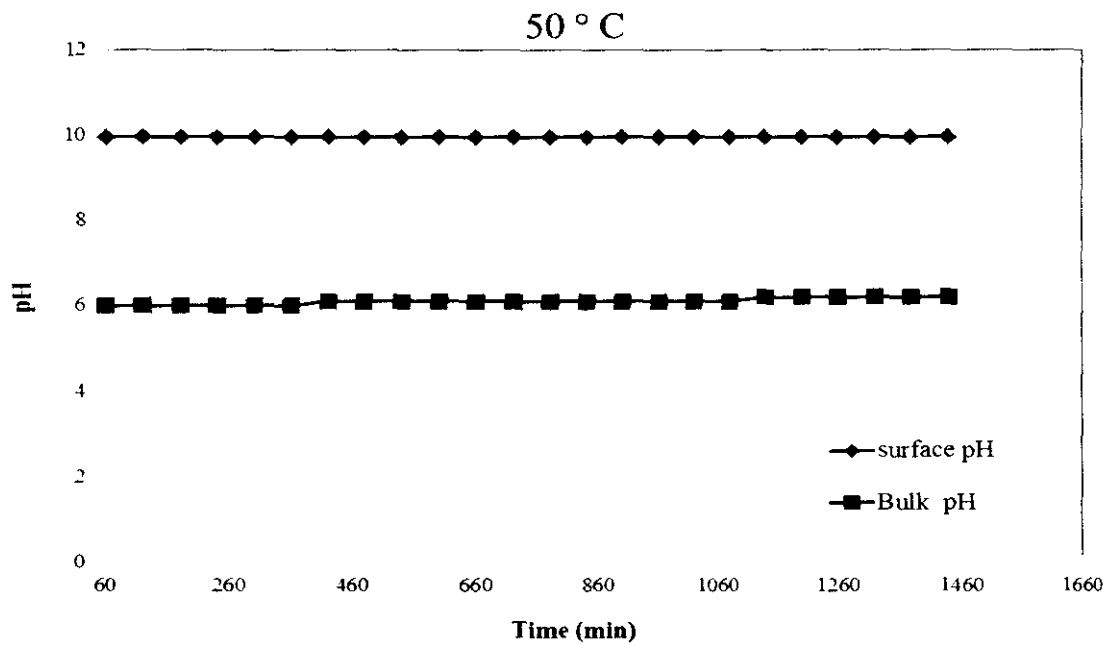


Figure 4.31: Surface pH measurement during X52 carbon steel corrosion under bulk pH 6.0; $p\text{CO}_2=0.88$ bar, temperature =50 °C, and $[\text{NaCl}] = 3\text{wt}\%$.

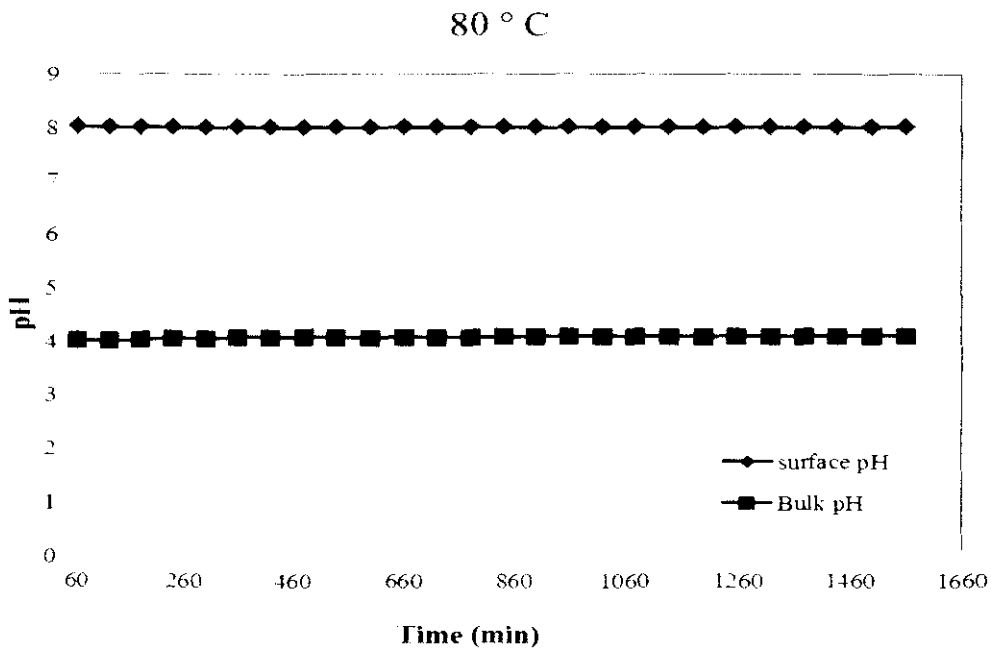


Figure 4.32: Surface pH measurement during X52 carbon steel corrosion under bulk pH 4.0; $pCO_2=0.53$ bar, temperature= 80 °C, and $[NaCl] = 3wt\%$.

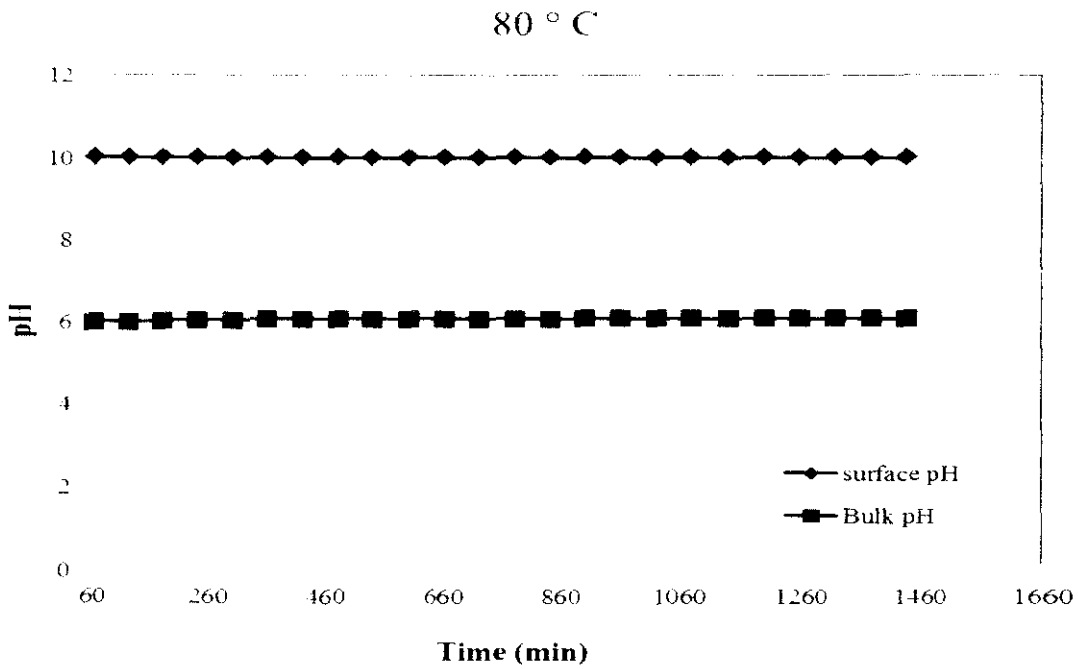


Figure 4.33: Surface pH measurement during X52 carbon steel corrosion under bulk pH 6.0; $pCO_2=0.53$ bar, temperature= 80 °C, and $[NaCl] = 3wt\%$.

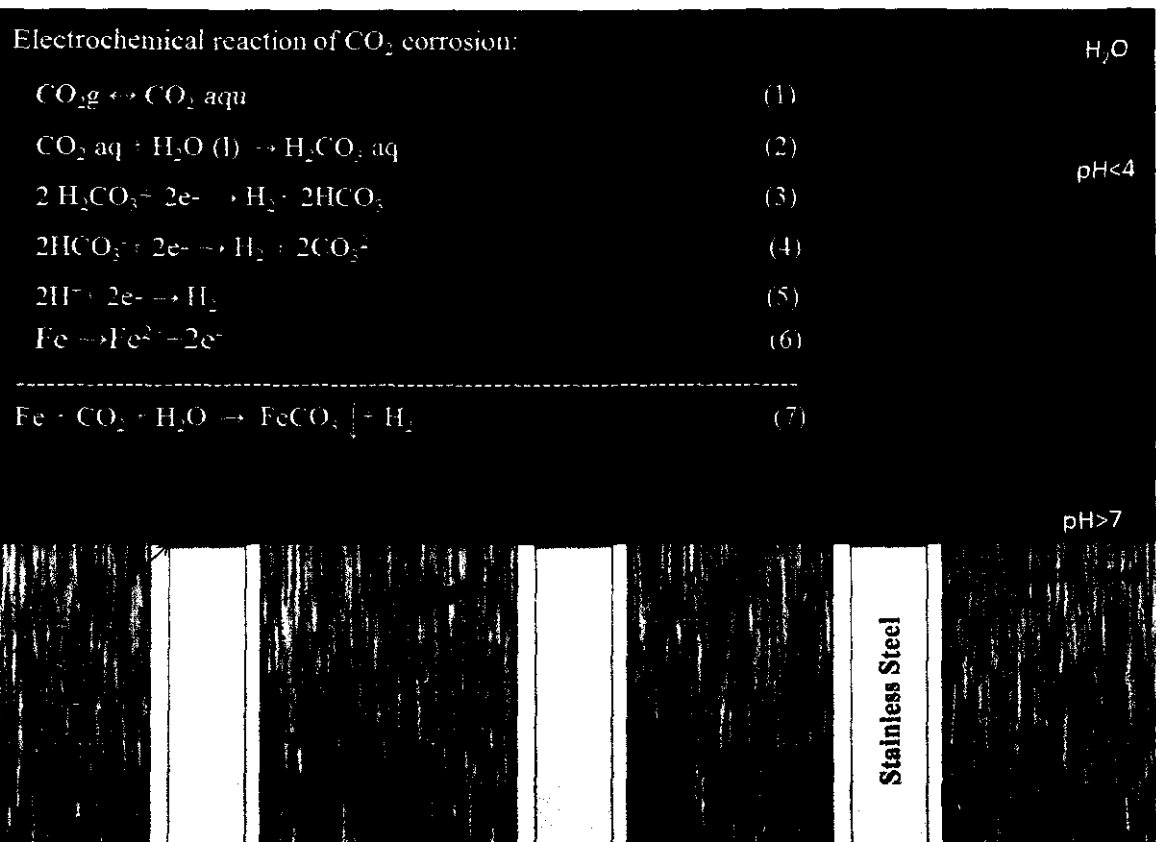


Figure 4.34: Electrochemical and chemical reaction on carbon steel surface during CO₂ corrosion.

4.4.3 SEM/EDX of corrosion product at three different temperatures

Figure 4.35 shows an SEM image of corroded carbon steel surface after exposure to CO₂ containing solution at 25 °C for 24 hours. Some corrosion product is created in metal surface but there is not any FeCO₃ film as evidence of the dominant corrosion product. Result of EDX from Figure 4.36 also confirms that formation of one kind of iron oxide is more dominant than formation of FeCO₃ due to more concentration of oxygen and iron ions.

In contrast, in higher surface pH and at higher temperature, the cubic crystalline shape of FeCO₃ was detected as it can be seen from Figure 4.37. This assumption is confirmed by EDX results which detected C element in the crystal grain as shown in Figure 4.38. The result shows that increasing temperature can increase formation of FeCO₃ as reported in literatures [3, 14]. Jiabin et al. [14] found that passive film is

Fe_3O_4 which is not a continuous film covering the steel surface, but is mainly cover boundary areas between the FeCO_3 crystals.

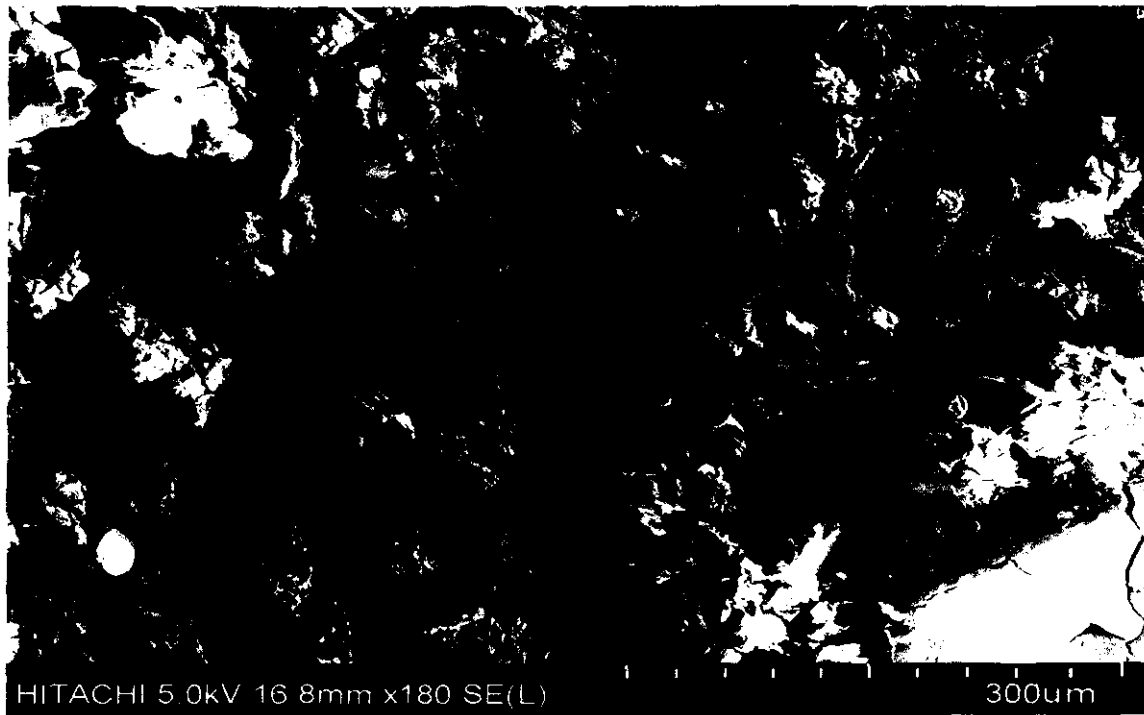


Figure 4.35: SEM image of corroded X52 carbon steel surface at 25 °C, bulk pH=4.

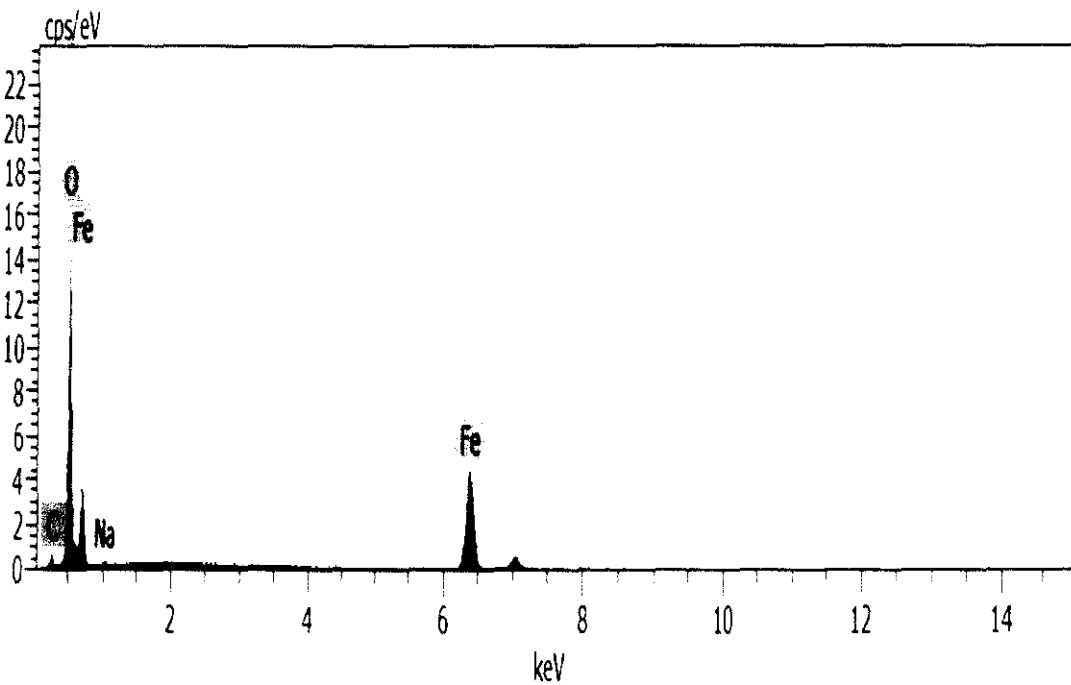


Figure 4.36: EDX result of CO_2 corrosion product of X52 carbon steel at 25 °C, bulk pH=4.

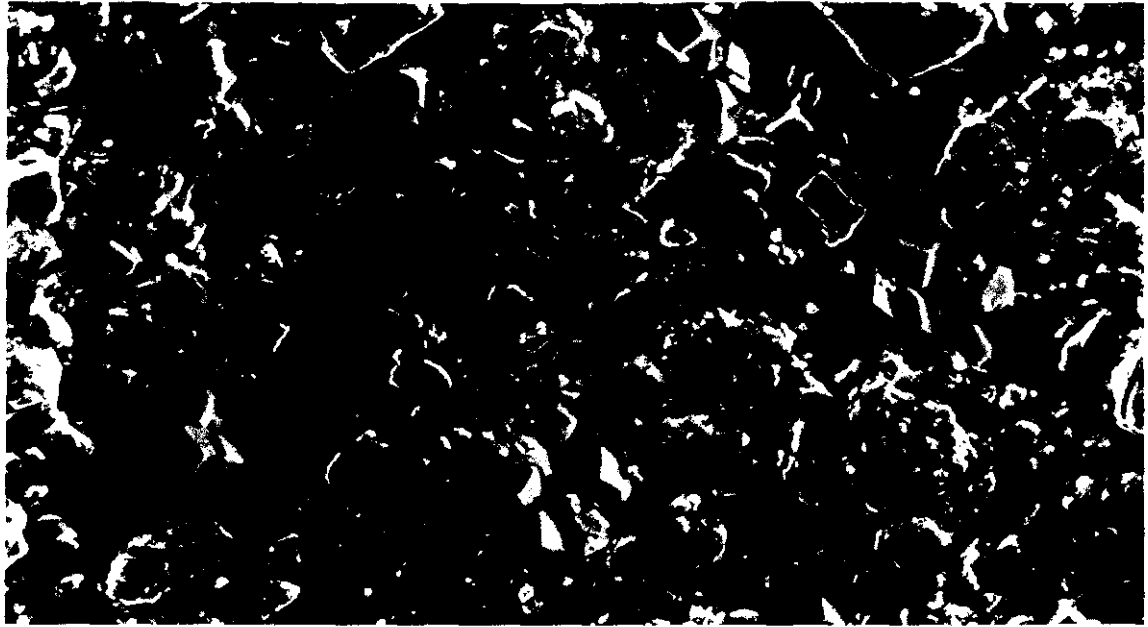


Figure 4.37: SEM image of corroded X52 carbon steel surface at 80 °C, bulk pH=4.

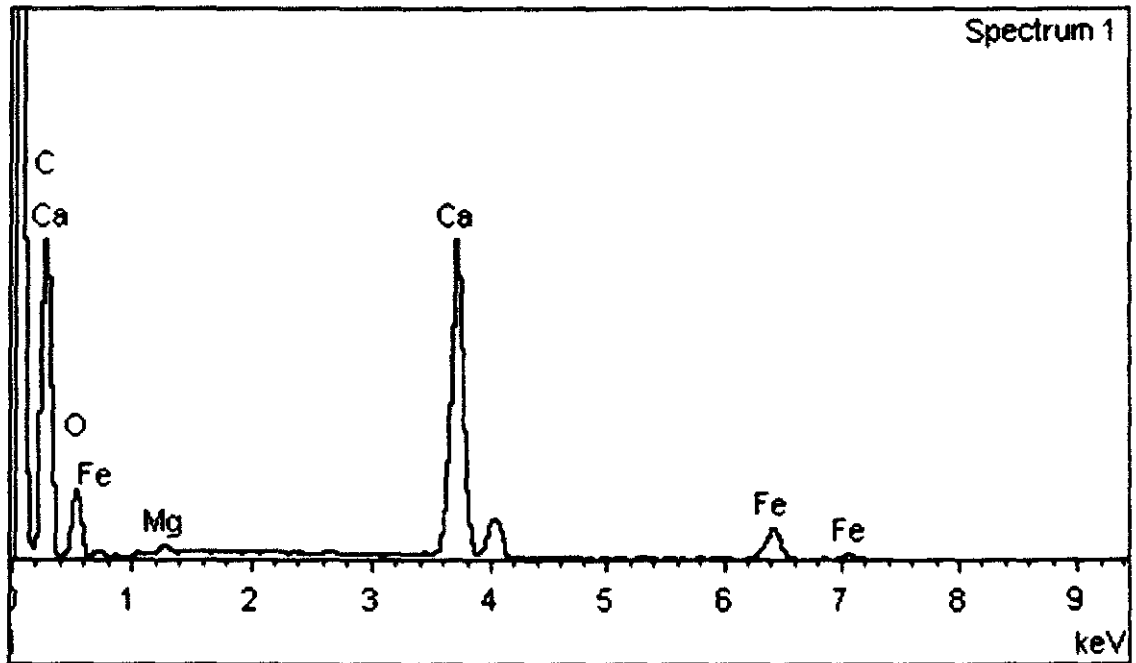


Figure 4.38: EDX result of CO₂ corrosion product of X52 carbon steel at 80 °C, bulk pH=4.

SEM images and EDX result of similar samples as mentioned above in bulk pH=6 solution are shown in Figure 4.39 to 4.42. It can be concluded that increasing temperature and bulk pressure create a favorite condition in metal surface for FeCO₃ formation.

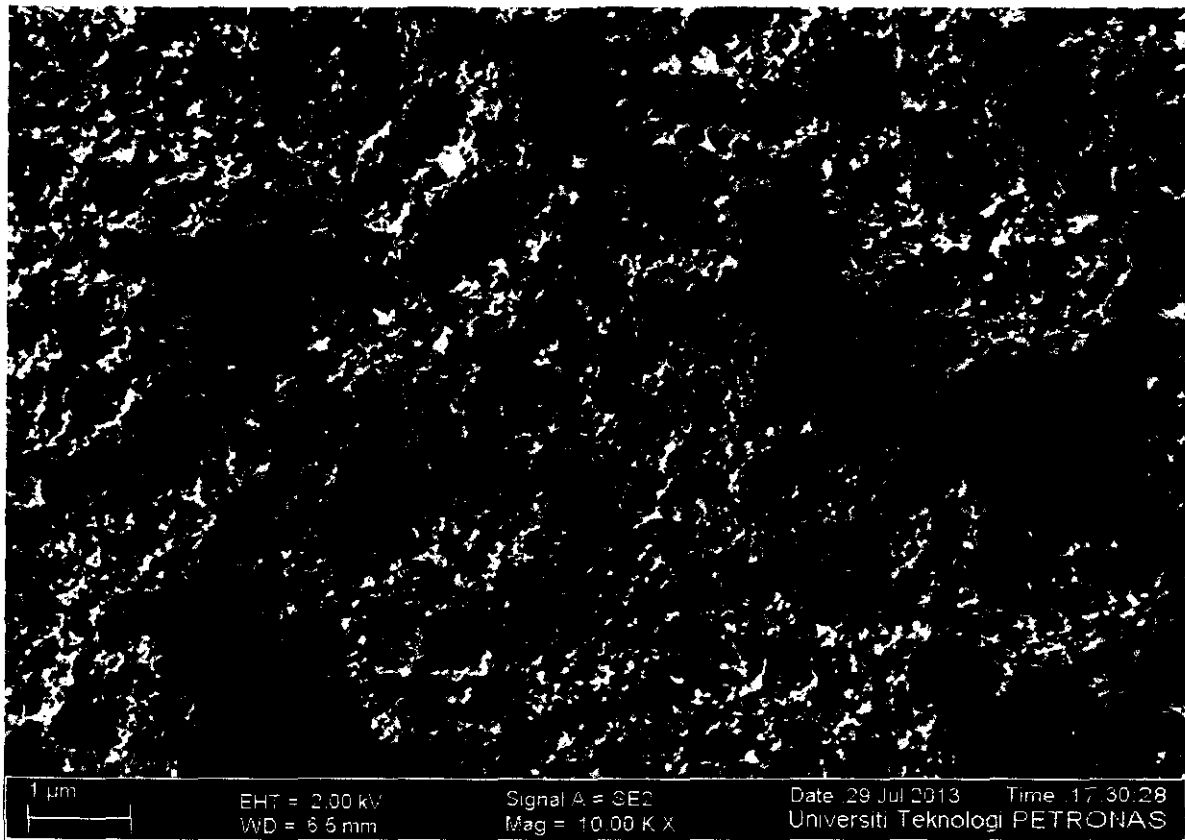


Figure 4.39: SEM image of corroded X52 carbon steel surface at 25 °C, bulk pH=6.

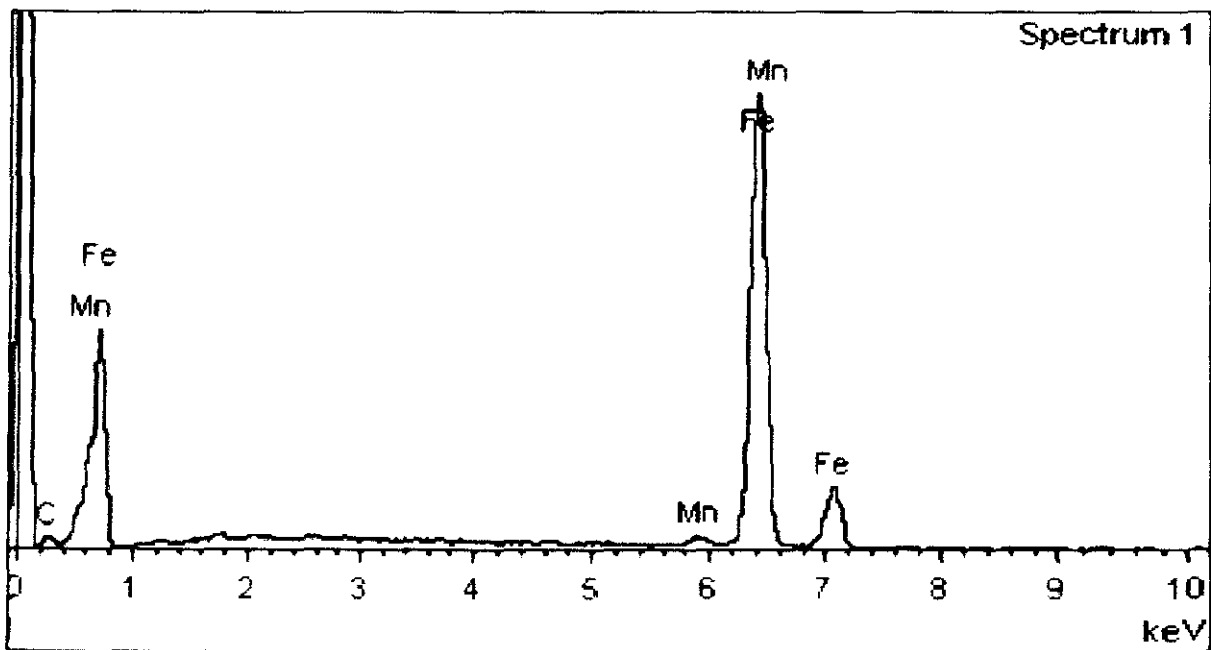


Figure 4.40: EDX result of CO₂ corrosion product of X52 carbon steel at 25 °C, bulk pH=6.

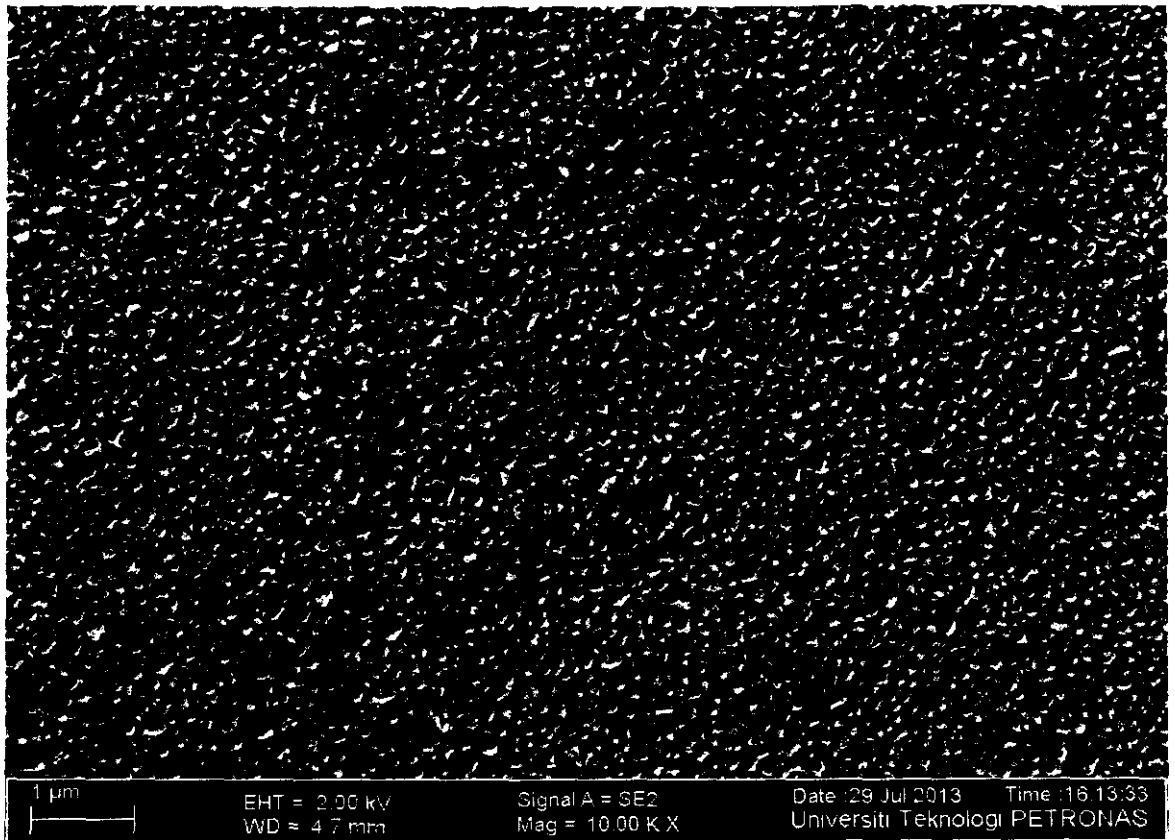


Figure 4.41: SEM image of corroded X52 carbon steel surface at 80 °C, bulk pH=6.

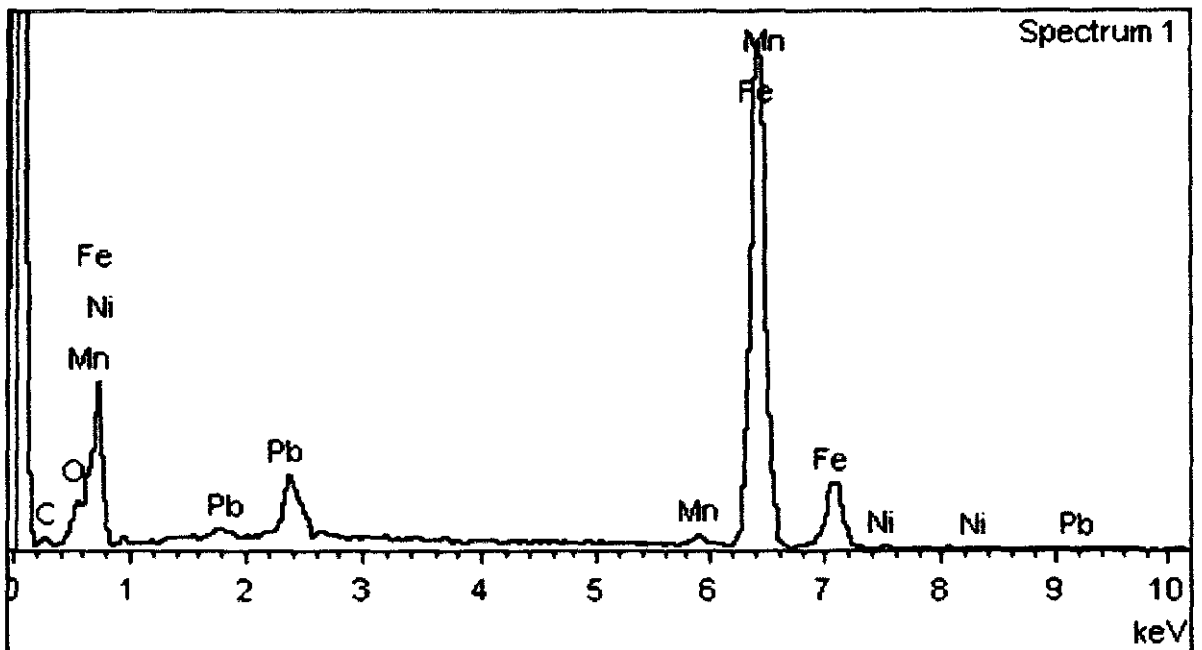


Figure 4.42: EDX result of CO₂ corrosion product of X52 carbon steel at 80 °C, bulk pH=6.

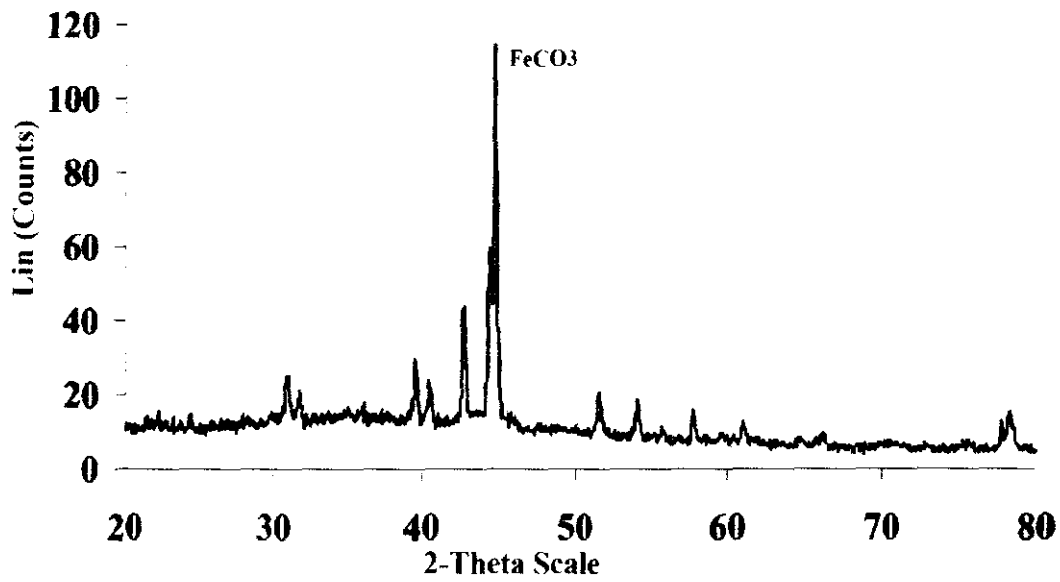


Figure 4.43: XRD spectrum for corrosion product on the surface of X52 carbon steel in CO₂-saturated 3% NaCl solution at 80 °C, bulk pH=6.

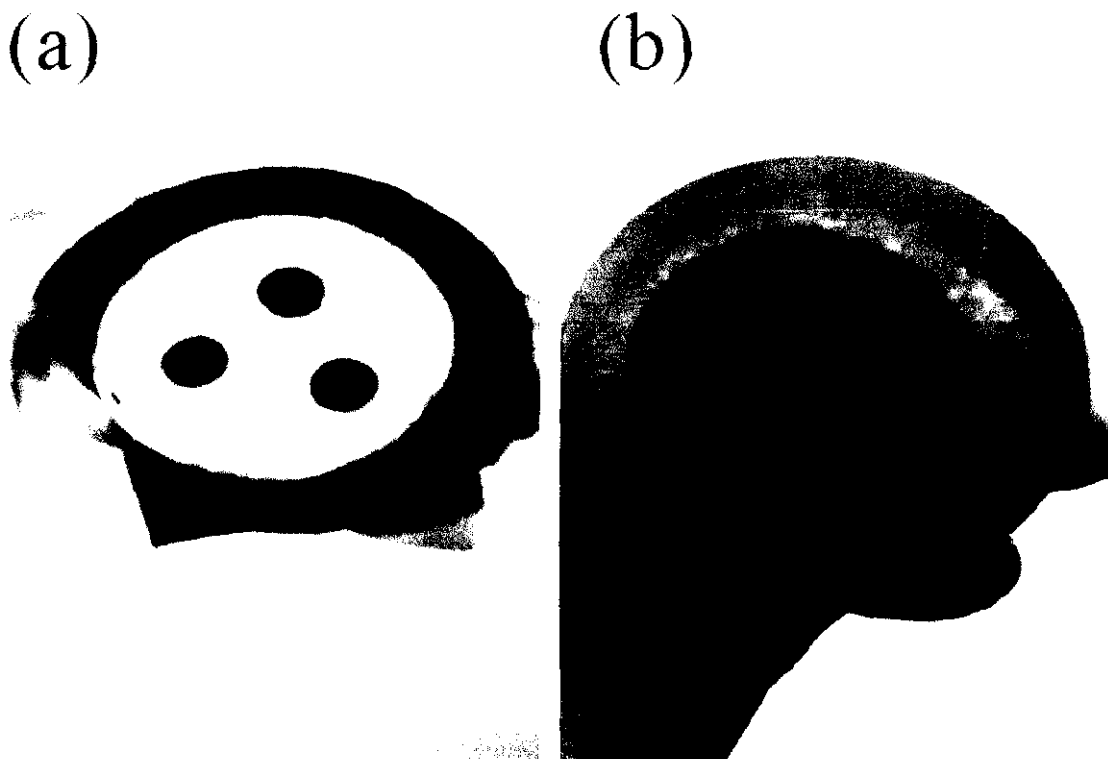


Figure 4.44: Surface of pH probe and carbon steel before (a) and after (b) exposure in CO₂-saturated 3% NaCl solution.

To confirm result of Figures 4.42 and 4.41 and show corrosion product is FeCO_3 , an XRD experiment was done on corrosion. XRD result is shown in Figure 4.43 which shows dominant composition of corrosion product is FeCO_3 . The IrO_x pH sensor should have a stable potential and remain strongly adhered for at least several hours to weeks if it will be used in corrosion monitoring. The OCP responses of the IrO_2 films to varying pH were tested for three weeks and then investigated by visual inspection under a microscope which also clear from Figure 4.44. Result showed no obvious signs of film delamination or degradation. Also, the OCP response of the IrO_x pH sensor showed fluctuations of ± 5 mV per pH unit over the three week period.

4.4.4 Conclusion

The pH value of the X52 carbon steel/solution interface was monitored for the first time using the in-situ pH microsensor of iridium oxide during the CO_2 corrosion at 25, 50, and 80°C. The design confirms that the measurement was able to determine the pH change correctly at the substrate/solution interface, which is a key requirement for studying the mechanism of electrochemical reactions and the relationship between corrosion process and the pH at the working electrode/solution interface during the corrosion. In all cases, surface pH or the interfacial pH increased compared with bulk solution pH after the corrosion process began. This result is in good agreement with theoretical hypothesis and prediction.

4.5 Under deposit pH measurement in CO₂ corrosion with a novel microelectrode pH probe

As mentioned in section 4.3, many electrochemical reactions taking place in corroding metal surface under deposit consume or produce protons. The pH in the near metal surface under deposit can therefore be significantly altered during the reaction and there is a need for in situ pH measurements tracing this near surface pH under deposit.

4.5.1 pH probe and experimental set-up for under deposit pH measurement

The proposed surface pH probe is mentioned in section 3.3.4 and depicted in Figure 3.5. A combination of three IrO_x pH sensors was used in probe design to enhance accuracy of pH measurement. Experimental set-up was same as mentioned in section 4.3: just a cap was used to be filled with Agar deposit. Schematic Design of pH measurement probe for monitoring of pH and corrosion under deposit is shown in Figure 3.7.

The prepared electrodeposited IrO_x film showed good stability and fast response time. The electrochemical characteristics of IrO_x pH microelectrodes were investigated before their application in surface pH measurement under deposit. The response of electrodeposited IrO_x electrodes to exposure to a series of universal buffer solutions in the pH range between 4 and 9 is shown in Figure 4.45 depicts a linear super-Nernstian response resulting in a sensitivity of -77.18 mV/pH for combination of three IrO_x pH sensors.

The OCP responses of the IrO_x films to varying pH were experienced for two weeks. After two weeks, visual inspection under a microscope indicated no obvious signs of film delamination or degradation. Also, the OCP response of the IrO_x film to varying pH remained at an average of ≈ 77 mV per pH unit with fluctuations of ± 5 mV per pH unit over the two week period.

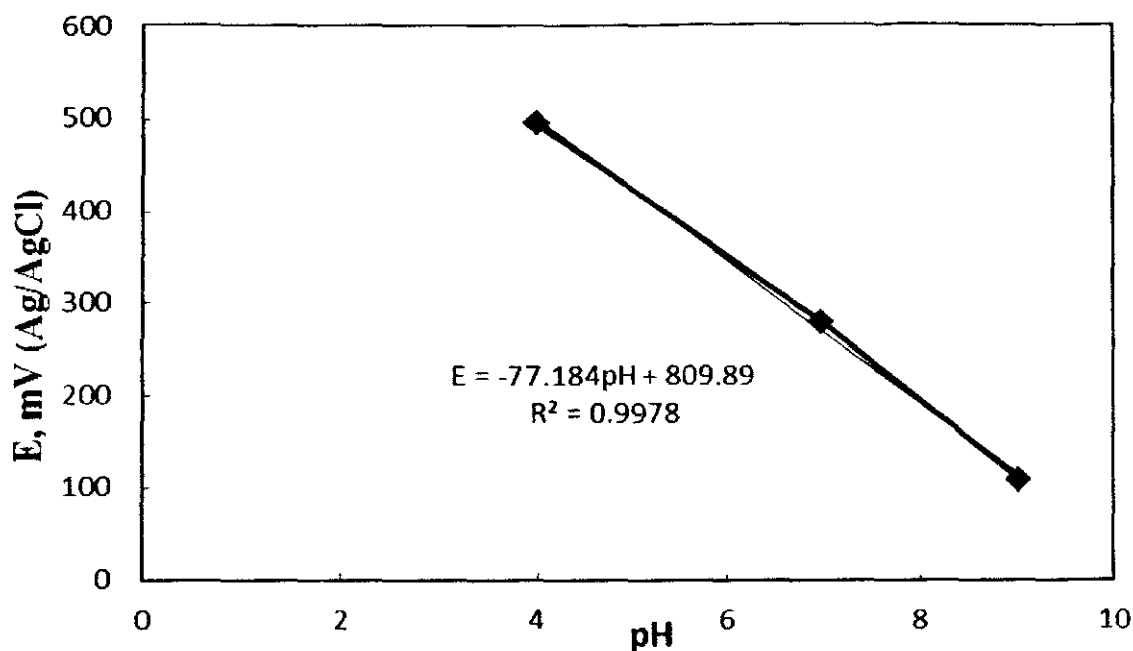


Figure 4.45: Potentiometric response of AlrO_x pH electrode in the pH range of 4–9 at a temperature of 25 °C.

4.5.2 Surface pH measurement under deposit in CO_2 corrosion at three different temperatures

Carbon steel electrode assembled with three pH sensors covered with 5 mm Agar as deposit was exposure to CO_2 -saturated 3% NaCl solution as depicted in figure 4.46. Chemical and electrochemical reaction on the carbon steel surface changed pH on the surface. Experiment was done at three different temperatures; 25, 50, and 80 °C. Also, corrosion rate of carbon steel was measured by using another Potentiostat in conjunction with an Ag/AgCl reference electrode.

Generally, reactions of (4-8) to (4-16) mentioned in section 4.3 also occur in metal surface under deposit, although these reactions will be limited due to difficulties in mass transport. Under deposit conditions, the deposit can be limit immigration of ions from metal surface to solution or vice versa. Then nature of corrosion process will be changed under deposit condition. Corrosion rate will be increased or decreased depend on properties of corrosion product.

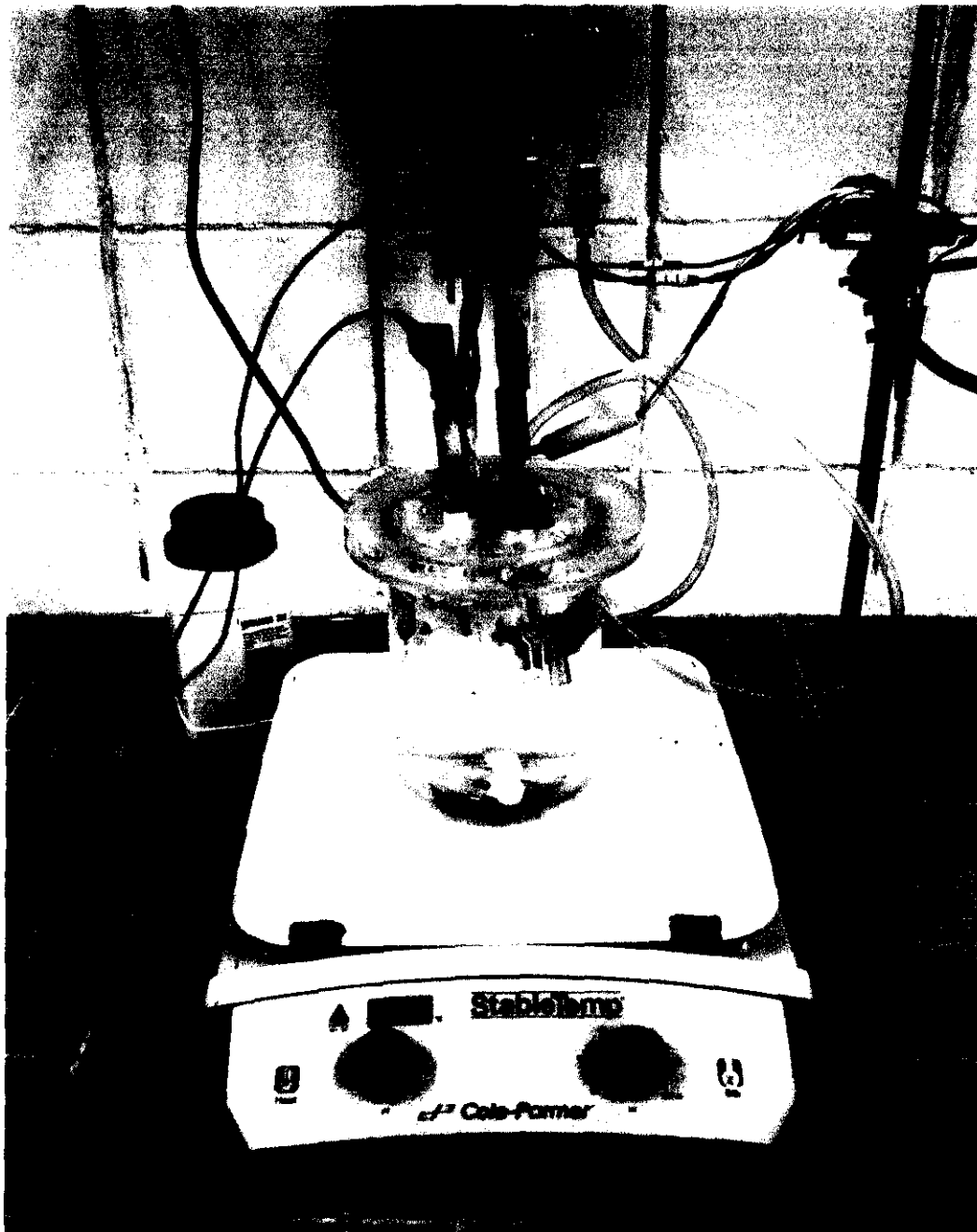


Figure 4.46: Set-up for measuring corrosion rate and near surface pH on carbon steel corroding surface under deposit at three different temperatures: 25, 50, and 80 °C.

Result of surface pH measurement at 25 °C and pH=4 is shown in figures 4.47. A stable surface pH was reported after one hour initial variation which is nearly 2 pH units higher than the bulk pH.

The pH of metal surface under deposit increased gradually up to pH=8 after exposure in CO₂-saturated 3% NaCl solution compared to the bulk solution pH

(pH=6) as is demonstrated in Figure 4.48. The pH of bulk solution and metal surface were recorded every one hour for 24 hours with a normal pH probe and in-situ IrO_x pH sensor embedded in carbon steel, respectively.

As mentioned before, one of the significant cathodic reactions in the CO_2 corrosion process is the reduction of H^+ ions, thus pH plays an important role in the cathodic reaction. It was reported that there is a change in the pH immediately adjacent to the electrode surface in the electrolyte and it has a main effect on the physical properties of precipitates (corrosion product) such as iron carbonate and iron sulphide [132]. Although this phenomenon will be effected by deposit due to mass transfer decreasing.

The achieved results correspond to steady state pH values are shown from Figure 4.47 to 4.52. In all cases, a significant higher surface pH values were measured with temperature growing. As mentioned before and later will be confirmed in Figure 4.60 and 4.61, corrosion rate is higher at the higher temperature due to consumption of more protons which results in a higher surface pH measurement. Furthermore, CO_2 dissolves less in the solution at higher temperatures and creates a weaker buffer solution. Water chemistry model calculation shows only half of the CO_2 dissolves at $80\text{ }^\circ\text{C}$ compared with $25\text{ }^\circ\text{C}$ [5]. Both mechanisms contribute to a higher surface pH at higher temperature. Regarding to all fact discussed above, existing of agar as deposit can change mass transfer and other chemical reaction which we expect in metal surface. As it is clear surface pH value is less than same condition without deposit.

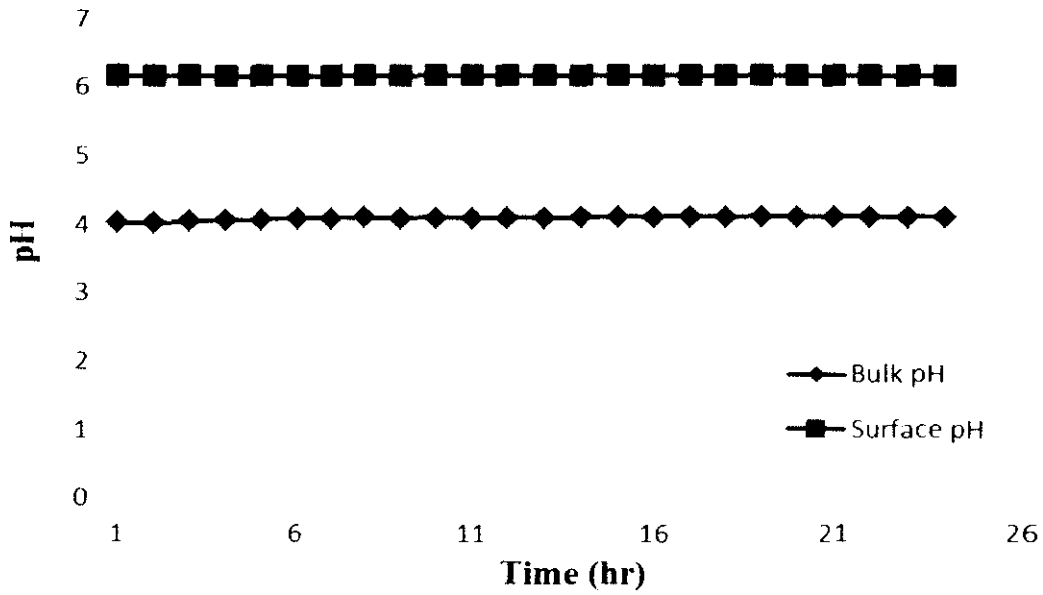


Figure 4.47: Surface pH measurement under deposit during X52 carbon steel corrosion under bulk pH 4.0; $p\text{CO}_2=0.97$ bar, temperature= 25 °C, and $[\text{NaCl}] = 3\text{wt}\%$.

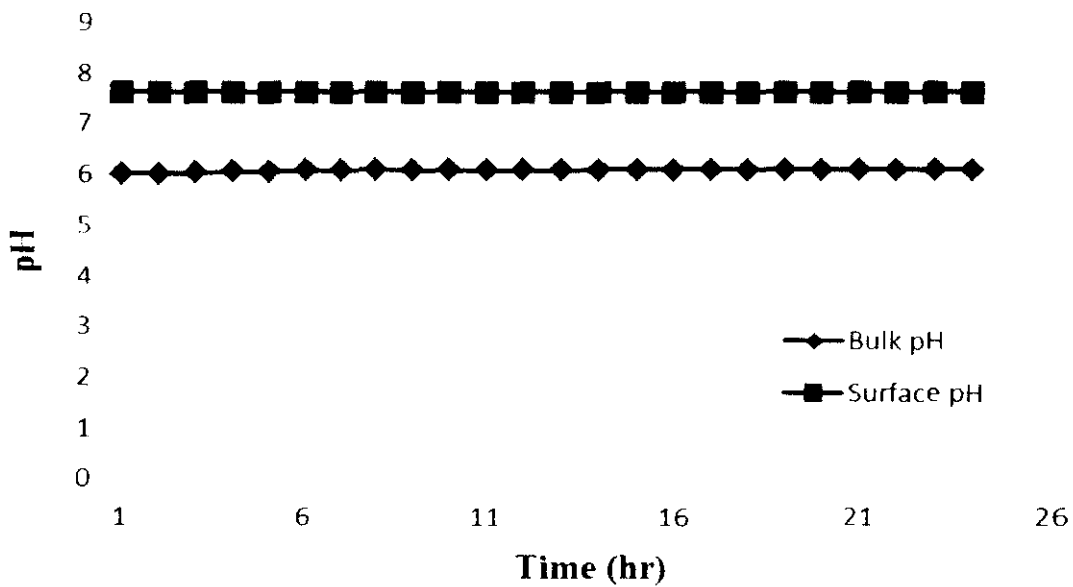


Figure 4.48: Surface pH measurement under deposit during X52 carbon steel corrosion under bulk pH 4.0; $p\text{CO}_2=0.97$ bar, temperature= 25 °C, and $[\text{NaCl}] = 3\text{wt}\%$.

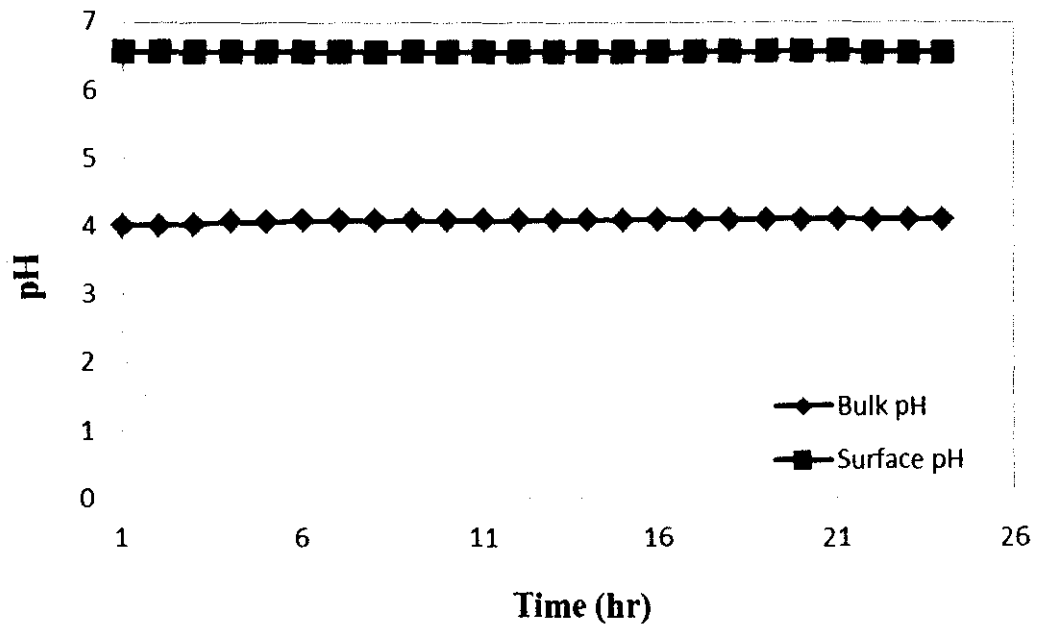


Figure 4.49: Surface pH measurement under deposit during X52 carbon steel corrosion under bulk pH 4.0; $p\text{CO}_2=0.88$ bar, temperature =50 °C, and [NaCl] = 3wt%.

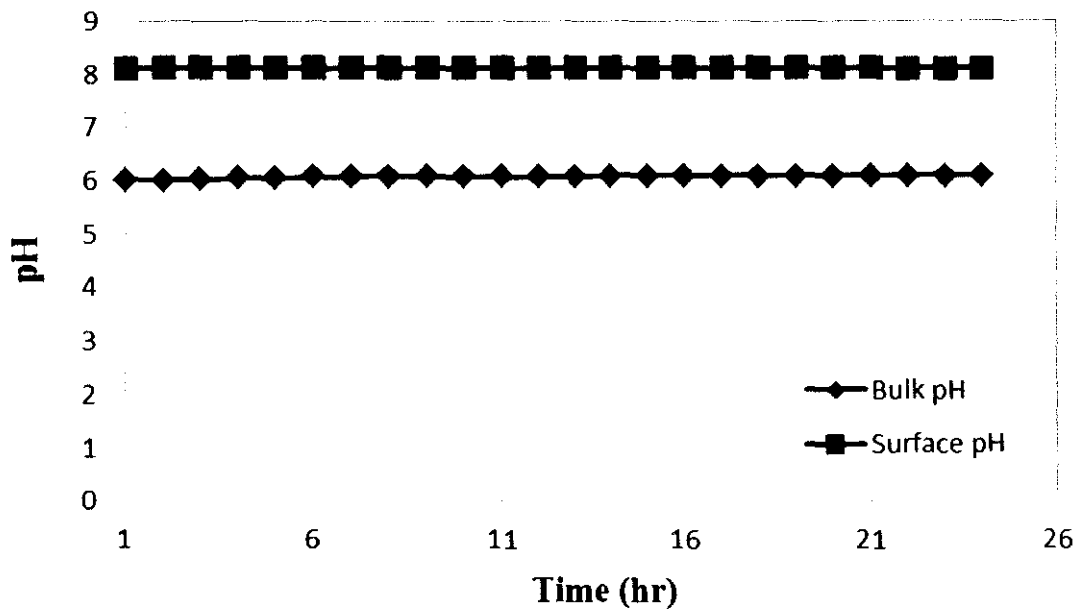


Figure 4.50: Surface pH measurement under deposit during X52 carbon steel corrosion under bulk pH 6.0; $p\text{CO}_2=0.88$ bar, temperature =50 °C, and [NaCl] = 3wt%.

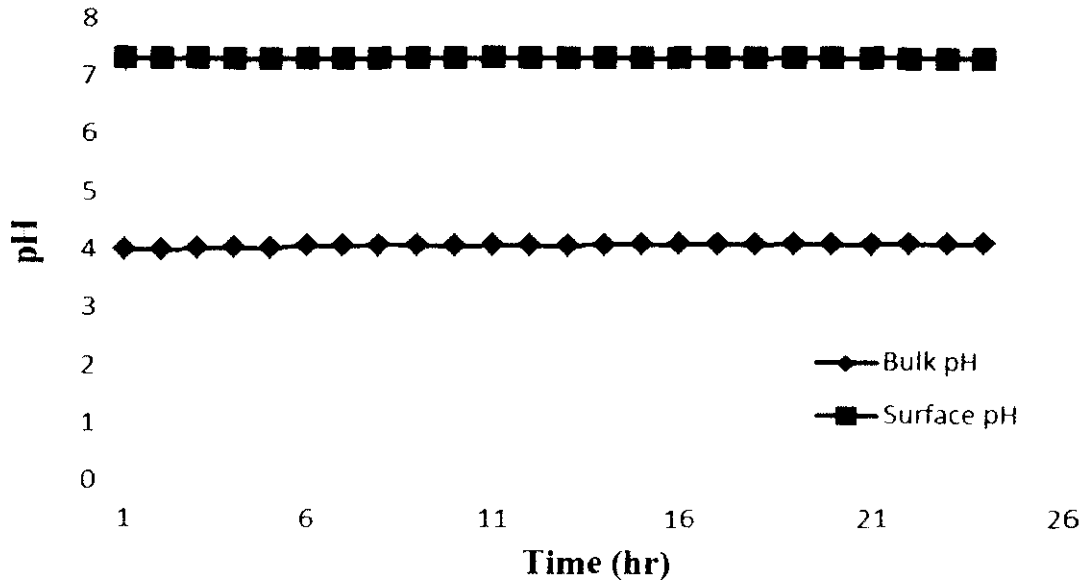


Figure 4.51: Surface pH measurement under deposit during X52 carbon steel corrosion under bulk pH 4.0; $p\text{CO}_2=0.53$ bar, temperature= 80 °C and $[\text{NaCl}] = 3\text{wt}\%$.

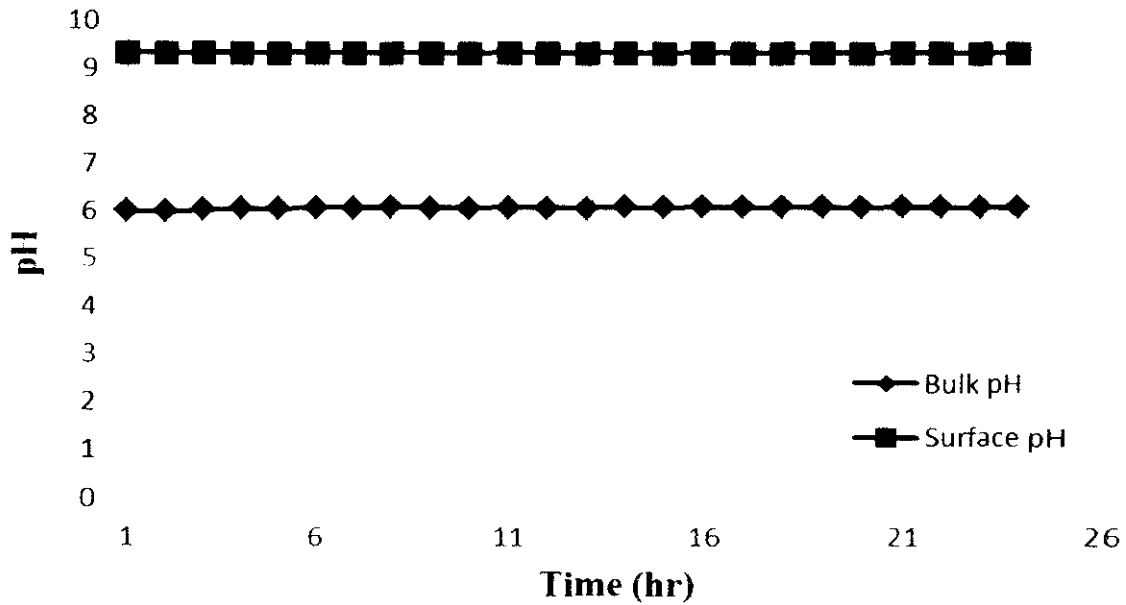


Figure 4.52: Surface pH measurement under deposit during X52 carbon steel corrosion under bulk pH 6.0; $p\text{CO}_2=0.53$ bar, temperature= 80 °C and $[\text{NaCl}] = 3\text{wt}\%$.

4.5.3 SEM/EDX of corrosion product at three different temperatures

Figure 4.53 to Figure 4.58 show surface morphology (face view) and EDX results of the under deposit X52 steel in pH=4 and pH=6, 3% NaCl solution saturated with CO₂ at temperature; 25 and 80 °C, respectively.

However pH condition was proper for creating of FeCO₃ film, it seems that changing in mass transport affected the nature of corrosion product. Regarding to FESEM images and EDX result, it can be concluded that FeC₃ film is likely to form than FeCO₃ film.

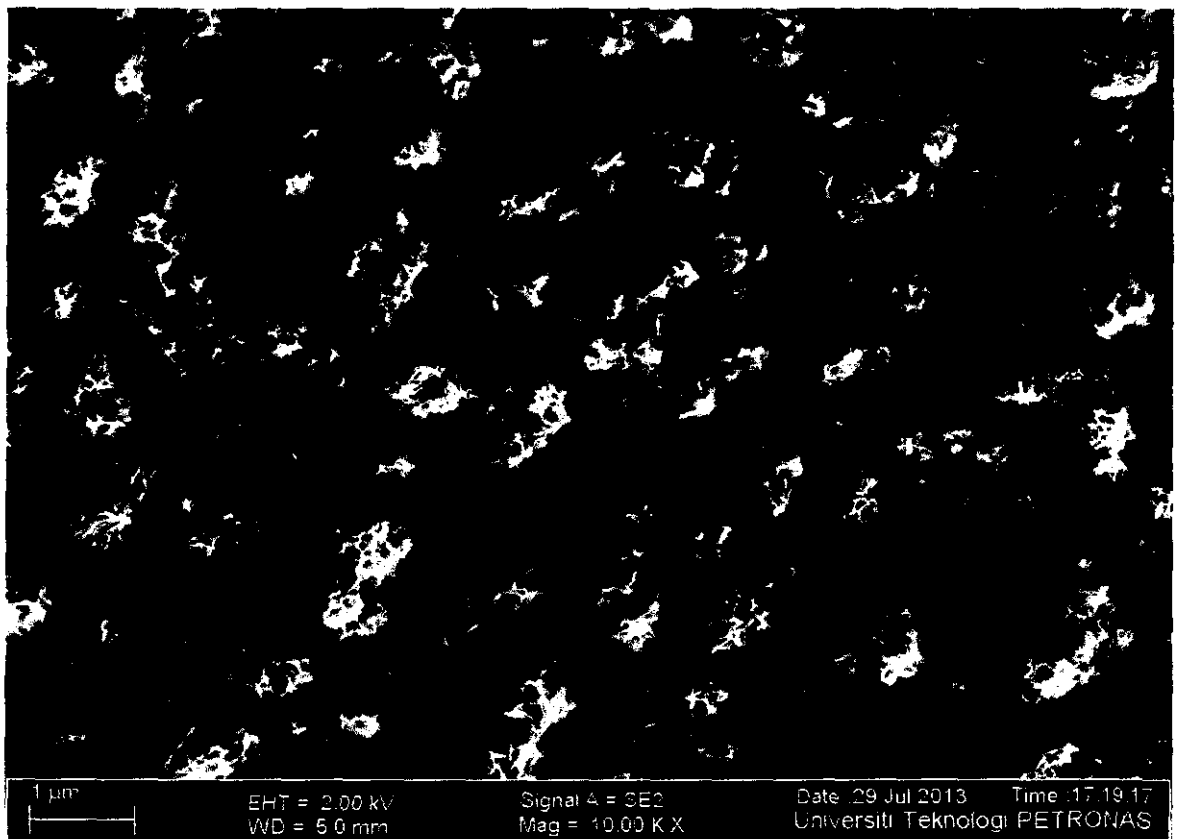


Figure 4.53: SEM image of corroded X52 carbon steel surface at 25 °C, pH=4

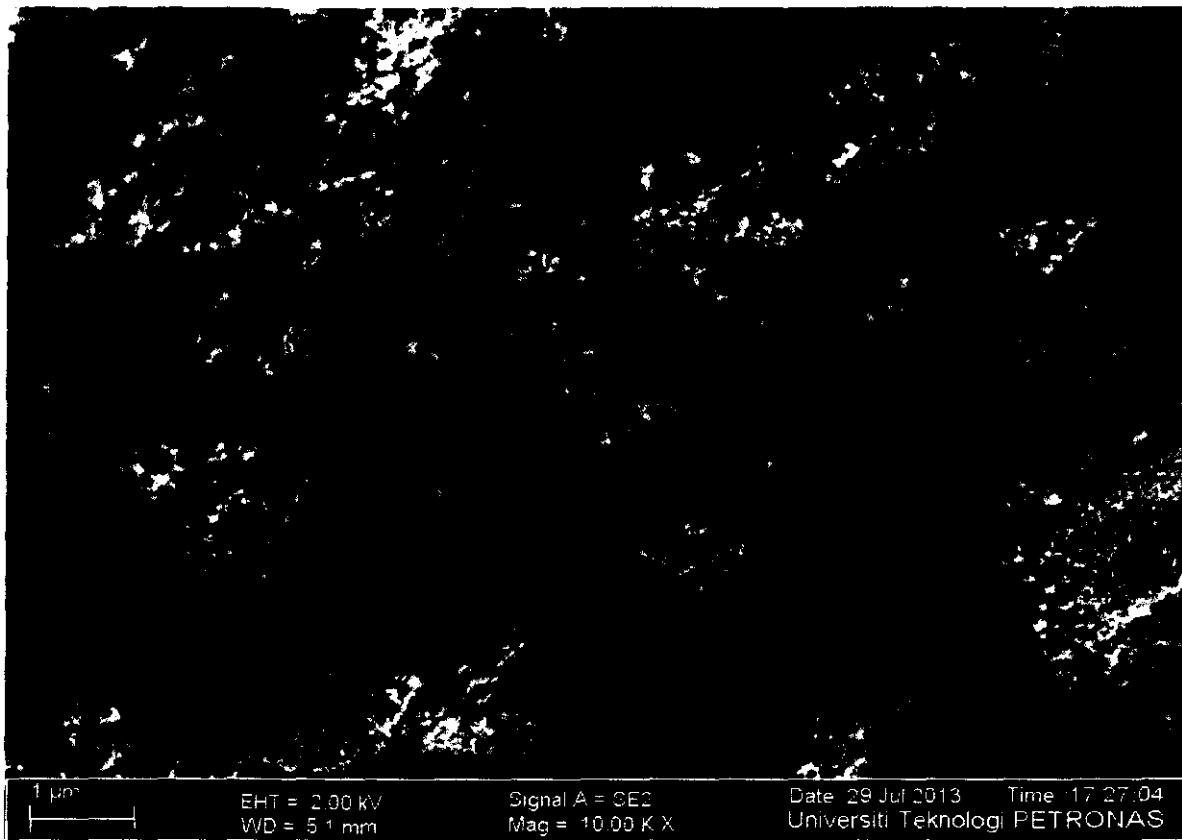


Figure 4.54: SEM image of corroded X52 carbon steel surface at 25 °C, pH=6

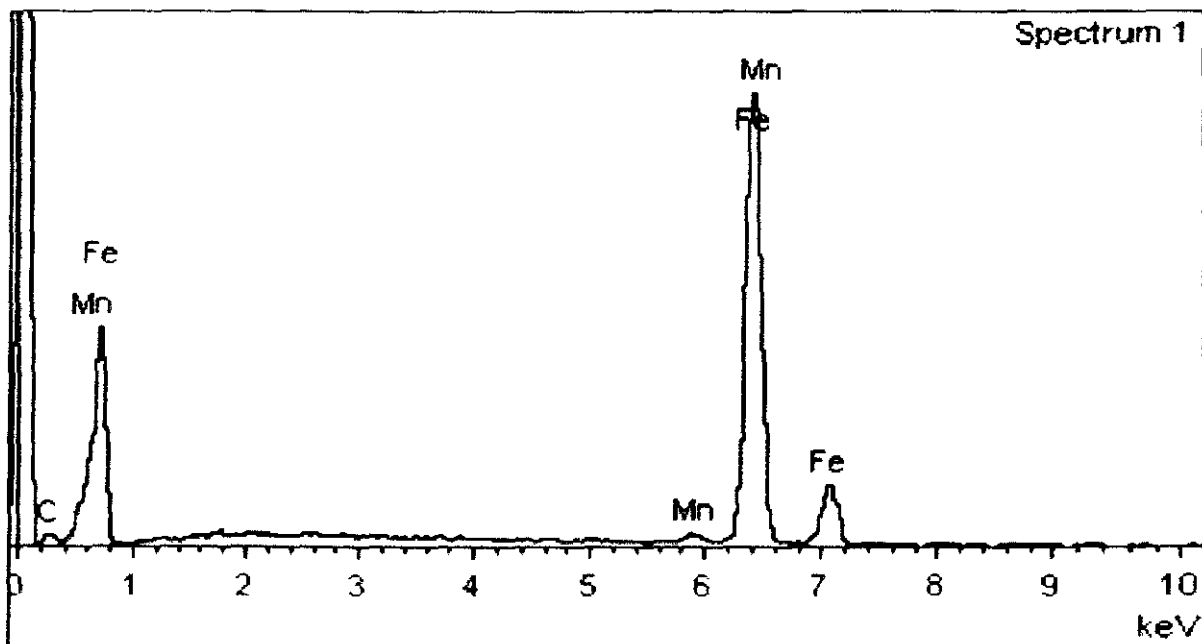


Figure 4.55: EDX result of CO₂ corrosion product of X52 carbon steel at 25 °C,
pH=6.

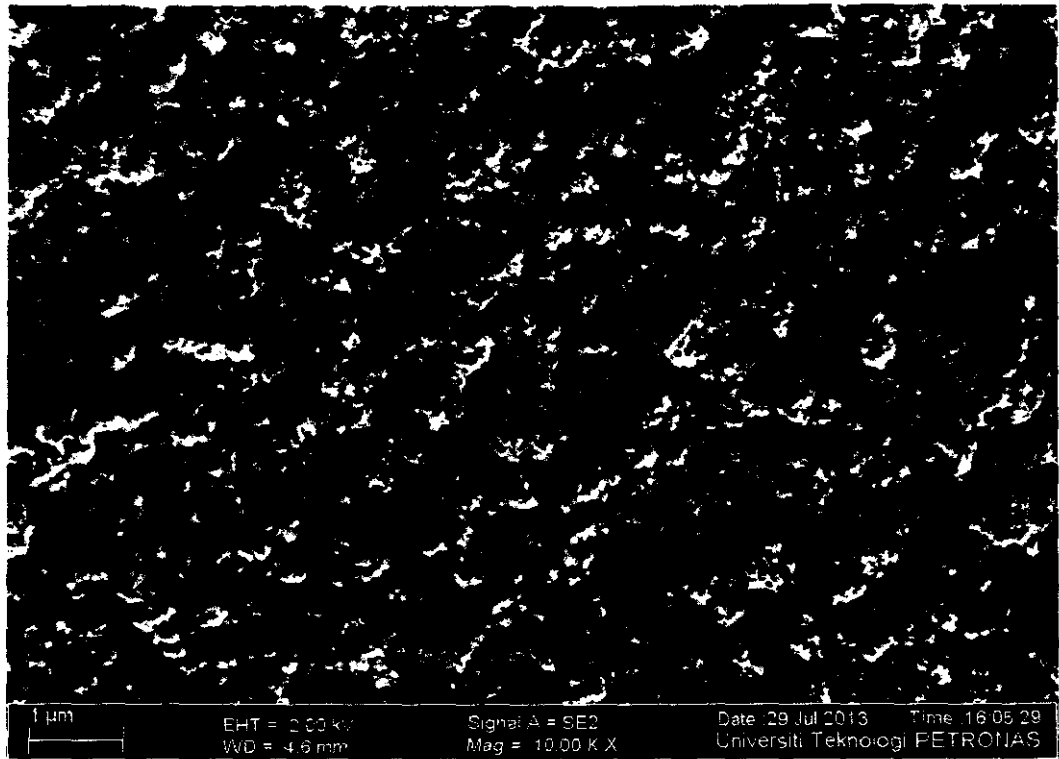


Figure 4.56: SEM image of corroded X52 carbon steel surface at 80 °C, pH=4.

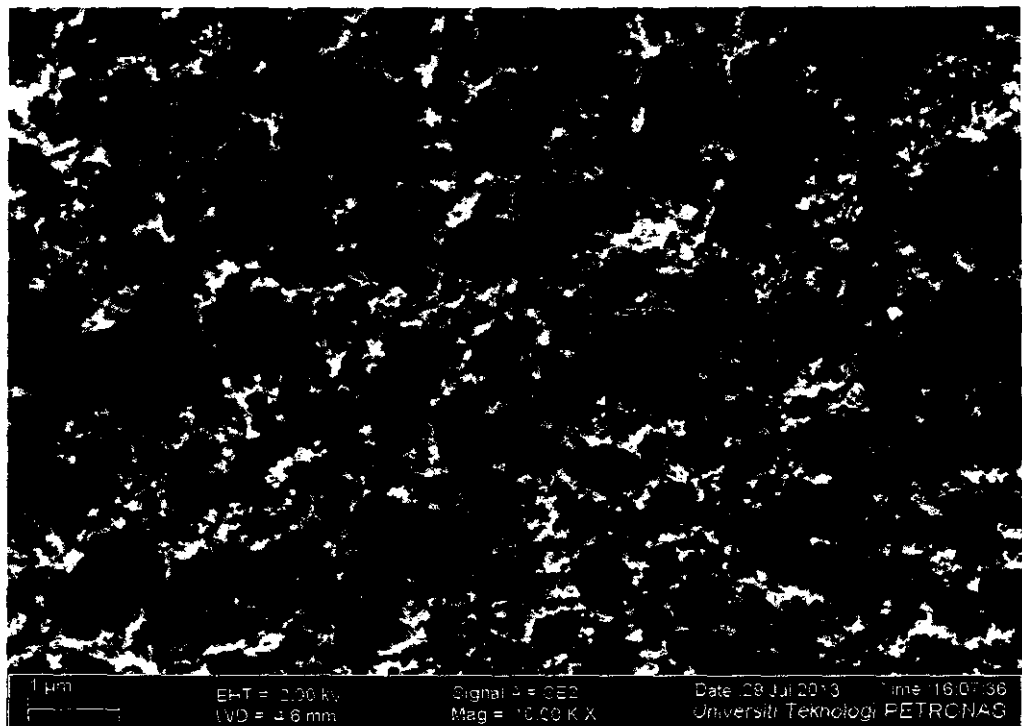


Figure 4.57: SEM image of corroded X52 carbon steel surface at 80 °C, pH=6.

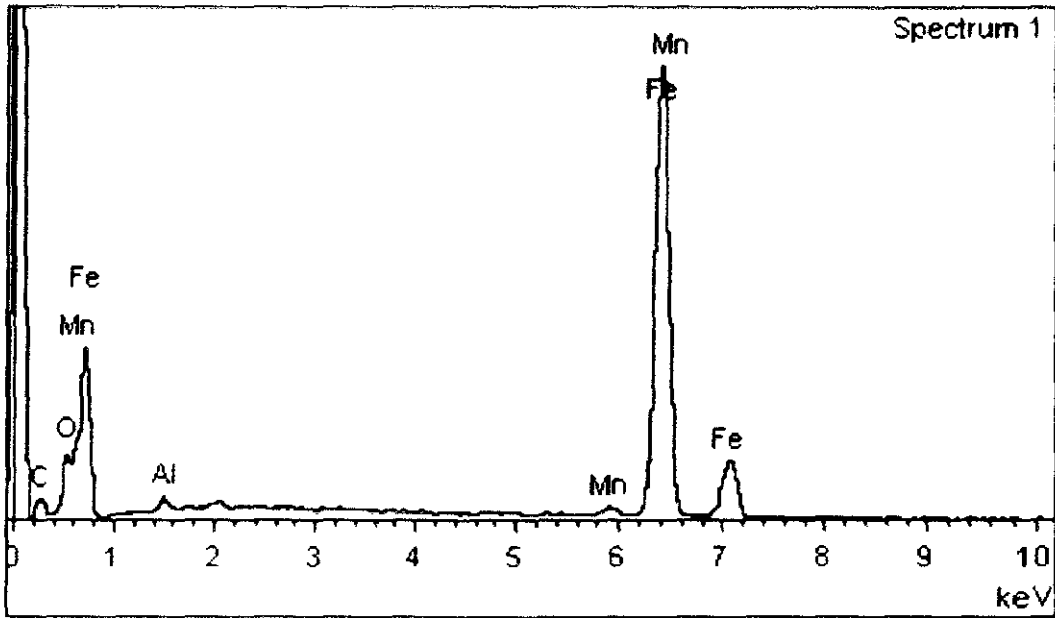


Figure 4.58: EDX result of CO₂ corrosion product of X52 carbon steel at 80 °C.
pH=6.

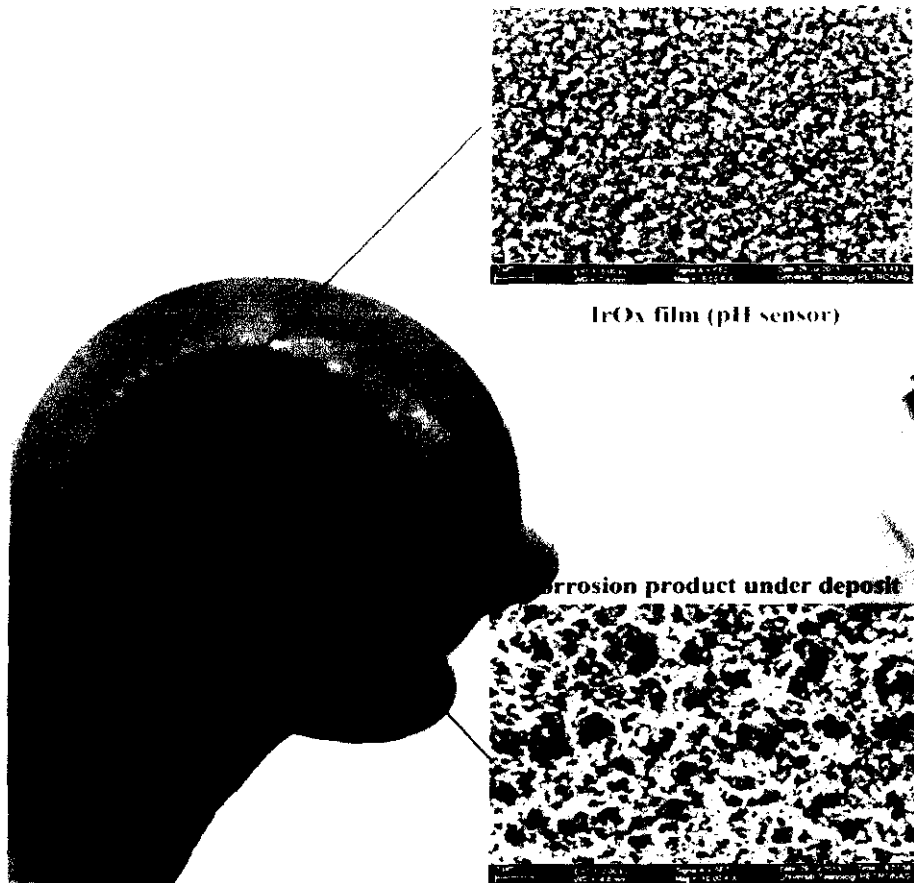


Figure 4.59: Surface of pH probe and carbon steel after exposure in CO₂-saturated 3% NaCl solution under deposit.

A top view picture of employed pH probe after experiment is shown in figure 4.59 which shows surface of pH sensor is stable after CO₂ corrosion experiment.

4.5.4 Corrosion rate in bulk pH=4

Corrosion rate of X52 carbon steel under deposit was simultaneously measured at different temperature by means of another potentiostat and long term LPR approach. As can be seen from Figure 4.60, first corrosion rate increased then decreased due to formation of protective corrosion product layer. In contrast, Figure 4.61 shows corrosion rate of sample at 80 °C gradually increased and then became stable due to non-stable corrosion product film.

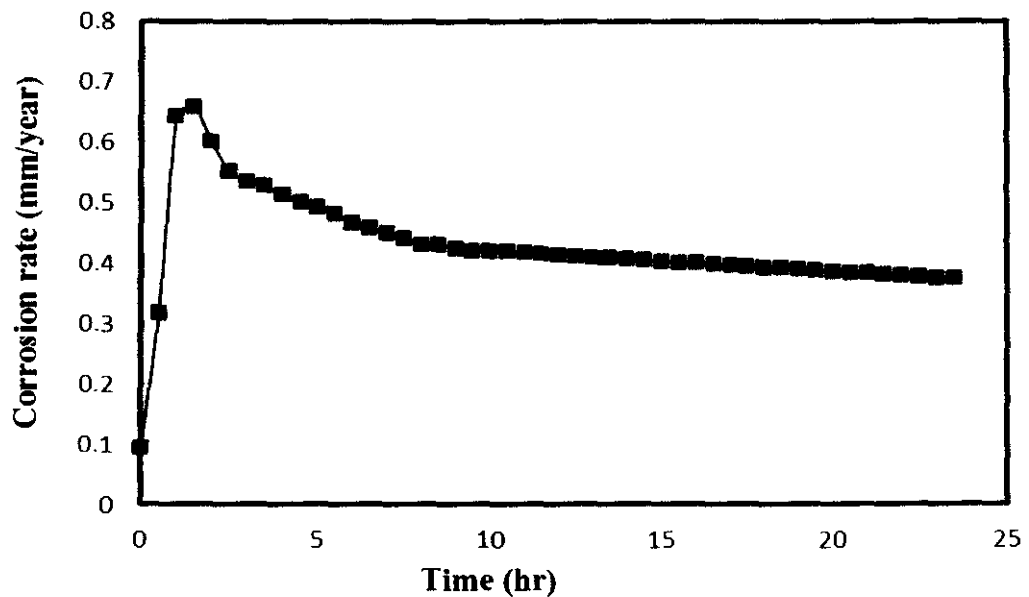


Figure 4.60: Corrosion rate of X52 carbon steel in the 3% NaCl solution at 25 °C under deposit, bulk pH=4.

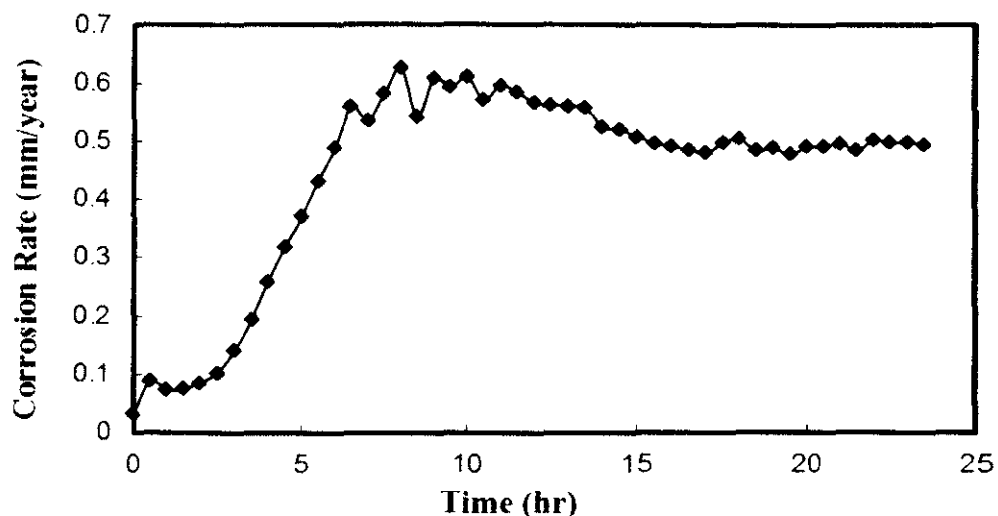


Figure 4.61: Corrosion rate of X52 carbon steel in the 3% NaCl solution at 80 °C under deposit, bulk pH=4.

4.5.5 Conclusion

The pH value of the X52 carbon steel under deposit (agar) was monitored for the first time using the in-situ pH microsensor of iridium oxide during the CO₂ corrosion at 25, 50, and 80°C. The design approves that the measurement was able to determine the pH change correctly under agar, which is a critical requirement for studying corrosion under deposit. In all cases, metal surface pH under deposit increased compared with bulk solution pH after the corrosion process began. This result is in good agreement with theoretical hypothesis and prediction.

CHAPTER 5

CONCLUSIONS AND FUTURE WORK

5.1 Conclusions

Based on statistical and experimental investigations that have been done in this research work, following conclusions were achieved:

- This work demonstrates the efficiency of response surface methodology in modeling and investigating the effect of various factors on IrO_x electrodeposition. Statistical results showed that the significant effect of scan rate on the IrO_x layers is higher than those of temperature and number of cycles.
- The results of the electrochemical experiment indicated that all fabricated electrodes were conductive and reduced the impedance of the stainless steel electrode. The CV result showed that CSC_C increased with an increase in the electrodeposited layer. However, the FESEM images revealed that cracks in electrodeposited layer also increased with an increase in IrO_x thickness.
- After successful result of electrodeposited IrO_x on stainless steel as pH sensor, a novel probe design with combination of pH sensors and carbon steel working electrode proposed for real-time measurement of pH on corroding carbon steel surface for better corrosion monitoring in CO₂ environment with or without deposit.

- The pH value of the X52 carbon steel /solution interface was monitored at 25, 50, and 80°C. The design confirms that the measurement was able to determine the pH changes correctly at the substrate/solution interface, which is a key requirement for studying the mechanism of electrochemical reactions and the relationship between corrosion process and the pH at the working electrode/solution interface during the corrosion. In all cases, surface pH or the interfacial pH increased compared with bulk solution pH after the corrosion process began. This result is in good agreement with theoretical hypothesis and prediction.
- The pH value of the X52 carbon steel under deposit (agar) was also monitored at 25, 50, and 80°C. The design approves that the measurement was able to determine the pH changes correctly under agar, which is a critical requirement for studying corrosion under deposit. In all cases, metal surface pH under deposit increased compared with bulk solution pH after the corrosion process began. This result is in good agreement with theoretical hypothesis and prediction.

5.2 Recommendation for Future Works

The research reported above investigates just using proposed pH probe for CO₂ corrosion.

More extensive studies will be invaluable. Some ideas developed here can be referred to for future studies:

- Proposed pH probe design in this study can be used to monitor surface pH measurement in other environment such as: H₂S and acidic solution.

- Regarding to purposes, material of working electrode which was carbon steel in our study can be changed.
- IrO_x was used as pH sensor material in our study, can be changed to any other sensing material for monitoring of any other ions in corroding surfaces which is very useful for monitoring of MIC or any other kind of corrosion.
- More effort can be done by using proposed pH probe for high pressure environment by just changing mounting material to a high pressure resistant resin.

REFERENCES

1. Han, J. "Galvanic Mechanism of Localized Corrosion for Mild Steel in Carbon Dioxide Environments", Ohio University (2009).
2. Dugstad, A., "Fundamental Aspects of CO₂ Metal Loss Corrosion-Part 1: Mechanism", *CORROSION 2006*, vol., pp. paper no. 06111, 2006.
3. Sun, W., Chokshi, K. & Nescic, S., "Iron Carbonate scale growth and the effect of Inhibition in CO₂ corrosion of mild steel", *CORROSION 2005*, vol., 2005.
4. Han, J., Yang, Y., Nescic, S. & Brown, B.N., "Roles of passivation and galvanic effects in localized CO₂ corrosion of mild steel", *CORROSION 2008*, vol. paper No. 08332, 2008.
5. Han, J., Brown, B.N., Young, D. & Nešić, S., "Mesh-capped probe design for direct pH measurements at an actively corroding metal surface", *Journal of applied electrochemistry*, vol.40(3), pp. 683-690, 2010.
6. Li, W., Brown, B., Young, D. & Nescic, S., "Investigation of Pseudo-Passivation of Mild Steel in CO₂ Corrosion", 2013.
7. Kakooei, S., Ismail, M.C. & Ari-Wahjoedi, B., "An overview of pH Sensors Based on Iridium Oxide: Fabrication and Application", *International Journal of Material Science Innovations*, vol.1(1), pp. 62-72, 2013.
8. Marzouk, S.A.M., "Improved electrodeposited iridium oxide pH sensor fabricated on etched titanium substrates", *Analytical chemistry*, vol.75(6), pp. 1258-1266, 2003.
9. Kakooei, S., Ismail, M.C. & Wahjoedi, B.A., "Electrochemical Study of Iridium Oxide Coating on Stainless Steel Substrate", *Int. J. Electrochem. Sci*, vol.8, pp. 3290-3301, 2013.
10. Kermani, B., "Materials optimization for oil and gas sour production", *CORROSION 2000*, 2000.
11. Ferreira, F.B.A., Silva, F.L.G., Luna, A., Lago, D.C.B. & Senna, L., "Response surface modeling and optimization to study the influence of deposition parameters on the electrodeposition of Cu-Zn alloys in citrate medium", *Journal of applied electrochemistry*, vol.37(4), pp. 473-481, 2007.
12. Honarvar Nazari, M., Allahkaram, S. & Kermani, M., "The effects of temperature and pH on the characteristics of corrosion product in CO₂

- corrosion of grade X70 steel", *Materials & Design*, vol.31(7), pp. 3559-3563, 2010.
13. George, K. & Nešić, S., "Investigation of carbon dioxide corrosion of mild steel in the presence of acetic acid-Part 1: Basic mechanisms", *Corrosion*, vol.63(2), pp. 178-186, 2007.
 14. Nordsveen, M., Nešić, S., Nyborg, R. & Stangeland, A., "A mechanistic model for carbon dioxide corrosion of mild steel in the presence of protective iron carbonate films-Part 1: Theory and verification", *Corrosion*, vol.59(5), pp. 443-456, 2003.
 15. Ezuber, H.M., "Influence of temperature and thiosulfate on the corrosion behavior of steel in chloride solutions saturated in CO₂", *Materials & Design*, vol.30(9), pp. 3420-3427, 2009.
 16. Wong, J.E. & Park, N.E., "Further Investigation on the Effect of Corrosion Inhibitor Actives on the Formation of Iron Carbonate on Carbon Steel", *CORROSION 2009*, 2009.
 17. Salama, M.M. & Brown, B.N., "A Study of Factors Affecting CO₂ Corrosion and Inhibitor Effectiveness Using a Multi-Phase Flowloop", *CORROSION 2009*, 2009.
 18. Gulbrandsen, E., Foss, M. & Sjøblom, J., "INTERACTION OF CARBON DIOXIDE CORROSION INHIBITORS WITH CORROSION PRODUCTS DEPOSIT", *CORROSION 2008*, 2008.
 19. Sun, W. & Nešić, S., "Kinetics of Corrosion Layer Formation: Part 1-Iron Carbonate Layers in Carbon Dioxide Corrosion", *Corrosion*, vol.64(4), pp. 334-346, 2008.
 20. Crolet, J., Thevenot, N. & Nesic, S., "Role of conductive corrosion products in the protectiveness of corrosion layers", *Corrosion*, vol.54(3), pp. 194-203, 1998.
 21. Howell, A.G., "Under Deposit Corrosion Mechanisms in Boilers", *CORROSION 2006*, 2006.
 22. Reus, H.D., Gough, M.D., Durnie, W.D., *et al.*, "Test methodologies and field verification of corrosion inhibitors to address under deposit corrosion in oil and gas production systems", *CORROSION 2005*, 2005.

23. Huang, J., Brown, B., Choi, Y.-S. & Nešić, S., "Prediction of Uniform CO₂ Corrosion of Mild Steel Under Inert Solid Deposits", CORROSION 2011, 2011.
24. Menendez, C., Jovancicevic, V., Zhu, Z.M., Morton, M. & Stegmann, D., "New Method for Assessing Corrosion Under Iron Sulfide Deposits and CO₂/H₂S Conditions", CORROSION 2011, 2011.
25. Nyborg, R. & Foss, M., "Experience With an Under Deposit Corrosion Test Method With Galvanic Current Measurements", CORROSION 2011, 2011.
26. Xue, H., Cheng, F.Y., Zhu, Z., Tajallipour, N. & Teevens, P.J., "Internal Pitting Corrosion of X80 Pipeline Steel under Deposited Sand Bed in CO₂-Saturated Solutions", CORROSION 2011, 2011.
27. Romankiw, L.T., "Specific Ion Activity Measurement at an Electrode during Electrolysis". IBM Technical Disclosure Bulletin, vol.13(1), pp. 69-70. 1970.
28. Dexter, S.C. & Lin, S., "Calculation of seawater pH at polarized metal surfaces in the presence of surface films", Corrosion, vol.48(1), pp. 50-60, 1992.
29. Little, B.J., Lewandowski, Z., Funk, T. & Roe, F. Spatial Distribution of pH at Mild Steel Surfaces Using an Iridium Oxide Microelectrode. (DTIC Document, 1994).
30. Wipf, D.O., Ge, F., Spaine, T.W. & Baur, J.E., "Microscopic measurement of pH with iridium oxide microelectrodes", Analytical chemistry, vol.72(20), pp. 4921-4927, 2000.
31. Bezbaruah, A.N. & Zhang, T.C., "Fabrication of anodically electrodeposited iridium oxide film pH microelectrodes for microenvironmental studies", Analytical chemistry, vol.74(22), pp. 5726-5733, 2002.
32. Cogan, S., Troyk, P., Ehrlich, J., *et al.* Charge-injection waveforms for iridium oxide (AIROF) microelectrodes. Vol. 2 1960-1963 Vol. 1962 (IEEE, 2003).
33. Lu, Y., Wang, T., Cai, Z., *et al.*, "Anodically electrodeposited iridium oxide films microelectrodes for neural microstimulation and recording", Sensors and Actuators B: Chemical, vol.137(1), pp. 334-339, 2009.
34. Zimer, A.M., Lemos, S.G., Pocrifka, I.A., Mascaro, L.H. & Pereira, E.C., "Needle-like IrO/Ag combined pH microelectrode", Electrochemistry Communications, vol.12(12), pp. 1703-1705, 2010.

35. Wei, C., Bard, A.J., Nagy, G. & Toth, K., "Scanning electrochemical microscopy. 28. Ion-selective neutral carrier-based microelectrode potentiometry", *Analytical chemistry*, vol.67(8), pp. 1346-1356, 1995.
36. Lewandowski, Z., Lee, W., Characklis, W. & Little, B., "Dissolved oxygen and pH microelectrode measurements at water-immersed metal surfaces", *Corrosion*, vol.45(2), pp. 92-98, 1989.
37. Klusmann, E. & Schultze, J., "pH-microscopy—theoretical and experimental investigations", *Electrochimica acta*, vol.42(20), pp. 3123-3134, 1997.
38. Romankiw, L.T. pH Changes at the Cathode during Electrolysis on Ni, FeCu and their Alloys and a Simple Technique for Measuring pH Changes at Electrodes. in *the Symposium on Electrodeposition Technology, Theory and Practice* 301–325 (1987).
39. Deligianni, H. & Romankiw, L., "In situ surface pH measurement during electrolysis using a rotating pH electrode", *IBM Journal of Research and Development*, vol.37(2), pp. 85-95, 1993.
40. Steegstra, P. & Ahlberg, E., "Influence of oxidation state on the pH dependence of hydrous iridium oxide films", *Electrochimica acta*, 2012.
41. Steegstra, P. & Ahlberg, E., "In situ pH measurements with hydrous iridium oxide in a rotating ring disc configuration", *Journal of Electroanalytical Chemistry*, 2012.
42. Ji, J., Cooper, W., Dreisinger, D. & Peters, E., "Surface pH measurements during nickel electrodeposition", *Journal of applied electrochemistry*, vol.25(7), pp. 642-650, 1995.
43. Deslouis, C., Frateur, I., Maurin, G. & Tribollet, B., "Interfacial pH measurement during the reduction of dissolved oxygen in a submerged impinging jet cell", *Journal of applied electrochemistry*, vol.27(4), pp. 482-492, 1997.
44. Díaz, S., Mattos, O., Barcia, O. & Fabri Miranda, F., "ZnFe anomalous electrodeposition: stationaries and local pH measurements", *Electrochimica acta*, vol.47(25), pp. 4091-4100, 2002.
45. Nobial, M., Devos, O., Mattos, O.R. & Tribollet, B., "The nitrate reduction process: A way for increasing interfacial pH", *Journal of Electroanalytical Chemistry*, vol.600(1), pp. 87-94, 2007.

46. Yoshinobu, T., Iwasaki, H., Nakao, M., *et al.*, "Application of chemical imaging sensor to electro generated pH distribution", Japanese journal of applied physics, vol.37(pp. L353-L355, 1998).
47. Yoshinobu, T., Harada, T. & Iwasaki, H., "Application of the pH-imaging sensor to determining the diffusion coefficients of ions in electrolytic solutions", Japanese journal of applied physics, vol.39(pp. 318, 2000).
48. King, F., Litke, C. & Tang, Y., "Effect of interfacial pH on the reduction of oxygen on copper in neutral NaClO₄ solution", Journal of Electroanalytical Chemistry, vol.384(1), pp. 105-113, 1995.
49. Schlesinger, M. & Paunovic, M. *Modern electroplating*, (Wiley, 2011).
50. Gamburg, Y.D. & Zangari, G. *Theory and practice of metal electrodeposition*, (Springer Science+ Business Media, 2011).
51. Vidal-Iglesias, F.J., Solla-Gullón, J., Herrero, E., Rodes, A. & Aldaz, A., "Do you really understand the electrochemical Nernst equation?", *Electrocatalysis*, pp. 1-9, 2012.
52. Janata, J. & Josowicz, M., "Peer Reviewed: A Fresh Look at Some Old Principles: The Kelvin Probe and the Nernst Equation", *Analytical chemistry*, vol.69(9), pp. 293A-296A, 1997.
53. Roach, K. "Electrochemical models for electrode behavior in retinal prostheses. M. Eng", Master of Engineering in Computer Science and Engineering. Department of Electrical Engineering and Computer Science, Massachusetts Institute of Technology (2003).
54. Bard, A. & Faulkner, L., "Electrochemical methods: principles and applications", *Electrochemical Methods: Principles and Applications*, 2001.
55. Bard, A.J. & Faulkner, L.R. *Electrochemical methods: fundamentals and applications*, (Wiley New York, 1980).
56. Evans, D.H., O'Connell, K.M., Petersen, R.A. & Kelly, M.J., "Cyclic voltammetry", *Journal of chemical education*, vol.60(4), pp. 290, 1983.
57. Bioanalytical Systems, I. *Instruction Manual for Basi Epsilon for Electrochemistry*. (2000-2009).
58. Lasia, A. *Electrochemical impedance spectroscopy and its applications*. in *Modern aspects of electrochemistry* 143-248 (Springer, 2002).

59. Macdonald, D.D., Sikora, E. & Engelhardt, G., "Characterizing electrochemical systems in the frequency domain", *Electrochimica acta*, vol.43(1), pp. 87-107, 1998.
60. de Levie, R., "The admittance of the interface between a metal electrode and an aqueous electrolyte solution: some problems and pitfalls", *Annals of biomedical engineering*, vol.20(3), pp. 337-347, 1992.
61. Mailley, S., Hyland, M., Mailley, P., McLaughlin, J. & McAdams, E., "Electrochemical and structural characterizations of electrodeposited iridium oxide thin-film electrodes applied to neurostimulating electrical signal", *Materials Science and Engineering: C*, vol.21(1), pp. 167-175, 2002.
62. Da Silva, G., Lemos, S., Pocrifka, L., *et al.*, "Development of low-cost metal oxide pH electrodes based on the polymeric precursor method", *analytica chimica acta*, vol.616(1), pp. 36-41, 2008.
63. Martinez, C.C.M., Madrid, R.E. & Felice, C.J., "A pH Sensor Based on a Stainless Steel Electrode Electrodeposited With Iridium Oxide", *Education, IEEE Transactions on*, vol.52(1), pp. 133-136, 2009.
64. Arikawa, T., Takasu, Y., Murakami, Y., Asakura, K. & Iwasawa, Y., "Characterization of the structure of ruo2-iro2/ti electrodes by exafs", *The Journal of Physical Chemistry B*, vol.102(19), pp. 3736-3741, 1998.
65. Thanawala, S.S., Baird, R.J., Georgiev, D.G. & Auner, G.W., "Amorphous and crystalline IrO₂ thin films as potential stimulation electrode coatings", *Applied Surface Science*, vol.254(16), pp. 5164-5169, 2008.
66. Ross D. Meyer, S.F.C., Member, Trung H. Nguyen, R. David Rauh, "Electrodeposited Iridium Oxide for Neural Stimulation and Recording Electrodes", *IEEE Transactions on Neural Systems and Rehabilitation Engineering*, vol.9(1), pp. 2-11, 2001.
67. Song, I., Fink, K. & Payer, J., "Metal oxide/metal pH sensor: Effect of anions on pH measurements", *Corrosion*, vol.54(01), 1998.
68. Van Ooyen, A., Topalov, G., Ganske, G., Mokwa, W. & Schnakenberg, U., "Iridium oxide deposited by pulsed dc-sputtering for stimulation electrodes", *Journal of Micromechanics and Microengineering*, vol.19(7), pp. 074009, 2009.

69. Lee, I.-S., Whang, C.-N., Park, J.-C., Lee, D.-H. & Seo, W.-S., "Biocompatibility and charge injection property of iridium film formed by ion beam assisted deposition", *Biomaterials*, vol.24(13), pp. 2225-2231, 2003.
70. Wessling, B., van Ooyen, A., Mokwa, W. & Schnakenberg, U. Iridium sputtered at varying pressures and target-substrate-distances evaluated for use as stimulation electrode material. in *Engineering in Medicine and Biology Society, 2006. EMBS'06. 28th Annual International Conference of the IEEE* 3353-3356 (IEEE, 2006).
71. Yang, H., Kang, S.K., Shin, D.H., Kim, H. & Kim, Y.T. Microfabricated iridium oxide reference electrode for continuous glucose monitoring sensor. Vol. 1 103-106 vol. 101 (IEEE, 2003).
72. Franklin, R.K., Joo, S., Negi, S., Solzbacher, F. & Brown, R.B. A comparison of fabrication methods for Iridium Oxide reference electrodes. in *IEEE SENSORS 2009 Conference* 1086-1089 (IEEE, 2009).
73. Macur, R.A. Iridium-iridium oxide electrode for measuring of blood pH and other fluids (Google Patents, 1973).
74. O'Hare, D., Parker, K.H. & Winlove, C.P., "Metal-metal oxide pH sensors for physiological application", *Medical engineering & physics*, vol.28(10), pp. 982-988, 2006.
75. Chiao, J.C. & Huang, W.D. Amorphous IrOx Film pH Sensor. (Google Patents, 2010).
76. Huang, P. & Kreider, K.G. Electrochemical evaluation of solid state pH sensors for nuclear waste containment. (Nuclear Regulatory Commission, Washington, DC (USA). Div. of Engineering; National Bureau of Standards, Washington, DC (USA). Center for Chemical Engineering, 1988).
77. Kreider, K., "Iridium oxide thin-film stability in high-temperature corrosive solutions", *Sensors and Actuators B: Chemical*, vol.5(1-4), pp. 165-169, 1991.
78. Prasad, R., "Assessment and Control of MIC in the Oil Industry in the 20th Century", *CORROSION 2000*, 2000.
79. Lewandowski, Z., Funk, T., Roe, F., *et al.*, "Spatial distribution of pH at mild steel surfaces using an iridium oxide microelectrode". *ASTM Special Technical Publication*, vol.1232, pp. 61-61, 1994.

80. Kim, Y.J., Lee, Y.C., Sohn, B.K., Lee, J.H. & Kim, C.S., "A novel pH microsensor with a built-in reference electrode", *Journal-Korean Physical Society*, vol.43(1), pp. 769-772, 2003.
81. Roe, F., Lewandowski, Z. & Funk, T., "Simulating microbiologically influenced corrosion by depositing extracellular biopolymers on mild steel surfaces", *Corrosion*, vol.52(10), 1996.
82. Carroll, S. & Baldwin, R.P., "Self-Calibrating Microfabricated Iridium Oxide pH Electrode Array for Remote Monitoring", *Analytical chemistry*, vol.82(3), pp. 878-885, 2010.
83. Kurzweil, P., "Metal oxides and ion-exchanging surfaces as pH sensors in liquids: State-of-the-art and outlook", *Sensors*, vol.9(6), pp. 4955-4985, 2009.
84. Burke, L.D., Mulcahy, J.K. & Whelan, D.P., "Preparation of an oxidized iridium electrode and the variation of its potential with pH", *Journal of electroanalytical chemistry and interfacial electrochemistry*, vol.163(1), pp. 117-128, 1984.
85. Pickup, P.G. & Birss, V., "A model for anodic hydrous oxide growth at iridium", *Journal of electroanalytical chemistry and interfacial electrochemistry*, vol.220(1), pp. 83-100, 1987.
86. Quan, H., Kim, W., Chung, K. & Park, J., "Surface renewable hydrogen ion-selective polymeric composite electrode containing iridium oxide", *Bulletin-Korean Chemical Society*, vol.26(10), pp. 1565, 2005.
87. Huang, W.D., Hsu, L.C., Wang, J., *et al.* Investigation of repeatability of sol-gel iridium oxide pH sensor on flexible substrate. in *Smart Materials, Nano- and Micro-Smart Systems*, Vol. 7269 726916-726916-726919 (International Society for Optics and Photonics, 2008).
88. Huang, W.D., Wang, J., Ativanichayaphong, T., Chiao, M. & Chiao, J. Development of an IrOx micro pH sensor array on flexible polymer substrate. (Society of Photo-Optical Instrumentation Engineers, 2008).
89. Karthigeyan, A., Gupta, R., Scharnagl, K., *et al.*, "A room temperature HSGFET ammonia sensor based on iridium oxide thin film", *Sensors and Actuators B: Chemical*, vol.85(1), pp. 145-153, 2002.
90. Yamanaka, K., "Anodically Electrodeposited Iridium Oxide Films(AEIROF) from Alkaline Solutions for Electrochromic Display Devices", *Japanese journal of applied physics*, vol.28(part 1), pp. 632-637, 1989.

91. Pikulski, M. & Gorski, W., "Iridium-based electrocatalytic systems for the determination of insulin", *Analytical chemistry*, vol.72(13), pp. 2696-2702, 2000.
92. Terashima, C., Rao, T.N., Sarada, B.V., Spataru, N. & Fujishima, A., "Electrodeposition of hydrous iridium oxide on conductive diamond electrodes for catalytic sensor applications", *Journal of Electroanalytical Chemistry*, vol.544(pp. 65-74, 2003.
93. Ges, I.A., Ivanov, B.L., Schaffer, D.K., *et al.*, "Thin-film IrOx pH microelectrode for microfluidic-based microsystems", *Biosensors and Bioelectronics*, vol.21(2), pp. 248-256, 2005.
94. Ryyänen, T., Nurminen, K., Hämäläinen, J., Leskelä, M. & Leikkala, J., "pH electrode based on ALD deposited iridium oxide", *Procedia Engineering*, vol.5(pp. 548-551, 2010.
95. Meyer, R.D., Cogan, S.F., Nguyen, T.H. & Rauh, R.D., "Electrodeposited iridium oxide for neural stimulation and recording electrodes", *Neural Systems and Rehabilitation Engineering, IEEE Transactions on*, vol.9(1), pp. 2-11, 2001.
96. Mayorga Martinez, C.C., Madrid, R.E. & Felice, C.J., "Electrochemical and geometrical characterization of iridium oxide electrodes in stainless steel substrate", *Sensors and Actuators B: Chemical*, vol.133(2), pp. 682-686, 2008.
97. Petit, M.A. & Plichon, V., "Anodic electrodeposition of iridium oxide films", *Journal of Electroanalytical Chemistry*, vol.444(2), pp. 247-252, 1998.
98. Zhang, J.M., Shi, Q., Yang, C. & Dong, Q.F., "In-situ pH measurement at the electrode/solution interface", *Chinese Chemical Letters*, vol.11(7), pp. 617-620, 2000.
99. Marzouk, S.A.M., Ufer, S., Buck, R.P., *et al.*, "Electrodeposited iridium oxide pH electrode for measurement of extracellular myocardial acidosis during acute ischemia", *Analytical chemistry*, vol.70(23), pp. 5054-5061, 1998.
100. C. M. Nguyen, H.C., W. D. Huang, and J.-C. Chiao, "An Electro-Deposited IrOx Thin Film pH Sensor", *BMES Biomedical Engineering Society Annual Meeting*, vol., 2011.
101. Ges, I.A., Ivanov, B.L., Werdich, A.A. & Baudenbacher, F.J., "Differential pH measurements of metabolic cellular activity in nl culture volumes using

- microfabricated iridium oxide electrodes", *Biosensors and Bioelectronics*, vol.22(7), pp. 1303-1310, 2007.
102. Elsen, H.A., Monson, C.F. & Majda, M., "Effects of electrodeposition conditions and protocol on the properties of iridium oxide pH sensor electrodes", *Journal of The Electrochemical Society*, vol.156(1), pp. F1-F6, 2009.
 103. Park, J., Kim, J. & Quan, H., "A surface renewable iridium oxide-glass composite hydrogen ion electrode", *Microchemical Journal*, vol.95(1), pp. 102-106, 2010.
 104. Park, J.M. & Kim, J.Y. Surface Renewable Iridium Oxide-Glass or Ceramic Composite Hydrogen Ion Electrode. (US Patent App. 12/846,791, 2010).
 105. Marzouk, S.A.M., Buck, R.P., Dunlap, L.A., Johnson, T.A. & Cascio, W.E., "Measurement of extracellular pH, K⁺, and lactate in ischemic heart", *Analytical biochemistry*, vol.308(1), pp. 52-60, 2002.
 106. Zhang, J., Lin, C., Feng, Z. & Tian, Z., "Mechanistic studies of electrodeposition for bioceramic coatings of calcium phosphates by an in situ pH-microsensor technique", *Journal of Electroanalytical Chemistry*, vol.452(2), pp. 235-240, 1998.
 107. Tanabe, H., Togashi, K., Misawa, T. & Kamachi Mudali, U., "In situ pH measurements during localised corrosion of type 316LN stainless steel using scanning electrochemical microscopy", *Journal of materials science letters*, vol.17(7), pp. 551-553, 1998.
 108. Kirk, R.E. *Experimental design: Procedures for the behavioral sciences*, (SAGE Publications, Incorporated, 2012).
 109. Rouhi, J., Mahmud, S., Hutagalung, S.D. & Kakooei, S., "Optimisation of nanooxide mask fabricated by atomic force microscopy nanolithography: a response surface methodology application", *Micro & Nano Letters, IET*, vol.7(4), pp. 325-328, 2012.
 110. Box, G.E. & Draper, N.R., "Empirical model-building and response surfaces: Wiley Series in probability and mathematical statistics", *Empirical model-building and response surfaces: Willey series in probability and mathematical statistics*, 1987.
 111. Carley, K.M., Kamneva, N.Y. & Reminga, J. Response surface methodology. (DTIC Document, 2004).

112. Porooh-Seritan, M., Gutt, S., Gutt, G., *et al.*, "Design of experiments for statistical modeling and multi-response optimization of nickel electroplating process", *Chemical Engineering Research and Design*, vol.89(2), pp. 136-147, 2011.
113. Orhan, G., Hapçı, G. & Keleş, Ö., "Application of Response Surface Methodology (RSM) to Evaluate the Influence of Deposition Parameters on the Electrolytic Cu-Zn Alloy Powder". *Int. J. Electrochem. Sci.*, vol.6(pp. 3966-3981, 2011.
114. Ahmadi, M., Vahabzadeh, F., Bonakdarpour, B., Mofarrah, E. & Mehranian, M., "Application of the central composite design and response surface methodology to the advanced treatment of olive oil processing wastewater using Fenton's peroxidation", *Journal of Hazardous Materials*, vol.123(1), pp. 187-195, 2005.
115. Bajpai, S., Gupta, S., Dey, A., *et al.*, "Application of Central Composite Design approach for removal of chromium (VI) from aqueous solution using weakly anionic resin: Modeling, optimization, and study of interactive variables", *Journal of Hazardous Materials*, vol.227– 228(pp. 436– 444, 2012.
116. Bolton, S. & Bon, C. *Pharmaceutical statistics: practical and clinical applications*. (M. Dekker, 1997).
117. Oberg, A.L., Mahoney, D.W., Eckel-Passow, J.E., *et al.*, "Statistical analysis of relative labeled mass spectrometry data from complex samples using ANOVA". *Journal of proteome research*, vol.7(1), pp. 225-233, 2008.
118. Tolosa, V."A Micro-electrode Array Biosensor for Monitoring Changes in Neurotransmitter Concentrations in Vivo", Doctor of Philosophy, Chemical Engineering, UNIVERSITY OF CALIFORNIA (2010).
119. Standard, A. G102-89, Standard Practice for Calculation of Corrosion Rates and Related Information from Electrochemical Measurements. in *Annual Book of ASTM Standards*, *ASTM International*, West Conshohocken, PA, Vol. 3 (2006).
120. Stern, M. & Geary, A.L., "Electrochemical polarization I. A theoretical analysis of the shape of polarization curves", *Journal of The Electrochemical Society*, vol.104(1), pp. 56-63, 1957.
121. Rouhimaleh, J."Fabrication and Characterization of Nano-Gap Electrodes by AFM Using Local Anodic Oxidation and TMAH Wet Etching", PhD Thesis, School of Physics, Univerisiti Sains Malaysia (2012).

122. Castillo-Blum, S.E., Richens, D.T. & Sykes, A.G., "Oxidation of hexaaquairidium (III) and related studies: Preparation and properties of iridium (III), iridium (IV), and iridium (V) dimers as aqua ions", *Inorganic Chemistry*, vol.28(5), pp. 954-960, 1989.
123. Zhao, Y., Hernandez-Pagan, E.A., Vargas-Barbosa, N.M., Dysart, J.L. & Mallouk, T.E., "A high yield synthesis of ligand-free iridium oxide nanoparticles with high electrocatalytic activity", *The Journal of Physical Chemistry Letters*, vol.2(5), pp. 402-406, 2011.
124. Nakagawa, T., Bjorge, N.S. & Murray, R.W., "Electrogenerated IrO_x nanoparticles as dissolved redox catalysts for water oxidation", *Journal of the American Chemical Society*, vol.131(43), pp. 15578-15579, 2009.
125. Nakagawa, T., Beasley, C.A. & Murray, R.W., "Efficient electro-oxidation of water near its reversible potential by a mesoporous IrO_x nanoparticle film", *The Journal of Physical Chemistry C*, vol.113(30), pp. 12958-12961, 2009.
126. Raistrick, I., "Impedance studies of porous electrodes", *Electrochimica acta*, vol.35(10), pp. 1579-1586, 1990.
127. Meyers, J.P., Doyle, M., Darling, R.M. & Newman, J., "The impedance response of a porous electrode composed of intercalation particles", *Journal of The Electrochemical Society*, vol.147(8), pp. 2930-2940, 2000.
128. Blakemore, J.D., Schley, N.D., Kushner-Lenhoff, M.N., *et al.*, "Comparison of Amorphous Iridium Water-Oxidation Electrocatalysts Prepared from Soluble Precursors", *Inorganic Chemistry*, vol.51(14), pp. 7749-7763, 2012.
129. Cogan, S.F., Plante, T. & Ehrlich, J. Sputtered iridium oxide films (SIROFs) for low-impedance neural stimulation and recording electrodes. in *Engineering in Medicine and Biology Society, 2004. IEMBS'04. 26th Annual International Conference of the IEEE*, Vol. 2 4153-4156 (IEEE, 2004).
130. Sheng, Z.-L., Wan, P.-F., Dong, C.-L. & Li, Y.-H., "Optimization of total flavonoids content extracted from *Flos Populi* using response surface methodology", *Industrial Crops and Products*, vol.43(pp. 778-786, 2013.
131. Sun, Y.-X., Liu, J.-C. & Kennedy, J.F., "Extraction optimization of antioxidant polysaccharides from the fruiting bodies of *Chroogomphis rutilus* (Schaeff.: Fr.) OK Miller by Box-Behnken statistical design", *Carbohydrate Polymers*, vol.82(1), pp. 209-214, 2010.

132. Tebbal, S. & Hackerman, N., "Effect of the Liquid Film Thickness on the CO₂ Corrosion of Steel", *Corrosion*, vol.45(7), pp. 558-562, 1989.

LIST OF PUBLICATIONS AND ACHIEVEMENTS

Research Title	Author's Name	Recognition	Status
Electrochemical Study of Iridium Oxide Coating on Stainless Steel Substrate	Saeid Kakooei, Mokhtar Che Ismail, Bambang Ariwahjoedi	Int. J. Electrochem. Sci., 8 (2013) 3290 - 3301, indexed by ISI and SCOPUS (IF=3.729)	Published
An overview of pH Sensors Based on Iridium Oxide: Fabrication and Application	Saeid Kakooei, Mokhtar Che Ismail, Bambang Ariwahjoedi	International Journal of Material Science Innovations 1 (1), 62-72, 2013, indexed by ISC	Published
Fabrication of a surface pH sensor for CO ₂ corrosion monitoring	Saeid Kakooei, Mokhtar Che Ismail, Bambang Ariwahjoedi	Sensors, indexed by ISI and SCOPUS (IF=1.953)	Under review
Electrodeposition of Iridium Oxide by Cyclic Voltammetry: Application of Response Surface Methodology	Saeid Kakooei, Mokhtar Che Ismail, Bambang Ariwahjoedi	Surface and Interface Analysis, indexed by ISI and SCOPUS (IF=1.22)	Under review
Surface pH measurement during CO ₂ corrosion by a microelectrode pH probe	Saeid Kakooei, Mokhtar Che Ismail, Bambang Ariwahjoedi	Materials and Corrosion, indexed by ISI and SCOPUS (IF=1.208)	Accepted
A Novel pH Sensor Design for Corrosion Monitoring	Saeid Kakooei, Mokhtar Che Ismail, Bambang Ariwahjoedi	1- SEDEX 31,2013 2- ACADREX2012	1- 3rd Stage (Bronze Medal) 2- 2 nd stage (Silver Medal)

LIST OF PUBLICATIONS WHICH ARE NOT INCLUDED IN THE THESIS

JOURNALS:

1. Mahmoud Alimanesh, Jalal Rouhi, Norzaini Zainal, **Saeid Kakooei** and Zainuriah Hassan. "Growth of Vertically Aligned ZnO Nanorods Arrays by Hydrothermal Method", *Advanced Materials Research* Vol. 795 (2013) pp 616-619, (**Scopus and ISI index**)
2. **Saeid Kakooei**, S. Valid Jaber, Kourosh Sharifi, Mokhtar Che Ismail, Abolghasem Dolati. "Effect of anodic inhibitors on corrosion of carbon steel bar reinforced concrete", *International Journal of Material Science Innovations* 1 (2), 1-14, 2013
3. **Saeid Kakooei**, M.C. Ismail, Khaled Alawadhi, Mahmood Bataee. "Prediction of Heat Affected Zone (HAZ) Corrosion in CO₂ Environment by Artificial Neural Network", *Australian Journal of Basic and Applied Sciences*, 6(12): 134-140, 2012 (**Scopus and ISI index**)
4. Hengameh Hanaei, Fakhrul Razi B Ahmadun, Ehsan Mohammadpour, **Saeid Kakooei**. "Optimization of Carbon Nano Tubes Synthesis using Fluidized bed Chemical Vapor Deposition: A Statistical Approach", *Caspian Journal of Applied Sciences Research*, 2(3), 138-147, 2013 (**ISI index**)
5. **Saeid Kakooei**, Jalal Rouhi, Ehsan Mohammadpour, Mahmoud Alimanesh, Arash Dehzangi, "Synthesis and Characterization of Cr-Doped AL₂O₃ Nanoparticles Prepared Via Aqueous Combustion Method". *Caspian Journal of Applied Sciences Research*, 1(13), pp. 16-22, 2012 (**ISI index**)
6. **Saeid Kakooei**, Hossein Taheri, Mokhtar Che Ismail, Abolghasem Dolati. "Corrosion Investigation of A516-Gr70 and API 5LX70 Steels in H₂S Containing Solution", *Caspian Journal of Applied Sciences Research*, 1(11) , 2012: 1-10 (**ISI index**)
7. **Saeid Kakooei**, Hossein Taheri, Mokhtar Che Ismail, Abolghasem Dolati, "Corrosion Behavior of X70 pipeline Steel in Hydrogen Sulfide Containing Solutions", *Journal of Applied Sciences*, 12 (23): 2454-2458, 2012 / DOI: 10.3923/jas.2012.2454.2458 (**Scopus and ISI index**)
8. Dehzangi, F. Larki, S. D. Hutagalung, E. B. Saion, A. M. Abdullah, M. N. Hamidon, M. Navaseri, **S. Kakooei**, B. Y. Majlis, A. Kharazmi, Numerical investigation and comparison with experimental characterization of side gate p-type Junctionless silicon transistor in pinchoff state, *Micro & Nano Letters*, 2012, Vol. 7, Iss. 9, pp. 981–985. doi: 10.1049/mnl.2012.0590, (**IF=0.836**)
9. Hossein Taheri, **Saeid Kakooei**, Mokhtar Che Ismail, Abolghasem Dolati. "The effect of H₂S concentration and temperature on corrosion behavior of pipeline steel

A516-Gr70", Caspian Journal of Applied Sciences Research, May; 1(5), 2012, 1-47
(ISI index)

10. Jalal Rouhi, Shahrom Mahmud, Sabar Derita Hutagalung, Nima Naderi, **Saeid Kakooei**, Mat Johar Abdullah, "Controlling the shape and gap width of silicon electrodes using Local anodic oxidation and anisotropic TMAH wet etching", IOP, Semiconductor Science and Technology 27 (2012) 065001, (IF= 1.723) , <http://nanotechweb.org/ews/article/lab/49800>
11. **Saeid Kakooei**, Jalal Rouhi, Arash Dehzangi, Ehsan Mohammadpour, Mahmoud Alimanesh
"Synthesis and Characterization of Al₂O₃:Fe Nanoparticles Prepared via Aqueous Combustion", Caspian Journal of Applied Sciences Research, 1(12), pp. 1-7, 2012
(ISI index)
12. **Saeid Kakooei**, Mokhtar Che Ismail, Bambang Ariwahjoedi,
"Mechanisms of Microbiologically Influenced Corrosion: A Review, World Applied Sciences Journal, 2012, 17 (4): 524-531, (Scopus and ISI index)
13. Jalal Rouhi, Shahrom Mahmud, Sabar Derita Hutagalung, **Saeid Kakooei**,
"Optimization of nano-oxide mask fabricated by atomic force microscopy nanolithography: A response surface methodology application", Micro & Nano Letters, 2012, 7(4): 325-328, doi: 10.1049/mnl.2011.0658 (IF=0.836)
14. **Saeid Kakooei**, Hazizan Md Akil, Abolghasem dolati, Jalal Rouhi,
"The corrosion investigation of rebar embedded in the fibers reinforced concrete ", Construction and Building Materials 35 (2012) 564-570 (IF=2.293)
15. **Saeid Kakooei**, Hazizan Md Akil, Morteza Jamshidi, Jalal Rouhi,
"THE EFFECTS OF POLYPROPYLENE FIBRES ON THE PROPERTIES OF REINFORCED CONCRETE STRUCTURES ", Construction and Building Materials 27 (2012) 73-77 (IF=2.293)
16. Jalal Rouhi, Shahrom Mahmud, Sabar Derita Hutagalung, **Saeid Kakooei**,
"Fabrication of nano-gap electrodes via nano-oxidation mask by scanning probe microscopy nanolithography.", J. Micro/Nanolith. MEMS MOEMS 10, 043002 (Oct 04, 2011); doi:10.1117/1.3643480 (IF=1.194)

CONFERENCES:

1. Mahmoud Alimanesh, Jalal Rouhi, Norzaini Zainal, **Saeid Kakooei** and Zainuriah Hassan, "Growth of Vertically Aligned ZnO Nanorods Arrays by Hydrothermal Method", ICoSM2013 -Malaysia, 2013
2. **Saeid Kakooei**, S. Valid Jaber, Kourosh Sharifi, Mokhtar Che Ismail, Abolghasem Dolati, "Study of Calcium Nitrite and Sodium Molybdate, anodic inhibitors in reinforced concrete", The World Engineering, Science and Technology Congress (ESTCON2012), ICPER2012, Kuala Lumpur, Malaysia,

3. **Saeid Kakooei**, Hossein Taheri, Mokhtar Che Ismail, Abolghasem Dolati, "The effect of H₂S concentration on the corrosion behavior of two pipeline steel (A516-Gr70 and API 5LX70) in sour environment at 50°C", The World Engineering, Science and Technology Congress (ESTCON2012), ICPER2012, Kuala Lumpur, Malaysia.
4. **Saeid Kakooei**, Hossein Taheri, Mokhtar Che Ismail, Abolghasem Dolati, "Corrosion Behavior of X70 pipeline Steel in Hydrogen Sulfide Containing Solutions", The World Engineering, Science and Technology Congress (ESTCON2012), ICPER2012, Kuala Lumpur, Malaysia.
5. Arash Dehzangi, Farhad Larki, **Saeid Kakooei**, E. B. Saion, Sabar D. Hatagalung, M.N. Hamidon, "Study of the characteristic of the p-type junction-less side gate silicon Nano-wire transistor fabricated by AFM lithography", The First Iranian Student Scientific Conference In Malaysia, 9-10 April 2011, Kuala Lumpur
6. **Saeid Kakooei**, Jalal Rouhi, Arash Dehzangi, E.B. Saion, "Aqueous combustion synthesis of Fe doped Al₂O₃ Nanoparticles". The First Iranian Student Scientific Conference in Malaysia, 9-10 April 2011, Kuala Lumpur
7. Abed Esmaili, **Saeid Kakooei**, M. Ahochehr, M. Kiani, "Root Cause analysis of Corrosion Occurred in Fire Fighting Water System in Aryasasol Polymer Co. (ASPC)" , 12th corrosion national congress, May2011, Tehran, , Iran (Persian language)
8. Jalal Rouhi , Shahrom Mahmud , Sabar Derita Hutagalung . **Saeid Kakooei**. "A fabrication technique for nano-gap electrodes by atomic force microscopy nanolithography". INSC2011, 4-5 July, Malaysia.
9. Arash Dehzangi, **Saeid Kakooei***, Jalal Rouhi, , E.B. Saion, " The effect of heat treatment on the Fe doped Al₂O₃ Nanoparticles prepared by Aqueous combustion synthesis", INSC2011, 4-5 July, Malaysia

